THE FEASIBILITY OF THE UTILIZATION OF DROP-ON-DEMAND TECHNOLOGY IN THE

FABRICATION OF FLEXIBLE DOSING, POLY-PHARMACY, AND NOVEL MULTI-DRUG DESIGN

DOSAGE FORMS

By

MARLENA BROWN

A dissertation submitted to the

Graduate School – New Brunswick

Rutgers, The State University of New Jersey

and

The Graduate School of Biomedical Sciences

University of Medicine and Dentistry of New Jersey

in partial fulfillment of the requirements

for the degree of

Doctor of Philosophy

Graduate Program in Biomedical Engineering

written under the direction of

Professor PAUL TAKHISTOV

and approved by

New Brunswick, New Jersey

May 2014

ABSTRACT OF THE DISSERTATION

THE FEASIBILITY OF THE UTILIZATION OF DROP-ON-DEMAND

TECHNOLOGY IN THE FABRICATION OF FLEXIBLE DOSING, POLY-

PHARMACY, AND NOVEL MULTI-DRUG DESIGN DOSAGE FORMS

By MARLENA BROWN

Dissertation director:

Professor PAUL TAKHISTOV

Current and future trends in the delivery of Active Pharmaceutical Ingredients (API) have

led to an explosion into the research of the development and understanding of novel drug

delivery systems with the capacity to delivery drugs with increasing accuracy and

efficiency. The advent of the discoveries made in the human genome project enables

genetic and anthropometric information about individuals to be utilized to deliver tailored

strategies for the detection, treatment, and prevention of disease. Microdispensing and, in

particular, Drop-on-Demand (DoD) technology, is an optimum technology to employ in

this avenue because it allows for the delivery of customizable drug architecture due to its

innovative and modular design. DoD enables customization for use in personalized

medicine because it is based upon a building block methodology where the dosage and

the drug delivery system is adapted by determining key attributes and combining the

Active Pharmaceutical Ingredient (API) and polymer in a block matrix system.

The goal of this research is to examine the feasibility of the utilization of Drop-on-Demand (DoD) technology to manufacture drugs that enable flexible dosing, poly-pharmacy, and multi-drug design dosage forms. Applied to transdermal drug delivery, we wish to design Transdermal Drug Delivery Systems (TDDS) in an innovative and systematic approach.

We propose to (1) print multi drug dosage forms, (2) decrease the amount of layers currently used in the traditional system, and (3) create new dosage forms by printing the API, skin enhancers, additives, and adhesive components onto the same film with distinct patterns and configurations to achieve the desired dissolution results.

ACKNOWLEDGEMENTS

DEDICATION

I dedicate this dissertation to my parents Mae Brown & Jesse Brown, my sisters: Latisha Ramsey, Myra Brown-Williams, and Linda M. Brown, my grandmother, Inez Brown, and my aunts and uncles including Antoinette Brown, Carzell Brown, Wardell Brown, and Casey Hare - Thank you for believing always believing in me; even when I did not believe in myself. Thank you for providing me with endless love, direction, and support to make this work possible.

To my beautiful nieces and nephews: Davone, Danasha, Dajere, Kamora, Corynn, and Nevaeh, thank you for the joy you bring into my life.

To my friends Mrs. Kera Young, Mr. David Snead, and Mr. Evan Egerton, thank you for giving me the motivation and strength to learn from those events that made us smile, made us cry, built us up or tore us down. These moments both joyous and sad provided me with the motivation I needed to move forward. For this, I say thank you.

Table of Contents

LIST OF TABLES

LIST OF FIGURES

xi

1 INTRODUCTION

1.1 Motivation

One of the most significant challenges currently facing biotechnology and pharmaceutical companies is the development and delivery of drugs that fit an individual patient's biology and pathophysiology [1-3] . Recent advances and discoveries made in the human genome project allow for some genetic and anthropometric information about individuals to be utilized to deliver tailored strategies for the detection, treatment, and prevention of disease [2]. Individuals have varying sensitivities to and metabolize medications differently, and therefore require different dosages of medications. Two approaches can be utilized to determine dosage: (1) Pharmacogenomics (genetic information) [2] and (2) Environmental Factors (body mass, age, etc.). Microdispensing and, in particular, Drop-on-Demand (DoD) technology is an optimum technology to employ in this avenue because it allows for the delivery of customizable drug architecture due to its innovative and modular design. DoD enables customization for use in personalized medicine because it is based upon a building block methodology where the dosage and the drug delivery system is adapted by determining key attributes and combining the Active Pharmaceutical Ingredient (API) and polymer in a block matrix system.

The goal of this research is to examine the feasibility of the utilization of Drop-on-Demand (DoD) technology to manufacture drugs that enable flexible dosing, poly-pharmacy, and multi-drug design dosage forms. Applied to transdermal drug delivery, we wish to design TDDS in an innovative and systematic approach.

We propose to: (1) print multi drug dosage forms and (2) decrease the amount of layers currently used in the traditional system and (3) create new dosage forms by printing the API, skin enhancers, additives, and adhesive components onto the same film with distinct patterns and configurations to achieve the desired dissolution results.

1.2   Controlled-Release Rate Drugs

To overcome many of the problems associated with conventional drug delivery, research into controlled drug delivery and precision dosage formulation has been extensively studied. Controlled drug delivery enables decreased toxicity, improved efficiency, and increased patient compliance. Furthermore, precision dosage formulation permits increased accuracy of delivery to the intended target site and drug therapeutic effectiveness. Recently drug formulators, biochemists, and engineers have developed "smart" drug delivery systems that incorporate materials that can be manipulated to have vast impact on the delivery of the drug. Advanced drug delivery systems such as these include delayed release, sustained release, site specific targeting, and receptor targeting systems. Advanced drug delivery systems function to enable delivery of therapeutics intact to targeted portions of the anatomy via the utilization of a medium that allows for the control of the drug delivery through means of a chemical, physical, or physiological trigger. Current attempts in designing these systems have led researchers to focus on micro and nano sized structures as the foundation in the architecture for precise dosage formulation. The structures utilized include micelles, nano and micro hydrogels, microspheres, liposomes, biodegradable polymers, dendrimers, electro active polymers, carbon nanotubes, and a variety of other substances that exist on the micro and nanoscale level [4].

General polymer systems, i.e. microspheres, involve reservoir, matrix, or a combination of both designs to dispense the API. In the reservoir design encapsulation of the drug occurs by a polymer shell. The matrix devices physically capture the drug by dispersing it throughout a polymer network. These polymer drug delivery systems operate through diffusion or dissolution and the rate of drug release is dictated by Fick's diffusion equation or the Noyes Whitney Equation, respectively [5, 6]:

$$J = -D\frac{dC}{Dx} \tag{1}$$

$$\frac{Dc}{dt} = k_d A\left(C_s - C\right) = \frac{D}{h}A*\left(C_s - C\right) \tag{2}$$

J represents drug flux, D is the diffusivity, k represents the partition coefficient; A is the Area, C is the API concentration the donor compartment. C_s is the solubility of the Active Pharmaceutical Ingredient (API).

Benefits of controlled time release drugs include enhanced desired drug release profiles at the target site, reduction of the administration frequency of the drugs, simulation of nighttime dosing, simulation of multiple dosing of one or more drug(s), and the development of novel drug therapies [5]. Current time-release drug delivery systems, classified based on physical/chemical phenomenon that directly affect the drug release rate include (1) diffusion, (2) swelling, (3) osmosis, (4) erosion/degradation, and (5) "other".

1.2.1   Diffusion Based Drug Delivery

Diffusion can be defined as basic mass transport that controls the rate of drug release from various drug delivery systems [5]. Several types of species that currently rely on drug delivery mechanisms that diffuse in an out of drug delivery systems include water, drugs, water-soluble excipients (plasticizers, polymers, and/or fillers), acids, bases, and polymer degradation products [5].

In the case where the polymeric material is chosen such that drug diffusion through the macromolecular network is the slowest step, the systems are referred to "diffusion controlled". The structure of the diffusion controlled drug delivery systems can represent three distinct types: (I) reservoir systems, (II) monolithic systems, and (III) systems classified as other [5].

1.2.1.1 Reservoir Type

In reservoir systems the drug and the release rate-controlling polymer or lipid are physically separated. The drug is immersed in the core of the dosage form comprising the "reservoir" or "drug depot". The polymer lipid surrounds the drug and acts as a release rate-controlling membrane [5]. A clear core structure such as a pellet, capsule, or tablet can be utilized to surround the reservoir and polymer lipid. Reservoir systems can further be characterized by primary drug load and/or drug solubility fraction within the device [5]: reservoir devices with an activity source that is not constant and reservoir devices that maintain steady activity source. Reservoir devices with non-constant activity are the result of when the drug load is less than the solubility of the drug and drug molecules that leave the dosage form and are not replaced. As a result of this, drug concentrations at the inner peripheries of the rate-controlling membrane decrease with time resulting in lower drug-concentrations. This provides the primary mechanism for

diffusion [5]. In reservoir systems with unsteady activity source, if optimum sink conditions are present and the and the properties of the rate controlling membrane are constant [5], we observe diffusion resulting from first-order release kinetics [5]. In a reservoir device that maintains a steady activity source the primary drug concentration is larger than the drug solubility [5]. In this type of system the undissolved and dissolved drugs exist simultaneously in the drug reservoir. The undissolved drugs can be, for example, drug crystals and/or amorphous aggregates [5]. Here, only the dissolved drug molecules are able to diffuse out and the drug crystal and aggregates remain in the reservoir.

1.2.1.2 *Monolithic*

Monolithic systems can be described as homogenous mixtures where the drug and the matrix are not clearly separated with a core-shell structure [5]. Two types of monolithic systems can be described depending on the proportion of the initial drug load compared to the drug solubility ratio: (A) Monolithic Solutions and (B) Monolithic dispersions.

In monolithic solutions the drug is located throughout the matrix [5]. Here the drug molecule is individualized within a polymeric network and bypasses the dissolution step of the drug during drug release [5] resulting in possible enhanced bioavailability. This type of system may be optimum for delivering drugs that have poor aqueous solubility; however, the drug system should not be meta-stable or form poorly water-soluble drug crystals over time [5]. Monolithic dispersions contain both the dissolved and dispersed drugs. The drug release kinetics of monolithic systems are dependent on the device geometry. In simple monolithic systems where we do not have polymer dissolution/swelling, or coefficients dependent on time and position, we can utilize Fick's

2nd Law of Diffusion to determine drug-release kinetics dependent on device geometry and dimension [5, 7, 8]. One example of this is the classical Higuchi equation [5, 9] that describes the rate release for thin ointment films with insignificant edge effects containing a large amount of initial excess suspended drug particles within it. [10].

$$\frac{M_t}{A} = \sqrt{D(2C_0 - C_s)c_s t} \tag{3}$$

, where A is the thin film surface area, D is the drug diffusion coefficient, C_0 and C_s are the drug concentration of the initial load and the solubility of the drug, respectively. Advantages of this equation include its simplicity and application to drug delivery systems such as polymeric patches [10] and other drug systems where the delivery is controlled.

It is important to make sure that when applying this equation to other systems of controlled delivery that the following assumptions are met:

1.   The API solubility is significantly less than the initial drug concentration[5].
2.   The device geometry is similar to a thin film such that edge contributions can be regarded as negligible [10].
3.   The carrier molecule does not dissolve or swell.
4.   Drug diffusivity is constant.
5.   The thickness of the film is greater than the drug particle size.
6.   Perfect Sink conditions are met [5].

Other diffusion controlled drug delivery systems include coated pellets, tablets or capsules where the drug is contained within the core, or monolithic drug polymer/lipid

core encased within an additional polymer or lipid coating. In this instance both the core and the coating are involved in drug release [5].

1.2.2   Swelling Controlled Drug Delivery

Polymer swelling represents another avenue to achieve controlled drug delivery. In polymer swelling devices the polymeric matrix swells once it comes into contact with an aqueous media (i.e. HPMC matrix tablets [5, 10]). In polymer swelling, the overall span of the pathway increased. This results in a decreased concentration gradient and decreased drug release rates [10]. The mobility of the polymer molecules increases. This, in turn, enhances drug diffusivities throughout the polymer network [10]. An example of this phenomenon can be observed in the HPMC tablet. While dry, the drug-diffusion coefficient is near zero; however, in a completely swollen HPMC polymer matrix, the diffusivity can approach those that are in aqueous media [5, 10]. The polymer type used and the type of drug [10] will determine whether (a) an increase in pathway length or (b) an increase of mobility in the polymer matrix will dominate resulting in either a decrease or increase in release rates, respectively [5].

Another example of a swelling control system is a hydrogel. Hydrogels can be defined as polymeric networks that are hydrophilic with a three-dimensional structure [11]. The constitution of a hydrogel includes polymer chains that are cross-linked. The cross-linking occurs physically or through hydrogen bonding, covalent bonds, or Van der Waals interactions [11-14]. Hydrogels are comprised of insoluble polymers that have the ability to swell in water [11, 15] . Hydrogels have been used significantly in the expansion and growth of the "smart" and controlled drug delivery system [16].

Hydrogels are often used to encapsulate or trap the drug; thus, protecting the drugs from aggressive and acidic environments such as the low pH in the stomach [11]. Additionally, hydrogels provide necessary protection to API(s) and delicate proteins from the harsh environments proximate to the intended target site [11, 17-21].

1.2.3   Osmotic Controlled Drug Delivery

Osmotic controlled delivery systems utilize hydrostatic pressure to manipulate the drug release rate. Currently there are two types of osmotic systems: one-chamber device and a two-chamber device. In both devices a rigid semi-permeable membrane surrounds the compartment or compartments and the hydrostatic pressure differences are driven by water influx into the system due to osmosis [5].

In the one-chamber device, the flow of water is driven by differences in osmolarity between the drug and the surrounding bulk medium [5] and this hydrostatic pressure drives the drug solution/suspension through orifices in the film. Here the drug delivery rate is dependent on the diameter of the holes in the film. In the two-chamber device the membrane surrounds the compartment that contains the drug and a compartment that is filled with a water soluble excipient. The compartments are separated by a flexible membrane. The influx of water into the drug compartment is due to the osmotically active excipient [10, 22] located in the second chamber. The force of the movement of water against the flexible impermeable membrane causes it to deform and the drug solution/suspension is pushed out of the chamber through the orifice [5, 22].

1.2.4   Degradation/Erosion Controlled Drug Delivery

Degradation can be defined as a scission procedure in which micro-molecules are cleaved into shorter-chain molecules and eventually oligomers and monomers [5]. Erosion is the process in which material, i.e. monomers, oligomers, polymer backbone, and polymer, is lost from the polymer bulk [5]. Erosion can occur in two distinct manners: (1) heterogeneous or surface erosion and (2) homogeneous or bulk erosion [5] . In heterogeneous erosion the polymer cleavage rate is greater than the rate at which water penetrates into the device. For this reason, polymer degradation occurs only on the surface-near regions of the system and the device shrinks with time. The drug is released as the surrounding polymer matrix disappears and the inner structure (i.e., porosity, drug content, and distribution) is not disturbed [5]. In homogeneous erosion the water-penetration rate is larger than the polymer chain-cleavage rate. Here, the entire device is quickly wetted upon contact with water and polymer chain cleavage occurs throughout the system [5]. The drug is now mobile and diffuses out of the device.

In general terms, polymers that are very reactive due to functional groups present in their backbone degrade rapidly due to surface erosion [5]. Polymers that have less reactive functional groups are bulk eroding. As an example, Polyanhydrides are primarily surface-eroding polymers and poly(lactic acid (PLA) is an example of a bulk-eroding polymer [10].

1.2.5 Other

Additional styles of controlled drug delivery systems include systems which are overlaps or combinations of diffusion, swelling, osmotic, or degradation/erosion controlled systems. Pulsatile drug release systems (i.e., drug loaded pellets [10] and micro-chip

based time-controlled delivery systems) offer possible opportunities to enhance drug delivery.

Extended and sustained release design systems that are diffusive in nature and are manufactured as reservoir type designs use multi-tablet and microencapsulated drug systems. In multi-tablet design small spheroid 3-4 mm tablets are prepared and placed into gelatin capsule shells to provide the desired drug release. Each capsule consists of at least 8-10 mini-tablets which may be coated for delayed release or uncoated for immediate release [23, 24]. In microencapsulation solids, liquids, or gases, are entrapped into microscopic particles where the wall is comprised of thin coatings. Encapsulation occurs by dissolving the wall material (i.e. gelatin) into a solvent, usually water. The API is then added and the mixture is stirred until the desired API particle size achieved. At this point a solution of acacia, or other similar material, is added to concentrate the polymer into small liquid droplets. The solvent's low interfacial tension present at the material's wall causes the droplets to form a film encompassing the API particles. The result is a constant tight film coating that remains on the individual particles of the API [23, 24]. Common excipients used include gelatin, methyl or ethyl cellulose, and various waxes.

In a matrix system the drug and excipients are combined and made into granules. In oral formulations tablets are prepared with a cellulose derivative (i.e. Hydroxypropyl methylcellulose) that is distributed throughout the API formulation with granules made from wet granulation or roller compaction. Formation of the tablet occurs through compaction. During ingestion the tablet mixes with liquid and swelling of the polymer occurs causing a small concentration of drug to be released. Solid drug is assumed to

dissolve in the surface layer first. As the external tablet layer is completely hydrated and the surface layer becomes exhausted, the next layer starts depleting [24]. In this manner the API release rate is directed by tablet corrosion and diffusion [23, 24]. Insoluble plastics, fatty compounds, and hydrophilic polymers are used in matrix systems [6].

Delayed release systems rely on repetitive dosages of drug from an immediate release system such as an enteric coated tablet or repeat action tablets. Sustained release systems permit the drug to diffuse from the carrier system in a controlled slow method over an extended length of time. Specific targeting and receptor targeting systems use "ligand receptor models" to recognize a biological component and then deliver the Active pharmaceutical ingredient (API) to the desired physiological application site [25].

Systems in which dissolution determines the rate of drug release are also utilized. Similar to diffusion controlled systems either microencapsulation or matrix systems may be used but the excipients used vary greatly. Because dissolution is used to manipulate the release rate of the API in water soluble drugs, the coating of the drug with a suitable salt of slowly soluble material is performed. The coating of the API is done with varying materials of different thicknesses to approximate the desired dissolution rates. Materials utilized include ethyl cellulose, carnauba wax, shellacs, and gelatin [13].

Matrix systems, whether diffusion or dissolution controlled, can offer greater control and protection of the API by the incorporation of layered architectures in the matrix design. This is achieved by surrounding the matrix and encapsulated API by a drug free membrane that is biodegradable with slow erosion characteristics. This results in a matrix design that exhibits both delayed and controlled delivery. This occurs because

the drug free membrane, likely made of gelatin similar to microencapsulation, needs to be degraded prior to the erosion of the matrix and drug located in the interior of the membrane. An example of a layered system is given by Vogelhuber in the treatment of tumors. In this configuration a core of drug-filled polyanhydrides is encircled by a drug-free poly(lactide-co-glucocide) layer, then a second drug coating of polyanhydride [26]. Results of Vogelhuber's experiments showed that there was a two-phase drug release. The initial drug release occurred on day one and was due to the outer coating of polyanhydride. The second phase occurred two weeks later due to erosion of the inner drug-filled polyanhydride [26]. This demonstrates that one can utilize multi-layer coatings of substrates to achieve delayed and controlled release. Extending the concept of layering beyond two layers provides drug manufacturers with technology in which many different types of drugs could be deposited at precise locations onto the same or different layers to create various therapeutic effects. This concept is of significant interest because it has the potential to revolutionize the manner in which drugs are currently administered.

Other novel, more specific advanced drug delivery systems include biodegradable polymers, block copolymers, and micelle polymer drug delivery systems [4]. Biodegradable polymers are analogous to the hydrophilic matrix systems described previously, in which, upon contact with water, the polymer degrades and leaves behind the API. These polymers consist of naturally occurring material such as collagen, cellulose, and polylactic acid, all of which the body is able to metabolize.   Block copolymers are simply the use of multiple monomers in which networks are formed through joint polymerization. Block copolymers that encompass cross linked

hydrophobic and hydrophilic monomers are designated as polymer micelles. Micelles are unique in that they exist in the nanometer size scale and; therefore, are able to individually carry drug molecules [4]. The outer shell of a micelle, composed of hydrophilic monomers, protect the core where the API is located [4]. Similar to microencapsulated drug delivery systems, the API is released due to degradation of the polymer matrix dependent upon the specific type of the delivery that is manipulated by the manufacture design.

Nanogels are colloidal microgels that have diameters less than approximately 100 nanometers in size. The primary characteristic ability of colloidal microgels significant in drug delivery is the "stimulus-responsive" behavior exhibited [27]. This is, as explained by Das et al, the ability to undergo volume phase transitions when exposed to external stimuli [28]. These stimuli include temperature, ionic strength, solvent used, electric field, and ph. The response exhibited by the colloidal gel is the change in the gel size due to swelling. A colloidal gel will swell when osmotic and repulsive ionic forces are greater than the attractive forces of hydrogen, van der Waals, hydrophobic, and other specific interactions [28]. The delivery of the API occurs through swelling and deswelling of the gel through manipulation of external stimuli.

1.3   Transdermal Medicine

The delivery of drugs to the skin and into the systemic system can be defined as transdermal drug delivery [29]. Transdermal drug delivery can be used as an alternative to the traditional oral route of drug delivery and can be an optimum avenue for drugs that possess the correct physio-chemical and pharmacological properties. Ideal candidates for transdermal drug delivery include drugs with short half-life, narrow therapeutic windows,

drugs that experience significant first-pass metabolism, and drugs that require multiple dosing. The drugs utilized for transdermal drug delivery should be nonionic, have a MW of less than 500 Daltons, be soluble in both oil and water, possess a low melting point, and be potent [30].

The transport of drugs into and across intact skin can occur through micro-routes[31]. These include transport through the epidermis (intracellular or intercellular movement) across the horny layer, through the follicles of the hair, or through the utilization of sweat glands, also known as the appendageal route [31]. Delivery of drugs through the intercellular or intracellular routes require additional diffusion through the remaining dermis and epidermis [31]. Delivery via appendageal penetration enables the drug to seep out and diffuse into the epidermis and directly into the dermal layer [31-35]. Some research suggests that for molecules containing electrical poles movement through the sweat glands may produce decreased and shorter diffusion times [31] into the systemic system. The significance and success of each of these micro-routes is dependent on various factors including the type of diffusion (transitory or steady-state) [31], chemical and physical properties of the drug, overall dimension of the stratum corneum, skin moisture, metabolism, compactness of follicles, sweat glands, and properties of the vehicle [31].

Prior to the formulation of any drug for use in transdermal drug delivery it is important to develop a stable preparation of the active pharmaceutical ingredient with the accurate ratio of concentrations relative to the drug reservoir, skin layers, and membranes[31]. The type of drug delivery device that we utilize determines the type of flux that is necessary. For example, transdermal devices which use rate-controlling membranes need

to maintain a drug flux across the membrane that is sufficiently low to enable the skin to behave as a sink [31]. In the situation where the stratum corneum does not operate as a skink, the drug input and rate, is determined by the individual's skin[31] which can results in drastically varying concentration profiles.

1.3.1 Current Designs & Problems in Transdermal Drug Delivery

The interest in potential biomedical applications of rate controlled transdermal delivery has increased significantly during the last decades. This can be seen by the immense focus in research and development activities in academic, industrial, and health care institutions attempting to develop novel transdermal therapeutic systems for prolonged and continuous administration of active pharmaceutical ingredients [36]. Potential transdermal drug candidates included antihypertensive, antihistamine, anti-angina, anti-inflammatory, anti-arthritic, contraceptive, and steroidal drugs [36].

During the last 20 years considerable advancements have been made aimed at increasing the flux of drugs across the stratum corneum. These physical enhancements include the use of iontophoresis, sonophoresis, electroporation, and micro needles [22, 37, 38] . New innovative technologies designed to enhance the drug delivery across the stratum corneum brings about the need to design mathematical models that take this factor into consideration. Because the above mentioned technologies function only to the change the physical nature of the skin by enhancing the diffusion rate, our proposed dosage form offers an alternative that can be applied universally and is more efficient due to decreased manufacturing costs.

Clinical applications of the proposed model dosage form include the ability to deliver an accurate amount of drug for use in multi-day therapy with a single application, constant dosage drug levels, and the ability to immediately stop drug administration, if so desired. This type of dosage may also make possible the delivery of complex pharmaceuticals and other biotechnology drugs that are currently in development [39]. In the cosmetic industries accurately predicting the drug flux into the skin would be useful in applications in which creams were utilized to protect the skin from ultraviolet light, treatment in dermatitis and acne, and in analyzing the amount of cosmetic chemicals that may be transported into our skins via perfume, soap, lotions, etc.

The successful applications of this model can result in decreased costs of research and production of drugs or drug delivery systems, increased and efficient risk assessment in pharmaceutical, agricultural, and cosmetic industries, and decreases in the amount of resources needed in bringing a pharmaceutical, agricultural, and cosmetic product to market. In short it has the potential to results in greater profits for pharmaceutical and other industrial companies because fewer resources are wasted but products are built with greater quality; thus resulting in greater consumer satisfaction.

Diffusion in Transdermal Delivery

In order for the API to have an effective systemic effect, it must reach its target site. This entails traveling the distance from the skin surface to the target site [40] and requires that the drug possess certain physiochemical properties. These properties should enable the facilitation of the drug to chemically and physically attach to the stratum corneum, allow for diffusion of the drug through the epidermis, and the delivery of the API into the

dermal capillary networks [36]. Generally, the rate of API permeates $\left(\dfrac{dQ}{dt}\right)$ through the

layers of the skin is described as:

$$\frac{dQ}{dt} = P_s(C_d - C_r) \tag{4}$$

,where C_d is drug concentration on the skin (donor department) and C_r is the drug

concentration in the body. P_s is the skin coefficient of permeability [36]. P_s can be

calculated according to (5)

$$P_s = \frac{K_s D_{ss}}{h_s} \tag{5}$$

K_s is the penetrant drug molecule partition coefficient as it moves from a drug system

onto the stratum corneum, h_s is the skin thickness, and D_{ss} is steady-state diffusion

constant of the API molecule [36].
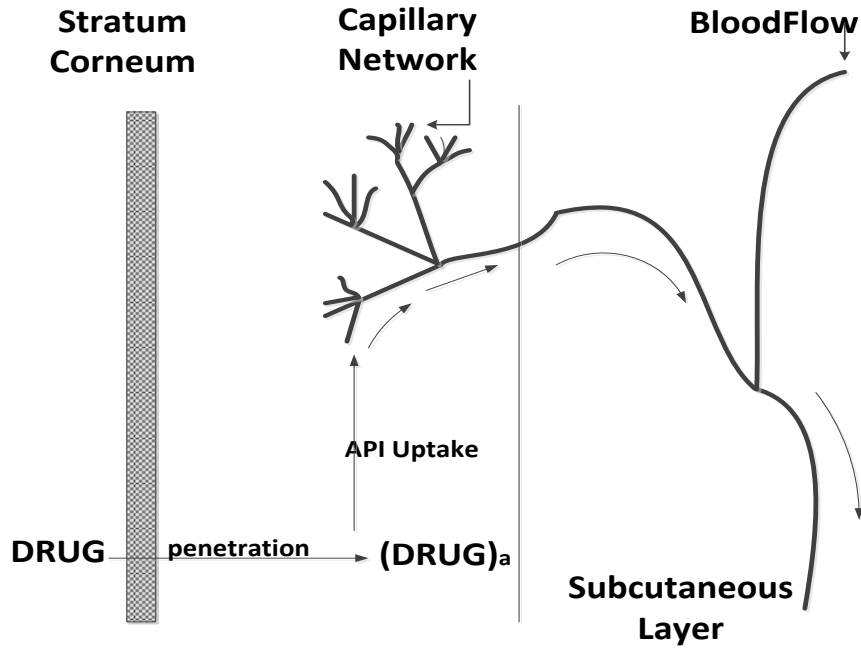
Figure 1: Schematic of multilayer skim model showing transdermal permeation of drug [36].

From equation (4) we observe that C_d must be significantly larger than the concentration

of the drug within the body, C_r, to obtain a steady level of drug diffusion into the skin

and across the stratum corneum [41]. Assuming that $C_d >> C_r$ equation (4) becomes

$$\frac{dQ}{dt} = P_s C_d \qquad (6)$$

and, $\frac{dQ}{dt}$, the rate of API penetration through the skin, becomes constant. To ensure that

C_d continues to be constant, we must make the drug release rate (R_r) steady or always

larger than uptake of the drug (R_a) by the skin [36]. If $R_r >> R_a$ than the API located

on the skin's surface should be kept at a concentration greater than or equal to that of the

saturation solubility of the API in the stratum corneum, C_s^e [36]. From this, $\dfrac{dQ}{dt}$, or the

maximum rate of API penetration can be expressed as

$$\left(\frac{dQ}{dt}\right)_m = P_s C_s^e \tag{7}$$

Analysis of equation (7) shows us that the magnitude of the API permeation rate is

dependent on the permeability coefficient, P_s, and the equilibrium concentration of the

API in the stratum corneum (C_s^e) [36].
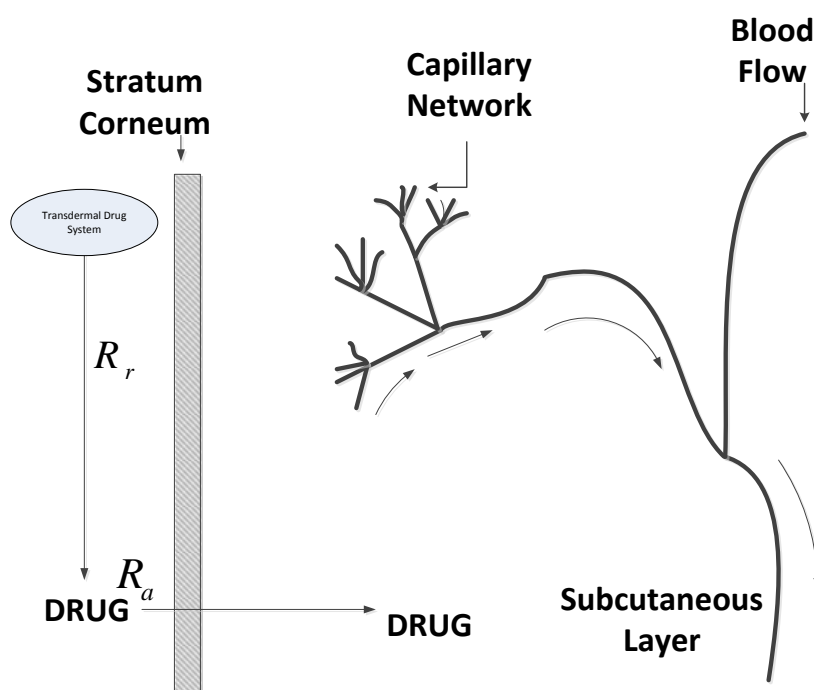
Figure 2: Illustration of the relationship between (Rr) and (Rs) of a transdermal system. [36].

The skin can be defined as a complex multilayered organ that produces the appendages

hair follicles, sebaceous, apocrine, and eccrine sweat glands [42] and is comprised of

heterogeneous cells and other extracellular components [10]. The skin is the body largest

organ and it serves to protect the body from heat, infectious materials, extreme

temperatures, and injury. In addition the skin is responsible, in part, for the maintenance of body temperature and storage of water and fat [43]. In its undamaged state the skin is a remarkable barrier and is near impenetrable to life-threatening organisms [43]. It is necessarily flexible, tough, strong, and significantly more complex than any man-made artificial material [5, 43]. Variation within the skin arises due to differences in thickness, composition, density of appendages, and biochemistry. The differences in skin can also be attributed to type, location in vivo, and strength.

 The skin is assaulted with toiletries, cosmetics, and medicated products almost on a daily basis [5]. Additionally it can become damaged through bruising, scraping, inspect bites, cuts, nicks, and assaults from an array of physical and chemical abuses greater than any other organ in the body [5], all of which can affect the skin structure. To understand how skin structure and function can affect drug permeation a review of skin anatomy and functionality is undertaken. For transdermal drug delivery purposes, the skin can be categorized into four structures. These include the innermost subcutaneous layer (hypodermis), dermis, the epidermis, and the external layer (stratum corneum) [44, 45] . In general discussions of the skin, the epidermis and the dermis constituent the skin and the stratum corneum is regarded as part of the epidermis [46]. The dermis encompasses the innermost subcutaneous tissue [46].

The epidermis consists of the epithelium composed of a keratinized outer layer, cells of the stratum spinosum, and an inner layer of basal cells [46, 47]. It is the stratum corneum (*horny layer*), consisting of anucleate cells, that offers the greatest barrier to toxins, and other microorganisms, heat, light, and the transdermal delivery of drugs. The stratum corneum is fundamentally metabolically inactive tissue composed hexagonal

building blocks. These building blocks are hexagonal flattened and stacked cells that were once viable [43]. Over most of the body the building blocks are layered between 15 − 25 cells deep [5]. The stratum corneum's thickness varies dependent on its location within the body. It can be as thick as a few hundred micrometers on the on the palms of our hand and soles of our feet [43]; however, over the majority of our body, the skin is approximately 10 μm [43] thick or less than 20% of the thickness of a sheet of paper [5]. The stratum corneum is a dense tissue, approximately $.25\frac{g}{cm^3}$ when dry and is continuously under formation. Microscopic flakes routinely dislodge and are replaced with new underlying cells, with a completely new horny layer occurring approximately every two weeks [5, 43].

1.3.2   Mechanism of Absorption

There are three primary manners that drug molecules can traverse the stratum corneum structure. The first method is the transcellular route. In this route the drug passes through keratinocytes and lipids to cross the stratum corneum. This path is thought to be the straightest and shortest path across the stratum corneum as compared to the intercellular route. The second avenue is the intercellular route. In this route the molecule remains in the lipid bilayer and travels around the keratinocytes [48] . The intercellular route primarily used during drug penetration because a large majority of drugs molecules are soluble in fats. The keratinocytes (of the intracellular route) consist primarily of proteins and few drugs are soluble in this environment [48, 49].   The third way a drug can penetrate the skin is via the sweat ducts utilizing the hair follicles or the sebaceous glands. This route is usually referred to as the shunt or appendageal route [29]. There has

been insufficient research of the contribution of the shunt route in transdermal drug delivery due to the inability to experimental in vitro models to distinguish between the three routes [29]; although Scheuplein concluded that the follicular shunt route resulted in the pre-steady state permeation of polar molecules and the flux of larger molecules that cannot traverse the stratum corneum easily [29, 50, 51]. In general, the shunt or appendageal route comprise only about 0.1 % [29, 52] of the area available for transdermal delivery and their overall contribution to the steady state flux is insignificant [29].

We examine the skin composition as layers of corneocytes of thickness of approximately 15 μm when dry and about 40 μm when hydrated that consists of keratin corneocytes existing in a web medium composed of fatty acids, cholesterol, triglycerides, and sterol/wax esters, and ceramides [29, 53]. The corneocytes are can be considered to be polygonal and flat (approximately 0 .2-1.5 μ thick and an average diameter of approximately 39 μm [29]. The lipid arrangement within the stratum corneum results in lipid phase characteristics that differs from other biological membranes [29]. Hydrocarbon chains are organized into areas within the lipid bilayer separating according to crystalline, gel, or liquid crystal phases [29]. These characteristics, along with the water component in the stratum corneum, all contribute to the relationship between the physiochemical properties of the drug, the composition of the stratum corneum, and the optimum choice of avenue for the delivery through the stratum corneum [29].

Previous research has suggested that hydrophilic molecules would diffuse through the aqueous areas approximate the external surface of the intracellular keratin strands and the

hydrophobic molecules probable route across the stratum corneum is through the lipid matrix (intercellular route) [29]. The idea that a drug will either take the intracellular route or intercellular route neglects the fact that the routes are not totally independent of one another and provides an oversimplification of the challenges of traversing across the stratum corneum [29]. Any API that crosses utilizing the transcellular router migrates into and diffuses out through the keratinocyte [29]. On the way to the next keratinocyte the chemical must move into and diffuse out of lipids that exists between the keratinocytes [29]. Partitioning into and diffusing out of lipophilic and hydrophobic regions is undesirable for many molecules [29]. For these reasons, the intercellular route is preferred and significant research has gone into understanding how to enhance delivery of drugs using the solubility properties of drugs in the lipid domain [29].

The percutaneous flux of a drug into the epidermis is dependent on various factors including type of drug vehicle used, initial concentration of drug in the vehicle, site of application, type of drug/chemical, and the thickness of the stratus corneum [48]. Transdermal delivery of drug through the skin is often predicted with little accuracy due to varied factors involved and the inability to manipulate the stratum corneum in advancing drug diffusion. For this reason most topical applications utilized for drug delivery are applied in "infinite" dose amounts. This results in non-efficient manufacturing, drug delivery, and bioavailability. To address this issue, recent advances in transdermal delivery focus on methods that enhance the delivery of the drug across the stratum corneum and the use of technologies that increase the quantity of drugs utilized in transdermal delivery.

1.3.3   Components of a transdermal system

A transdermal system can consist of the polymer matrix, the active pharmaceutical ingredient (API), penetration enhancers, rate controlling membrane, penetration enhancers, surfactants, components of the drug reservoir, backing laminates, and the adhesive layer [29].

The polymer matrix is an important component in the design of a transdermal dosage form [29]. The polymer matrix can be formulated in a manner to achieve the desired rate

of controlled drug delivery where the physical and chemical properties of the polymer and the drug will determine the mechanism of drug release [29]. Polymers that are used in in transdermal dosage form should have the following characteristics:

- Polymer should enable a large quantity of drug to be integrated into it

- The properties of the polymer, i.e., MW, temperature, melting point, etc. should permit the diffusion and release of the API

- Polymer should be inert with respect to the drug

- Ease of manufacture and fabrication

- Polymer should remain stable when added to API, excipients, etc.

- Polymer should not decompose due to body temp or high humidity conditions

- Polymer should be safe and non-toxic

Penetration enhancers and surfactants can be added to polymers to aid in the permeation of the API molecule. Penetration enhancers enhance the permeability of the skin by modifying the barriers to the flux of the drug [29]. Important properties of the penetration enhancers are that they should be non-reactive, nontoxic, non-irritating, pharmacologically inert, and the ability to act directly and for a specified duration [29].

Drug Reservoir: The drug reservoir is the temporary "storage" location of excess drug. In the drug reservoir the drug can be consistently dispersed throughout the polymer environment or exist as a suspension suspended in a liquid medium [36]. It is important that the reservoir is compatible with the API and promote the transfer of the API at the desired rate. Furthermore, the reservoir should be able to maintain the structure of the

dosage form. Common materials used in the drug reservoir included colloidal silica, HPC, and mineral oils [29].

Backing laminates are used in transdermal dosage forms to provide support [29]. The backing occludes the API from migrating out of the dosage form through the top. Laminates must be impermeable to the API, permeation enhancers, and surfactants [29]. Additionally, the backing should be elastic, flexible, possess tensile strength, and transmit moisture vapor at a low rate [29]. The laminate should be economically efficient, be chemically compatible with the other components of the dosage form, and should allow adhesive lamination [29]. Examples of layers include those comprised of aluminum vapor, polyethylene, heat seal, pigmented layers, and polyester [29].

Rate controlling membrane: The rate controlling membrane is used to manipulate the release rate of the API from the transdermal system [29]. Polymers usually serve as base materials for these type of membranes [29]. Materials that can be used in the rate controlling membrane are cellulose derivatives, chitosan, hydrogels, and poly-2-hydroxyethyl methacrylate (PHEMA) [29, 54].

Adhesive Layer: The adhesive layer is utilized to bond the transdermal system to the skin. Current classes of adhesives include polyisobutylene type pressure adhesives, silicone pressure adhesive, and acrylics pressure sensitive adhesives [29]. The pressure sensitive adhesive should be cause irritation and should adhere to the skin for a sufficient amount of time through a variety of environmental conditions.

The release liner is used to protect the transdermal delivery stems from contaminants and can avoid the potential loss of API that moved into the adhesive layer during storage [29].

The release lines consist of the base layer and a release layer. Materials that are utilized include silicon, Teflon, polyesters, foil, and Mylar [29].

1.3.4   Types of Transdermal Devices

Types of transdermal drug delivery systems include membrane moderated systems, adhesive delivery systems, matrix drug delivery systems, and micro reservoir drug delivery systems [36]. In systems where the drug reservoir is completely encapsulated in a partition made up of a plastic laminate membrane-moderated transdermal controlled drug delivery is achieved [36]. In membrane moderated transdermal systems the drugs migrate from the porous polymer membrane that has a specific drug permeability rate [36]. On the surface of the membrane an adhesive is applied [36]. The drug release rate can be manipulated through polymer concentration and composition, the permeability of the API in the polymer, and the type and width of the rate controlling membrane [36].

The drug rate of release is described by:

$$\frac{dQ}{dt} = \frac{C_r}{\left(\dfrac{1}{P_m} + \dfrac{1}{P_a}\right)} \tag{8}$$

Here C is the concentration of drug in the donor, P_a is the permeability coefficient of the adhesive layer; P_m is the permeability coefficient of the polymer membrane [36].

Drug in adhesive transdermal models contain API where the drug is dispersed within the adhesive layer [29, 36]. The adhesive layer is then attached to an impermeable backing that forms a drug layer [36]. A rate controlling adhesive polymer layer may be added to

the surface of the drug donor layer to further manipulate the drug release rate [36]. The rate of drug release in adhesive systems can be defined by:

$$\frac{dQ}{dt} = \frac{kD}{(h_a)}C_r \qquad (9)$$

Here k describes the segregation of the API from the reservoir to the adhesive layer [36].

In matrix diffusion controlled transdermal systems, the drug reservoir consists of the solid drug dispersed in a hydrophobic or hydrophilic polymer matrix [36]. The API is shaped into a polymer disc with specific area and thickness. This disc is then situated onto an occlusive base[36]. Here the adhesive polymer is not mounted to the surface of the API disc, the adhesive is spread around the perimeter of the transdermal patch. The drug release rate for matrix diffusion drug delivery systems is explained by the following equation:

$$\frac{dQ}{dt} = \sqrt{\frac{CC_r D}{2t}} \qquad (10)$$

C is the initial drug load, D is the drug diffusivity, C_r is the drug concentration in the donor compartment [36].

Microreservoir systems employ a combination of mechanisms from both the matrix dispersion systems and the reservoir system [29, 36]. The drug reservoir in this type of systems consists of suspended drug particles in an aqueous medium of a polymer that is water soluble. The drug solution is then dispersed into a hydrophobic polymer [36] through high-shear force. This process produces thousands of microscopic balls of drug reservoir [36]. To stabilize the dispersion the polymer chains are cross-linked producing a

circular API sphere of fixed surface area and thickness [36]. The drug sphere is then placed centrally on an adhesive pad [36]. The rate of drug release from a microreservoir controlled transdermal system is dependent on the fraction of the concentration in the bulk compared to the drug solubility (β') and the proportion API solubility in the medium to the total API concentration present at the peripheries of the polymer film α' [36]. The rate of drug can be defined by:

$$\frac{dQ}{dt} = \frac{D_p D_s \beta' K_p}{D_p \delta_d + D_s \delta_p \beta' K_p}\left[\alpha S_p - \frac{D_1 S_1(1-\alpha)}{\delta_1}\left(\frac{1}{K_1} + \frac{1}{K_m}\right)\right] \tag{11}$$

K_1, K_p and K_m are the partition coefficients that describe the partition of the drug from the liquid, polymer coating membrane, and the polymer matrix, respectively [36]. The drug diffusivities [36] are represented by D_1, D_p, and D_s.

Other types of drug delivery systems that employ mechanisms or a combination of mechanisms described above include the vapor patch and matrix system [29].

1.4 Personalized Medicine

For the past 20 years research focusing the genomic, environmental, and anthropometric information of a patient has been observed in an effort to deliver a more personalized approach to healthcare [55]. As indicated by Haselden et al, conventional methods of drug administration are based upon a reactive assessment of a patient's current medical state determined by biochemical and functional analysis and clinical signs and diagnosis [56]. Although this method has proven to be adequate in the successful treatment of a majority of populations, it fails to provide what may be the best treatment for the

individual [56]. Individual effective treatment requires comprehension of a person's the genetic, information, interaction with environment, personal lifestyle, and anthropometric information. This type of treatment paradigm has received considerable attention from academia, government, and private drug sponsor institutions [56].

Recent advances in personalized medicine focus primarily on pharmacogenomics; however, there has been some attention towards personalized drug delivery in other areas. "Targeted" diagnostics and therapeutics have been developed from information gauged from the individual's genetic makeup. On the pharmacogenomics front, genomic testing has been successful in enabling us to identify the probability of an individual inflicted with a specific disease, predict a patients response to disease and drug treatment, and provide patients with the optimum therapeutics [1, 2] to treat their disease or ailment.. Genetic tests have revealed that some patients' tailored drug treatment will require varying doses of medications. For example, the AmpliChip CYP450 (Roche Diagnostics) can anticipate the manner in which patients will metabolize some drugs [57].

Specifically, the personalized coalition for medicine points out that genotyping of drug enzymes has to resulted in enhanced drug dosing quantities for diseases and ailments such as heart disease, depression, anxiety, and cancer[58]. This has been beneficial in decreasing side effects, undesired drug interactions, and ineffective treatment [58]. This personalized medicine has seen success and has the potential to decrease unnecessary treatments, adverse side effects, and increase the efficacy of drug delivery and treatments [1] and patient compliance.

1.5   Drop-on-Demand Technology

Drop-on-Demand Technology can be utilized in the manufacture of personalized dosage forms. The following section (1.5) is summarized from my previous work detailed in "Automated Drop-on-Demand System with Real-Time Gravimetric Control for Precise Dosage Formulation." <u>Journal of Laboratory Automation</u> **18**(2): 152-160.

In all types of controlled drug delivery the key component is the design of a precise dosage formulation that permits enhanced control and prediction of the diffusion rate of the drug out of the carrier system and into the targeted area for therapeutic application. Unfortunately these designs are usually complicated, costly, and involve large scale manufacturing processing to obtain the resultant drug delivery system. The current methods of obtaining polymers result in poor or no control over particle size causing decreased control in release profiles during drug delivery applications. One of the more promising and forward thinking technologies that can be employed in the design of controlled delivery and precise dosage formulation is drop on demand technology for polymer printing and rapid prototyping. Ink Jet printing is based upon dot matrix printing technology where droplets of ink are released from a small orifice and are deposited onto a specific position on a material [59].

Applied to precision dosage formulations, ink jet technology can be used to drop precise dosages of drug formulation onto biopolymeric substrates to create functional and convenient drug delivery system.   In the design of DDS where adhesion occurs through surface interactions the ability to precisely control manufacturing processes and API concentration is critical. Drop on demand technology allows us to engineer adhesion

properties through the manipulation of polymer concentrations and dosage volume enabling the end-user to create substrate where the functional API can be encapsulated within a polymer cell (blister pack) or layered onto the surface with the API distributed evenly onto the film surface (edible film DDS).

In recent years ink jet technology (IJT) has been evaluated for its potential use in the creation and modification of biological substrates [60]. In particular drop on demand technology (DoD) has been employed in the patterned self-assembly of protein arrays, designed seeding of individual cells, printing of viable mammalian cells, and to a lesser extent, tissue engineering. In addition ink jet technology, as compared to other substrate modification techniques, is relatively inexpensive, flexible, simple, and expedient [61, 62].

Ink jet technology has long been a staple of the printing industry. Types of ink-jet technology include continuous and drop on demand systems [60]. In continuous ink-jet printing the ink is forced through the nozzle on a print head at high pressure by a mechanical pump. The drops are electrostatically charged resulting in a steady stream of charged ink particles that are ejected forward [63]. DoD printing systems can function as piezoelectric or bubble jet (thermal) printers. In these systems electrical signals are generated and sent to an actuator that creates a pressure waveform responsible for ejecting a droplet of ink onto the substrate [61]. In general consumer ink jet printers consist of a pressure ink reservoir, small diameter orifice to control dispensing volume, and a voltage dependent orifice [62]. Commercially designed printers can be used in

drop on demand systems for biological applications with only small modifications to accommodate for the use of "biological ink" and polymer substrates [64].
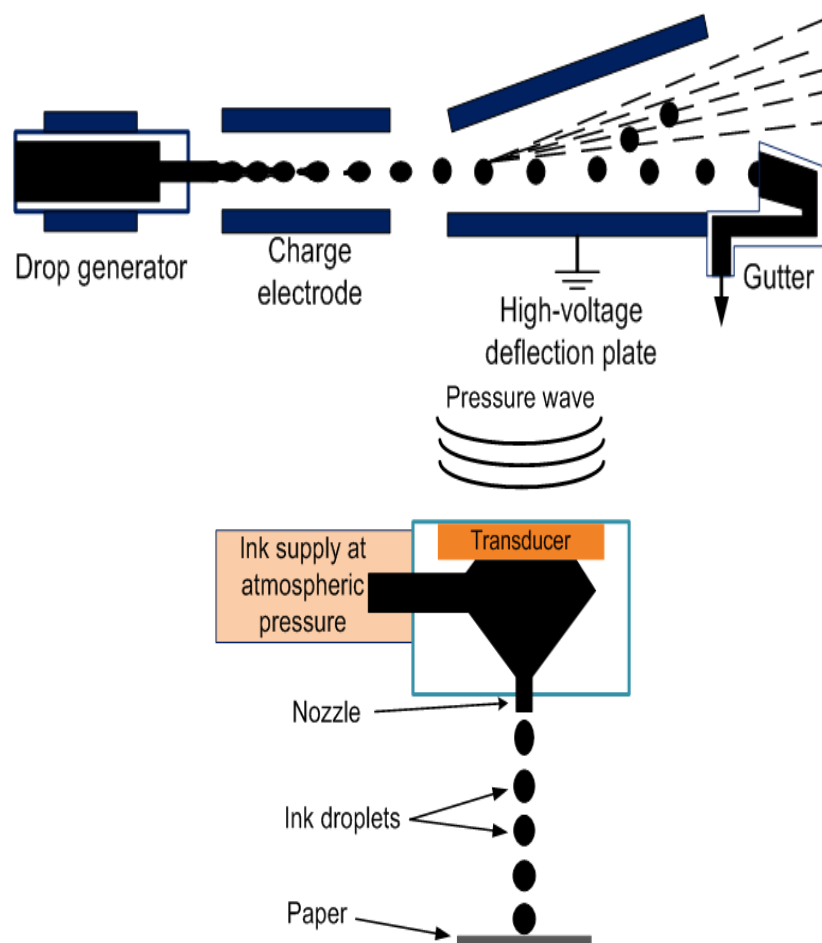
Figure 3: Continuous and Drop on Demand Technology

Applied biologically IJP has been used in drug screening, biosensors, and genomics [65]. Labile and fragile molecules such as DNA and other proteins, mammalian cells, and macromolecules have been successfully printed where greater than 90% of the cells were not lysed during printing [66]. In addition to single cells IJT has also been used to manufacture DNA protein arrays and in the modulation of cell attachment patterns.

Ink jet technology is optimum for our uses because it provides specialized control in the drop formation properties. In engineering adhesive properties it is critical that the radius, uniformity, and capacity of the droplet containing the polymer adhesive and API be precise within micron range error. Droplet size can play a significant role in binary surface interactions and can alter adhesion properties. Basaran details the advantages of utilizing drop on demand technology and declares that drop-based systems are optimum for processes which entail the manufacture of polymer particles [63]. Innovative techniques in ink jet technology enable the functionality of applications previously impossible with greater efficiency and control. Ganan-Calvo developed a combinatorial method based on Flow Focusing technology [67]. Figure 3 depicts the flow focusing device and procedure. In this method the polymeric solution (fluid 1) is injected into a capillary tube surrounded by *focused* water [68]. The polymeric solution flows through the tube towards the orifice that opens up to the flowing water stream (fluid 2). The water stream shapes the meniscus of fluid 1 into a cusp resulting in the jetting of fluid 1 out of the orifice [63, 67]. This technique permits the ejection fluid drops that are much smaller in diameter than the orifice and is capable of manufacturing drops with radii of 35-40 μm [63]. An expansion Ganan-Calvo, Martin-Banderas fluid flow technology was undertaken by Umbanhowar with the creation of monodisperse emulsions using co-flowing streams [63, 69]. Other noteworthy techniques used to create and control small radii from larger orifices include using voltage pulses of square waves and waveform 3 [68, 70]. Images of systems which enable enhanced control over particle properties such as radii using waveform techniques as described by Basaran are available in [63].
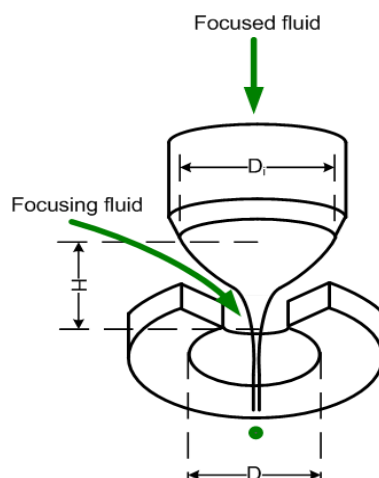
Figure 4: Flow Focused Methodology [67]

In recent years transdermal controlled delivery and precision dosing has increased in popularity due to its ability to deliver accurate dosing of toxic drugs, delivery of macromolecules, ease of application, and increased bioavailability of the API at the site of application. Ink Jet printing applied to transdermal and precision controlled drug delivery enables innovative drug delivery systems (DDS) that are efficient, adaptable, and effective. Current employed drug delivery applications utilizing Ink Jet Printing include the loading of drug coated stents, printing of protein molecules, needle free jet injection[71], and three-dimensional printing technology for oral drug dosage forms [72].

The application of IJT and DoD to biology is significant. Ink jet printing (IJP) allows for the generation of scaffolds that are complex in nature and highly vascularized. As compared to other techniques IJP is preferred due to its low cost, efficiency, high throughput rate, and ability to print bioink without chemical or biological alteration. IJT expands tissue engineering because it permits the printing of various bioinks, including hydrated or solvated molecules [65]. Moreover inkjet technology allows for greater

control in the positioning and location of spatial arrangement of materials in the scaffold. A major problem in tissue regeneration is the ability to carefully combine and organize cells and scaffolds into a geometric pattern that allows open and free communication between the cells to promote growth [66]. This factor proves to be especially significant where distinctive cell types are necessary to be placed in anatomical precise locations to achieve the desired biological function [66]. Ink jet printing offers potential solutions to this problem. Differing from micro contact printing and photolithographic techniques, IJP can create multiple surfaces using up to 200 nozzles where ink is injected simultaneously from each nozzle. With regards to tissue scaffolds this enables surface modification and precision cell placement to occur faster and with greater accuracy [62].

Summarized from my previous work in "Automated Drop-on-Demand System with Real-Time Gravimetric Control for Precise Dosage Formulation." <u>Journal of Laboratory Automation</u> **18**(2): 152-160 'Most all drug delivery applications which employ ink jet printing involve similar principles but with modifications specific to the desired application. In general a bio-ink, macromolecule, or drug is loaded into a cartridge of an ink jet printer and the drug is released in a controlled manner via thermal, piezoelectric, or pressure means' [68].

In needle free injections drugs, proteins, and other large macromolecules are deposited under the skin through utilizing jet injectors that propel liquid streams to velocities sufficient for skin penetration. This ink jet printers rely on springs or gasses to deposit liquid streams [71]. This method eliminates the need for painful or inaccurate doses through the use of hypodermic needles. Ink jet printing offers advantages to the coating of stents [73] because precise amounts of drug are able to be printed due to small

available printing area, expensive drug costs are minimized, results are usually controllable and reproducible [74]. In addition small quantities of drugs, i.e., 100 µg, are easily printed with low good efficiency and low error. The use of IJT in the manufacture of drug-coated stents increases drug bioavailability, patient compliance, and success rate of the stenting procedure. In three dimensional printing for use in oral delivery Ink jet printing is used to address traditional problems associated with oral dosage, such as decreasing drug release rates and diminished API precision., through the use of geometric configurations and patterning [75]. Solid objects can be created utilizing ink jet technology by printing into specific areas of sequentially deposited layers [75]. Three dimensional ink jet printing can produce drug delivery with zero order release rates, diffusion gradient based rates, cyclic drug release, and other controlled release mechanisms [75].
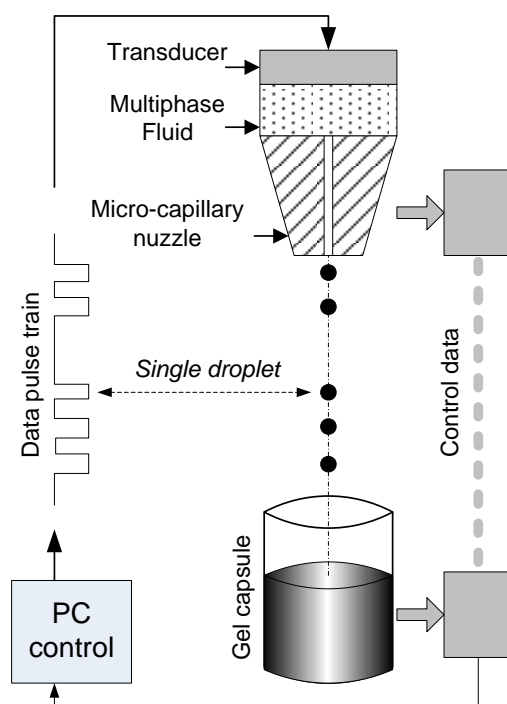
Figure 5 Schematic of a drop-on-demand micro-dispensing system [68].

The following paragraph is summarized from my previous work "Sahay, A., M. Brown, et al. (2013). "Automated Drop-on-Demand System with Real-Time Gravimetric Control for Precise Dosage Formulation." <u>Journal of Laboratory Automation</u> **18**(2): 152-160.

'The use of inkjet dispensing technology generally provides several advantages over syringe-pump based liquid handling. Figure 5 shows a schematic of a drop-on-demand ink-jet system. Because the technique is non-contact, delivery of the drop to a small location is not limited by the mechanical size of the tip [68]

2   MATERIALS AND METHODS

2.1   Materials

Materials used in film formation included polyethylene glycol(PEG) of molecular weights of 400, 1000, 1450, 1500, and 3350 and Hydroxypropyl cellulose powder (MW 100, 000) manufactured by TCI (Tokyo).. PEG 400 No. 443 was provided in liquid form by TCI Corporation of Tokyo. PEG of MW 1000(semisolid wax) and 1500 (white flakes) was supplied by Alfa Aesar Corporation (Ward Hill, MA).   J.T. Baker (Phillipsburg, NJ) provided PEG 1450 as a waxy soft solid. PEG 3350 was supplied by Sigma Chemical Company (St. Louis, MO) in powder form.

 Diiodomethane, 95%, stab with copper (Alfa Aesar, Ward Hill, MA), Distilled water (from tap), and BDH ethylene glycol, supplied by VWR (Chester, PA), were used as probe test liquids for surface energy calculation. Film was formed on No. 1 Corning (Lowell, MA) cover glass slips (22 X 40 mm in diameter), VWR # 2 cover glass slips (20X 20 mm), and Polystyrene VWR 60 X 15mm petri dishes.

Materials used in the fabrication of the transdermal form included poly(methyl methacrylate) (PMMA), in white powder form supplied by Spectrum Chemicals (New Brunswick, NJ) and the aromatic "safer" solvent Anisole supplied in liquid form from Alfa Aesar (Ward Hill, Massachusetts). These two materials were used to develop the PMMA thin film adhesive coating.   Nicotine Ditartrate (Fair Lawn, NJ) in powder crystalline form and Haloperidol in powder form was supplied by TCI America. Polyethylene (PE) served as the backing layer of the transdermal form was received from

VWR.   The transfer membrane utilized in the Franz diffusion cell studies was polyvinylidene fluoride. A brief summary of the components of the transdermal form can be seen in Table 1.

Transdermal Component	Material
Backing Layer	Poly Ethylene Film PENS, 76 μm thick with a 46μL thick adhesive layer
Adhesive	6% PMMA dissolved in anisole
Transfer Membrane	Bio Trace PVDF – polyvinylidene fluoride, 165μM
Active Pharmaceutical Ingredient	Nicotine Ditartrate, 99% ; Haloperidol

Table 1 : Components of modified Transdermal Delivery System

2.1.1   Active Pharmaceutical Ingredients

2.1.1.1   *Dopamine Hydrochloride*

Dopamine (DA) (3,4-dihydroxyphenylethyamine, is a natural occurring catecholamine neurotransmitter in the brain. It is the immediate precursor of hormone noradrenalin [76, 77] and is associated with pleasurable experiences such as sex and eating providing feelings of happiness or enjoyment for reinforcement of certain activities.   It is thought to regulate many activities including hormonal and cardiac activities [76]. Dopamine is a neurotransmitter in the sympathetic and central nervous systems and acts as a hormonal regulator in maintaining heart rhythm and blood pressure [76].   Lack of the presence of dopamine neurons in the brain is also noted in cases of Parkinson's disease, schizophrenia, and depression [76-79]

2.1.1.2   *Haloperidol*

Haloperidol is a hydrophobic molecule and a butyrophenone antipsychotic. It is also classified as a neuroleptic (tranquilizer) and acts a D2, D3, and D4 dopamine receptor

antagonist used for treatment in schizophrenia and mania. Its hydrophobicity and low molecular weight makes it an ideal drug for use in transdermal delivery [80, 81].

2.1.1.3   *Nicotine Ditartrate*

Nicotine ditartrate also known as nicotine bitartrate dihydrate or nicotine hydrogen tartrate is a crystalline salt of nicotine. It has been used in many applications of smoking cessation including as lozenges and in fast dissolving applications. Research shows that nicotine is stable during storage and is easily converted to an absorbable form in the mouth [31].

2.1.2   Biocompatible Film Substrate

2.1.2.1   *Hydroxypropyl Cellulose*

Hydroxypropyl cellulose (HPC) is a partially flexible, water soluble polymer. [82]. At high concentrations HPC can transition from a liquid crystal [82] The average At distance lengths of ca ~ 100 HPC remains stiff; however it becomes flexible are lengths greater than ca~100. [82].

2.1.3   Adhesive

2.1.3.1   *Polymethyl Methacrylate*

PMMA is a polymer that is used readily for many miniature electronic applications [73]. PMMA is utilized as a resist material for ultra-violet and micro lithographic processes [83]. PMMA is also used as a host in optical-electronic application because it can produce uniform layers, its transparency in visible wavelengths, and suitable class transition temperatures [84].   PMMA is also used to provide coating and as bonding

agent for wafers because it has excellent adhesion for most substrates [83]. An adhesive solution of PMMA was formed by mixing 6 grams of PMMA powder in 100 ml of anisole during continuous storage for a period of 24 hours.

2.2   Methods

2.2.1   Film Formation

Hydroxypropyl cellulose (HPC) forming solution was prepared by dispensing 0.10 grams of HPC powder in 100 ml of ethanol or DI water at room temperature. Solutions were placed on a stirrer for a period of 2 hours and then left to stand for 24 hours. Film solutions that were to be comprised of only HPC and ethanol were formed and diluted down to concentrations ranging from 0.1 % - 0.5% of HPC. Film solution for PEG &HPC blend films were prepared by diluting 0.010 grams of HPC in 100 ml of ethanol. All solutions remained constant at 0.10 % HPC but varying volumes of PEG were added to form different solutions concentrations for film preparation. Twenty different polymer blend solutions were utilized to form thin clear films on Corning cover glass slips.

Films were formed using either spin coating or free-casting techniques. In the free-casting method 750 micro liters of solution were placed onto polystyrene VWR 60 X 15 mm diameter Petri dishes and the liquid solution was allowed to spread. The petri dishes were placed under vacuum pressure for a 24 hour period. After 24 hours the petri dishes were placed in an oven and allowed to solidify. After solidification, the films were analyzed using optical microscopy techniques and digital images were captured using a Nikon Coolpix camera. Spin coated films were formed using a Laurell WS-400A-6NPP Lite Spin Coater. Corning cover glass slips were loaded onto the spin coater and placed

under vacuum pressure. 200 micro liters of film blend solutions were placed onto a cover glass slip and spun for 10 seconds at 1000 rpm.

2.2.2 Calculation of Surface Energy Parameters

To obtain surface energy measurements the Van Oss and Young methods were utilized [85]. In this method three liquids with known surface energy values are placed onto a solid such that three equations can be generated and utilized to find the surface energy parameters of the solid substrate [86, 87]. The defining equations are:

$$\gamma_L \cos\theta = \gamma_s - \gamma_{SL} \tag{12}$$

γ_L is the surface tension, θ is the initial impingement contact angle, γ_s is substrate surface energy, and γ_{SL} is the solid: liquid interfacial energy. The total surface energy is now expressed as:

$$\gamma^{TOT} = \gamma^{LW} + \gamma^{AB} \tag{13}$$

The term γ^{AB} can be defined in terms of electron parameters [88]:

$$\gamma_i^{AB} = 2\sqrt{\gamma_i^+ \gamma_i^-} \tag{14}$$

and the relationship relating the contact angle and the interfacial energy can be evaluated using the following equation[87, 89]:

$$\gamma_L\left(1+\cos\theta\right) = 2\left(\sqrt{\gamma_S^{LW}\gamma_L^{LW}} + \sqrt{\gamma_S^+\gamma_L^-} + \sqrt{\gamma_S^-\gamma_L^+}\right) \tag{15}$$

The Van Oss method [86] was used to calculate interaction energies between the film substrate and polyethylene glycol (PEG). Solution droplets of dopamine hydrochloride were deposited onto the films to observe contact angle measurement. Contact angles

were obtained employing the sessile drop method [90]. Goniometry and a KSV digital camera software system were utilized to capture images of drop impingement.

Optical goniometry for Surface energy/Surface Tension

To investigate how PEG concentration would affect the surface energy properties of the bio-edible substrate, contact angle (CA) goniometry was used. A Rame-Hart (Netcong, NJ) goniometry system was employed to accurately obtain initial contact angle measurements. The sessile drop method, without control of humidity in the ambient, at room temperature was used. The three liquids utilized included water (72.8 dyne/cm), diiodomethane (50.8 dyne/cm), and ethylene glycol (48.0 dyne/cm) [86, 91]. Advancing and receding contact angles were imaged using a Pixera Professional 1.2 MPixel 2.5 luc C-mount (San Jose, Ca) high resolution camera and software system.
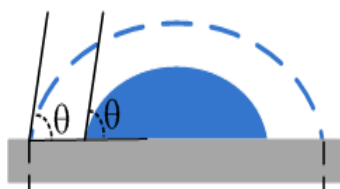
Figure 6 : Geometry of a Sessile droplet

The surface energy of the film is obtained by using sessile droplet method on an optical Rame-Hart goniometry (software KSV CAM101). In sessile drop method, a liquid droplet is deposited onto a substrate as in Figure 6. The final shape of the drop is dependent on the initial contact angle that the droplet makes upon impingement [92].

2.2.3   Thermal Analysis

The crystallinity of dopamine hydrochloride was characterized by differential scanning calorimetry (DSC) using a Perkin Elmer DSC 7 at the rate of 10^0C per minute. The DSC analyzer measures the flow of heat into or out of the investigated sample as function of temperature or time. The relationship between the heat flow, scanning temperature and time is in the form:

$$\frac{dq}{dt} = \frac{dq}{dT}\frac{dT}{dt} + H(T,t) \tag{16}$$
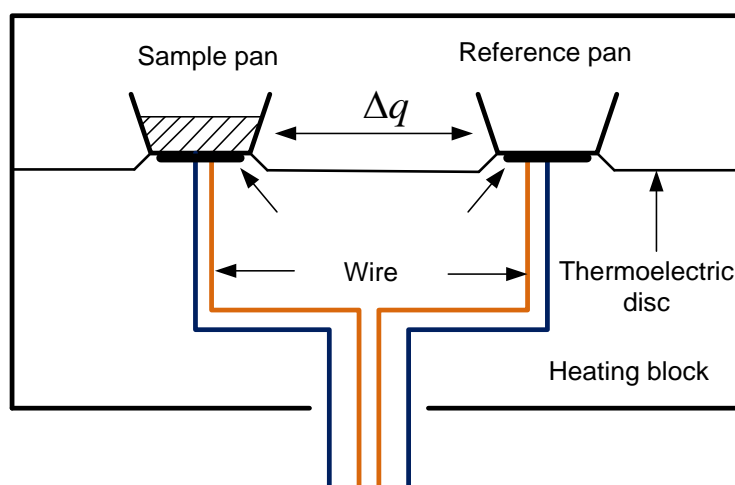
Figure 7 : Schematic diagram of differential scanning calorimetric cells [93].

In equation (16), the term dq/dt is the heat flow; dq/dT is heat capacity of the sample; dT/dt represents the scanning rate (the rate of heating or cooling); and $H(T,t)$ is the heat of thermal incident (i.e. glass transition or solid – liquid transition. Measurement of the heat flow enables us to characterize the crystallinity and thermal properties of a material. Figure 7 presents the schematic diagram of heat flux differential scanning calorimetric cells. Figure 8 presents a ty typical DSC thermogram [94].
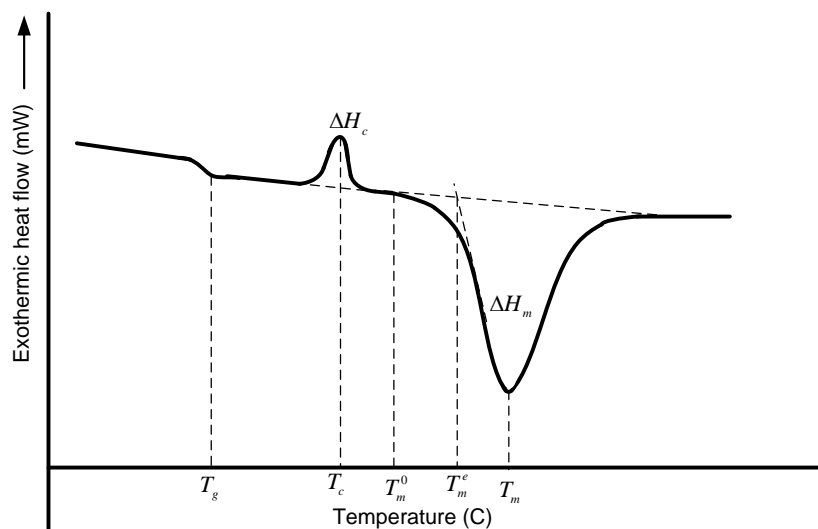
Figure 8: A typical DSC thermogram of a material [95].

2.2.4 Optical Microscopy

Digital images of film surface morphology were captured employing Nikon SMZ-10 A and Lomo MGC-10 optical microscopes and a Nikon Coolpix 995 Digital Camera. Digitized images enabled the dissimilarities in surface features to be magnified allowing for quantitative data and qualitative features to be extracted and utilized for comparison. Because the surface of the film substrate and that of the optical lens exhibited similar optical characteristics proper alignment of filament and condenser was undertaken to ensure proper observation. [96].

2.2.5 Atomic Force Microscopy

The Atomic Force Microscope, model Q-Scope 250 was used to provide three dimensional images of the surface and line profiles to enable height or width measurements. Other quantitative and qualitative data obtained included size,

morphology, surface texture, and roughness. Scans were taken in the range of hundreds of nanometers to provide ideal characterization of nanoparticles.

2.2.6   X-ray diffraction for characterizing crystallinity

X ray diffraction was utilized to differentiate between crystalline and amorphous final structures. Wide-angle x-ray scattering (WAXS) patterns of dopamine and/or HPC samples were obtained using a Bruker HiStar area detector[14].

The samples were prepared by first cutting the droplet area from the HPC film area and centering the ~3mm droplet in the 0.5mm x-ray beam.   For pure dopamine-HCl, a standard 1mm special glass capillary was used.

The Bruker GADDS software (Bruker-AXS, Madison, WI, *General Area Detector Diffraction System v4.1.03,* 2001) was used for data collection and chi integration. Programs WinPLOTR of the *FullProf 2000 Suite Program v1.10* [97] were used for displaying the data.

Materials can be described as crystalline when the molecules and atoms are arranged in a regular pattern which is positioned to the point of a lattice. The smallest volume element which is repetition in three dimensions describes the crystal and is called a unit cell. [95]. There are seven crystal systems, defined by combinations of crystal structures, described in

Table 2. When the incident X-ray beam is sent to a sample having interplanar spacing d of atomic plane, diffraction occurs only if Bragg's Law is fulfilled. The relationship among

interplanar distance, d, incident angle, θ, and wave length, λ, is $n\lambda = 2d\sin\theta$ where n is integers [95].
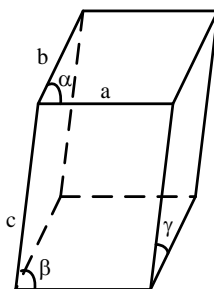
Figure 9: Unit cell

Table 2 : Crystal Systems

Crystal class	Axis system
Cubic	$a = b = c$; $\alpha = \beta = \gamma = 90^0$
Tetragonal	$a = b \neq c$; $\alpha = \beta = \gamma = 90^0$
Hexagonal	$a = b \neq c$; $\alpha = \beta = 90^0$; $\gamma = 120^0$
Rhobohedral	$a = b = c$; $\alpha = \beta = \gamma \neq 90^0$
Orthorhobic	$a \neq b \neq c$; $\alpha = \beta = \gamma = 90^0$
Monoclinic	$a \neq b \neq c$; $\alpha = \gamma = 90^0$; $\beta \neq 90^0$
Triclinic	$a \neq b \neq c$; $\alpha \neq \beta \neq \gamma \neq 90^0$

Data summarized from [98]

In most diffractometers, the X-ray wavelength λ is fixed allowing a family of planes can produce a diffraction peak only at a specific angle 2θ. Here, d is the perpendicular vector drawn from the unit cell to intersect the crystallographic plane[95]. The intensity of the diffraction peaks is determined by the organization of atoms in the whole crystal. The unit cell parameters are determined from the XRD spectrum through identification of the peak locations. Peak intensity areas represent the crystal atoms and the amorphous phase

is characterized by the baseline[95]. Figure 10 shows a schematic diagram of a typical XRD.
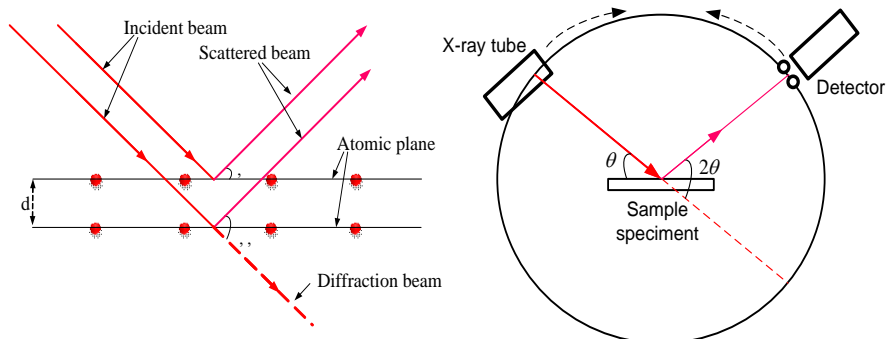
Figure 10: X-ray diffraction on a crystal (left) and the schematic of an X-ray diffraction[95].

2.2.7   USP Dissolution

In-vitro dissolution tests measure the rate and amount of dissolution or drug release from a drug dosage form in an aqueous media. The dissolution test is an important quality control procedure for the drug product and the results are linked to product performance in vivo [99]. The dissolution method used for a particular drug product in-vitro relates to the bioavailability of the drug in vivo. Furthermore, the dissolution method should be able to differentiate between degrees of product performance, changes in drug product formulation, and identify the biopharmaceutical quality of the dosage form [99].

The HP Agilent/ Varian VK 7000 / 7010 Dissolution Apparatus I (See Figure 11) was utilized to determine the dissolution profile for the dopamine solutions printed onto 2% HPC in varying patterns and amorphous or crystalline structure forms.

Dissolution studies were also undertaken for the transdermal dosage forms for nicotine droplets printed onto PE substrates.   Four distinct dosage forms were utilized tested.

These included (1) Traditional transdermal system: Nicotine droplets (no adhesive) printed onto PE, (2) Novel transdermal system: Nicotine droplets with PMMA adhesive printed adjacent to the API, (3) Monolithic transdermal: Nicotine ditartrate embedded in HPC polymer network, and (4) Reservoir Transdermal Drug System: Nicotine deposited onto PE and layered with thin PMMA adhesive. A total of 20 mg of drug was contained within each film for the dissolution studies.
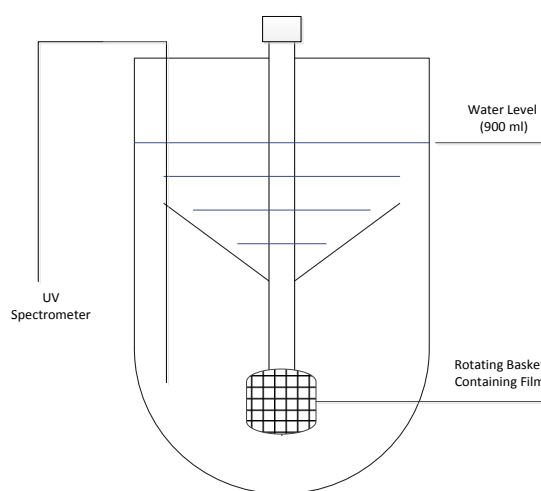
Figure 11: USP Dissolution Apparatus Type I

Additional dissolution studies were performed for a multi-drug transdermal dosage form. Films containing the drugs nicotine ditartrate and haloperidol were analyzed. Each film contained approximately 10 mg of Nicotine and 7.5 mg of haloperidol For all the films the following method was employed: Films were placed into baskets rotating at 250 rpm and lowered into a water bath at a temperature 37 degrees Celsius. The wavelength spectrum was set according to the UV Spectrum of the drugs and sample time point measurements were taken. Table 3 provides specifications about the dissolution experiments.

Drug	Film Size	Total Drug Amount (mg)/film	UV Detection Wavelength	Sample Time Points
Dopamine Hydrochloride	10*10 mm	2.8 mg	285	Every 3 minutes up to 2 hrs
Nicotine Ditartrate	25 *25 mm	10 mg; 20 mg	259	Every 3 minutes up to 24 hrs
Haloperidol	25*25 mm	7.5 mg	230	Every 5 minutes for the first 20 Minutes and every 30 minutes for an additional 2 hrs and 40 minutes

Table 3: Specification for the dissolution experiment

2.2.8   Franz Diffusion Cell Penetration Studies

Franz Cell Diffusion experiments were done to investigate in vitro penetration of nicotine across a PVDF membrane. Transdermal dosage forms were created by printing droplets of nicotine ditartrate onto the PE backing layer measuring 7.5 mm * 7.5 mm. In all experiments the nicotine droplets were deposited in the center of the film. The dosage forms were allowed to dry.   The film was then inverted so that the drug came into direct contact with the transfer membrane when placed onto the bottom area of the donor cell.

Transdermal Dosage Form Franz Diffusion Cell and HPLC Assay	
PVDF Membrane Assay	Formulations (3 each containing 0.5 mg of nicotine)
	Phosphate Buffer
	HPLC Grade Water
	Franz Diffusion Cells (receptor volume 5.1 mL, donor orifice diameter 5mm
HPLC Assay	Varian, Microsorb-MV 100-5 C18, 5μm particle size, 150 * 4.6mm size, column temp: 35°C
	HPLC Vials
	Injection 10μL
	Detection Wavelength : 259
	Mobile Phase A = Phosphate buffer 0.05M (PH=4 adjusted with Phosphoric acid) Mobile Phase B = Acetonitrile Isocratic A:B (50:50)

Table 4: Transdermal Dosage Form Franz Diffusion Cell Assay

Penetration profiles for the Nicotine "patches" was obtained using Franz Diffusion Cells. The amount of Nicotine penetrated was measured at the 2, 4, 6, 8, 10, 12, and 24 hour time points. The assay for the transdermal dosage forms can be seen in Table 4. Three Franz cells were used for each nicotine formulation. At each time point 250μL of receptor fluid was removed for HPLC analysis. The same volume of PBS was placed back into the sample. The date was corrected for drug lost at each sampling point. The sample fluid was stored in glass vials at approximately 4° C for 24 hrs until HPLC analysis. Each experiment was repeated 6 times.

2.2.9   Evaporation and Mass Flux

Weight measurements of drops were taken using an automated Labview program. The user input parameters include environment, measurement release and auto zero. The auto zero resets the scale to '0' the scale prior to each measurement [68].
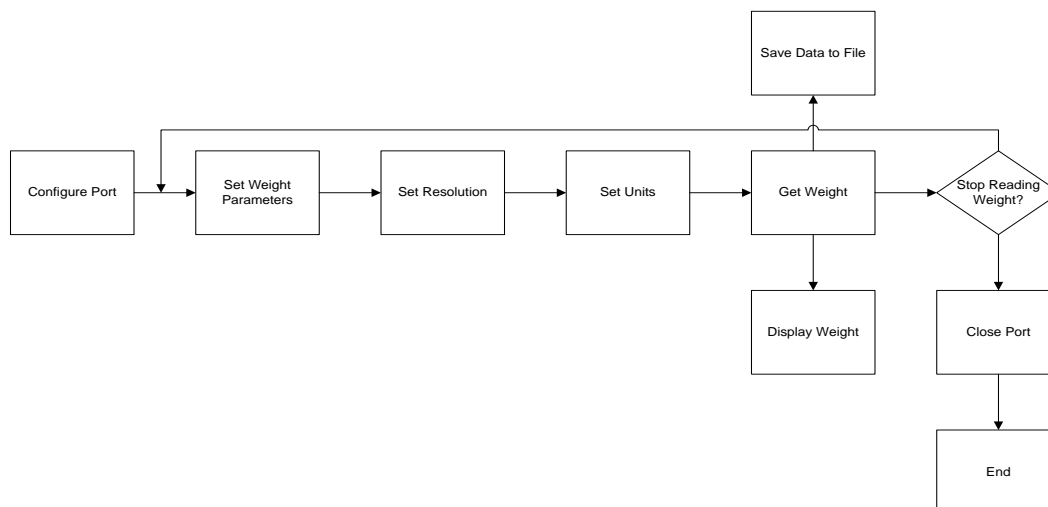
Figure 12 DoD Waveform Design

3 HPC: PEG POLYMER BLENDED FILMS WITH CONTROLLABLE ADHESIVE PROPERTIES

3.1 Utilization of HPC as polymer Film for Dosage Form

The design of a platform for drug delivery utilizing biopolymeric films and drop on demand technology requires intimate knowledge of drug release kinetics, chemical interactions, and adhesion characteristics. The adhesion between the edible film, added components, and the active pharmaceutical ingredient is of primary interest. Adhesion properties can be manipulated to alter the drug type and delivery of the active pharmaceutical ingredient. In particular biopolymeric edible film substrates can be manufactured in manners that enable drop on demand formulation for a variety of pharmaceutical compounds. This encompasses either blister type delivery, where the active compound is manufactured in a batch process and can be dispensed as blister cells, or as an edible film, where the drug is dispersed throughout the surface of the film strip.

Cellulose ethers have been employed in a multitude of drug delivery applications including ophthalmic, transdermal, and controlled delivery applications. In particular hydroxypropyl cellulose (HPC) has been used in rapid release formulation in the gastrointestinal tract due to its ready solubility and lack of interference in drug release profiles [100]. When preparing oral drug delivery systems cellulose ethers have traditionally been utilized in conjunction with plasticizers polyethylene glycol (PEG) or polyvinyl alcohol(PVA) [100]. In these systems, both the solubility parameters of the cellulose derivative and plasticizer [101] are important in determining polymer blend characteristics such as tensile strength, drug loading capacity, bioavailability, and adhesion. Literature reports that HPC values of solubility range from 21.7 – 23.6

$MPa^{1/2}$ [100], indicating greater or equivalent solubility with general cellulose derivatives used in drug formulations including hydroxypropyl methylcellulose, ethyl cellulose, and hydroxypropyl methyl cellulose phthalate [100]. Plasticizers can be added to polymers blends to reduce bitterness, increase strength, tear, toughness, and impact resistance, lower glass transition temperatures and enhance flow [100]. Data has shown that similarities in chemical structure between the polymer and the plasticizer increases plasticizer efficiency [100]. Cellulose derivative which contain large amounts of hydroxyl groups and are water soluble should be used with plasticizers that have similar characteristics such as polyols, polypropyl glycols, glycerol, and polyethylene glycols [100]. HPC and PEG were chosen as polymer blend materials for substrate film fabrication.

Hydroxypropyl cellulose (HPC) and polyethylene glycol (PEG) have been extensively studied as components in edible films and in other food and pharmaceutical technologies [102]. However, little attention has been given to the adhesion surface interactions that exist between substrates (i.e. hydroxypropyl cellulose, polyethylene glycol) and the active pharmaceutical ingredient. Current methodologies of drug delivery employing melts involve dispersing the API in the melt usually through a polymeric matrix. Processing of melts can be difficult due to intrinsic melt characteristics such as viscosity, rheology, shear rate, and temperature dependence and complex interactions observed within melts. This complexity hinders the ability of the end-user to successfully manipulate adhesion properties using small and low cost manufacturing. The design of a DDS utilizing surface properties to control adhesion is more efficient, cost-effective, and can be implemented with fewer complexities as compared to the conventional system of

drug delivery using melts through API dispersion. The objective our work is to identify, analyze, and manipulate adhesion characteristics of mixed polymer blends of HPC and PEG in order to engineer biopolymeric film suitable for use in the design and architecture of a precise dosage formulation utilizing drop on demand technology.

3.2   Theories of Adhesion

Adhesion properties are vital and affect the basic physiochemical nature of the drug delivery system. Molecular factors that can influence adhesion include the hydrophilic regions, molecular weight, cross-linkages, hydrogen bonding, surface tensions, and other functional groups. Theories of adhesion include the physical absorption theory, chemical bonding, diffusion theory, electrostatic theory, mechanical interlocking, and weak boundary layer theories[103, 104]. In our analysis we examined Lifshitz (LW) interactions and capillary forces in the determination of the mechanism of adhesion for our polymer blend substrate.

3.2.1   Physical Adsorption

The physical absorption theory occurs due to attractions between permanent and induced dipoles. These attractions are known as Van der Waals interactions and consist of three types: attraction between two dipoles, attraction between a nonpolar molecule and a dipole, and attractive forces between two nonpolar molecules (also known as dispersion forces) [104]. Van der Waals forces are inversely proportional to the sixth power of the separation distance and are the weakest contributing force to adhesive bonds.

3.2.2   Mechanical Interlocking

Wetting of the surface is necessary for the occurrence of adhesion due to mechanical interlocking. Rough micro and nano scale surfaces containing irregularities and cracks are penetrated by liquid adhesives in mechanical interlocking. The adhesive liquid later solidifies and the two polymer surfaces become interlocked on either sides resulting in mechanical bondage. In examination of mechanical interlocking phenomena capillary forces are considered in the examination of surface irregularities of nanometer scale film [105]. The penetration of liquid into rough pores causes tensile forces that significantly increase the area. The increase in area brings about capillary forces. These forces are the driving force that cause the work of adhesion between the polymers [106]. Equations describing capillarity can be derived from Young-Laplace Equation [106]

$$\Delta P = \gamma \left(\frac{1}{R1} + \frac{1}{R2} \right) = 2\gamma H \qquad (17)$$

,where Δp is the interface pressure differential, γ the surface tension, H is the average curvature. R_1 and R_2 are the radii of curvature. Equation (17) displays the relationship between the pressure difference , the liquid surface tension, and the average radius of curvature [107]. Assuming simple geometry and that R_1 and R_2 are equal we obtain the capillary Equation   (18) relating height of the liquid column to the liquid-air surface tension, and the droplet contact angle.

$$h = \frac{2\gamma \cos\theta}{\rho g r} \qquad (18)$$

, where ρ is the density, g is the gravitational acceleration, r is the pore radius, θ is the contact angle, and γ is the liquid-air surface tension. Equation (18) was utilized to

explore the significance of PEG MW, contact angle, and PEG concentration in film surface morphology and adhesion due to mechanical interlocking.

3.2.3   Work of Adhesion

Luner et al [85] explored the significance of intermolecular interaction and thermodynamic work of adhesion and concluded that, in cellulose ethers, the Lewis-base component play no role in the work of cohesion or total surface energy [85] but instead facilitate in advancing the work of adhesion between substrates [85]. For cellulose ethers, the Van der Waals (LW) interactions serve as the primary contributor to the work of adhesion [85].   From this result the author further surmises that the work of adhesion calculation can be used as an indicator to determine the significance of the acid–base interaction contribution. [85] Work of adhesion, WA, is defined as:

$$W_A = \gamma_1 + \gamma_2 - \gamma_{12} = W_A{}^{LW} + W_B{}^{LW} \tag{19}$$

3.3   Polymer Blend Miscibility

Polymer blends are created by the mixture of polymers with varied chemical structures. The resulting polymer blend mixture possesses different properties midway between the two individual polymer components [108].   Miscible polymers blend due to changes in thermodynamic entropy for which polymers favor increased entropy stemming from polymer chain chaos. In the absence of entropy effects polymer blend miscibility is determined by the equilibrium of small enthalpic and non-configurational entropic effects [109]. The balance that exists between enthalpic and entropic effects is responsible for variations of the polymer blend macromolecular structure.

Miscibility between polymers may only exist for a specific set of conditions or not at all. In the instances of immiscible polymer blends compatibility between polymers is forced through the addition of copolymers. Compatibilization increases dispersion by increasing the total apparent volume, increase interactions between phase, strengthens the interface, and increases the interactions between dispersed drops [109]. The polymer blends viscosity, elasticity, and yield stress increases with the addition of a copolymer. The overall performance of the blended polymer is reliant on the properties of the polymeric components, concentration, spatial arrangement, and morphology. Flow imposed morphology and thermodynamics are responsible for the arrangement of polymeric components in space [109].

In general thermodynamic properties of binary polymer blends may be described by the Flory-Huggins Theory using the binary interaction parameter χ_{12} that is proportional to the interfacial tension of the polymer and solvent, γ_{12} [110]. The theory predicts different material behavior over varying degrees of conditions such as gases, low molecular weight organic liquids, metals, and glassy polymers. χ_{12} is used in the determination of miscibility of materials in polymers and in the computation of the phase diagram of polymer blends. As discussed previously blending and miscibility of polymers are due to changes in entropy. Entropy is interpreted from the change in Gibbs free energy Equation (20)

$$\Delta Gm = RT \left[n_1 \ln \theta_1 + n_2 \ln \theta_2 + n_1 \theta \chi_{12} \right] \tag{20}$$

,where n_1 and n_2 are the number of moles and θ is the volume fraction of components 1 and 2. χ_{12} accounts for the energy of intermingling molecules of the polymer and solvent. R is the universal gas constant. T is the temperature measured in Kelvin. The interaction parameters and interfacial tension enable the calculation of the osmotic pressures used in the prediction of polymer solubility in the solvent

3.4   Surface Morphology

3.4.1   Macroscale

Optical microscopy detailed macro scale morphology and revealed that increased amounts of PEG plasticizer would result in increased irregular surface pores. Figure 13 and Figure 14 show optical images of surface morphology film formed by free casting with increasing concentrations of PEG.
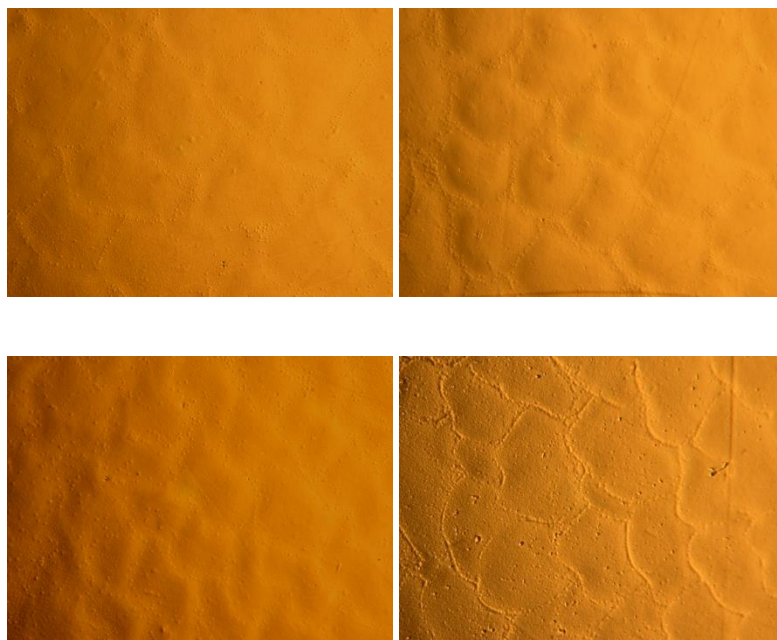
Figure 13 Surface Morphology of Polymer blends on PS support. Peg concentration (A) 1.2% ,(B) 1.35%, (C)1.75%, (D) 2%
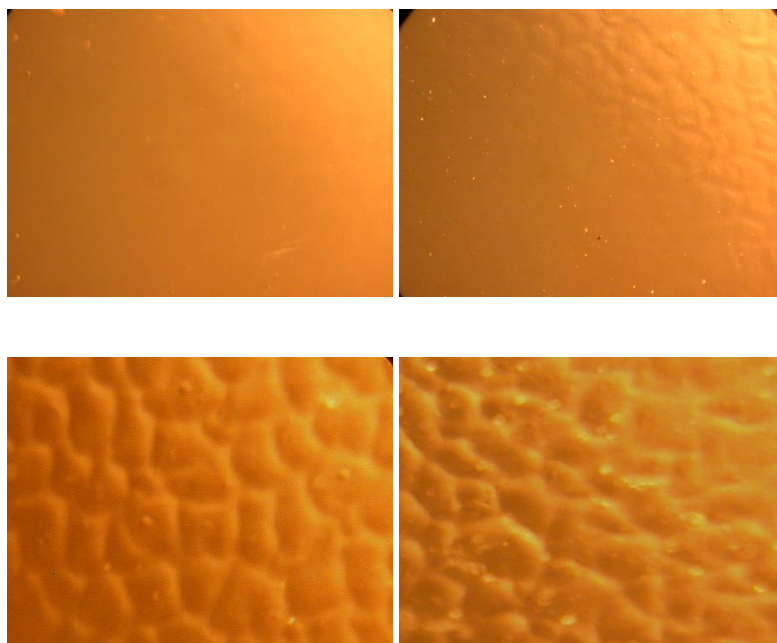
Figure 14 Surface Morphology of Polymer blends on Glass support. Peg concentration (A) 1.2%, (B) 1.35%, (C) 1.75%, (D) 2%

Film composed of very little PEG and .10% HPC by weight result in a very smooth film with no observable grains or irregularities. Increasing the PEG concentration to 1.2% causes slight perturbations in the surface where boundaries start to form. Further increases in PEG volume produce randomly distributed non uniform islands resulting in differences in heterogeneity throughout the film surface. HPC:PEG films experience deformation because the evaporation of the solvent, ethanol, causes the PEG concentration in the polymer to enlarge and polymerization ensues. Polymerization results in stress induced islands caused by the desire of the film to relieve pressure on the surface of the thin films. Macrostructure morphology differed slightly depending on the support material utilized. Films created with Polystyrene (PS) as a support formed grains that appeared to be more flat. Glass supported films formed grains that were greater in height with more defined barriers. The difference in heterogeneity observed is attributed to the fact the polystyrene and PEG have low miscibility with each other as compared to

PEG and glass. Contact angle goniometry and subsequent surface energy computation show that interaction energies between the PS and PEG are less than that of the PS and Glass. As a result clustering of independent monomers occurs [111] on glass support because interaction energies between electrostatic interactions are greater.

3.4.2   Microscale

Micro scale investigation of film morphology for spin coated film was conducted utilizing AFM analysis. Spin coated films were created on glass support with varying concentrations of added plasticizer. The amount of irregular pores was found to increase with increasing concentration of PEG. Lower PEG concentration decreased the diameter size of the pore while greater PEG concentration increased pore size. The increased amount of irregular pores observed with the addition of PEG is due to the interference of the PEG with the evaporation of ethanol. Spontaneous deformation occurs when the surface of a thin film becomes unstable due to pressure increases and increases in local film thickness [112]. For thin films deformation and pore formation can occur due to (1) true ruptures in the film leading to the formation of cylindrical dry spots on the surface and (2) saturation of the initial instability [112]. AFM Images and pore size distribution of the polymer film is shown in

Figure 15.
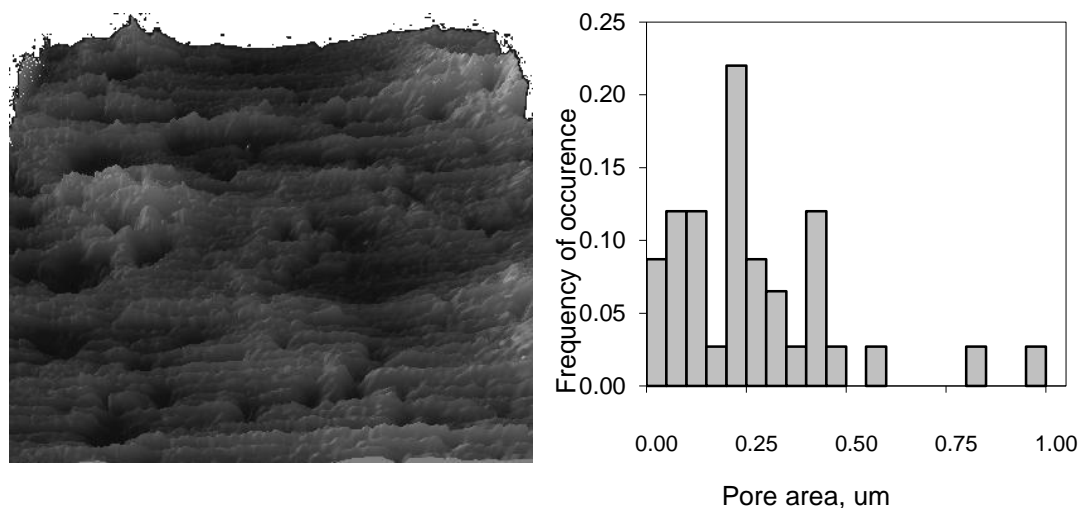
Figure 15: Histogram of Pore Size Distribution

Pore distribution analysis provides data that the irregularities are not uniform. Pore diameters range in size from 0.01 to $1.0\,\mu m^2$. The average are of pores appears to be approximately $0.35\,\mu m^2$ with the majority of the pore having an area of $0.2\,\mu m^2$. As observed by the image larger pore sizes are observed but at much lower frequencies. To correct for the problems of non-heterogeneity and film deformation, Iyer et al propose introduction of an elastomeric interlayer to reduce deformation resulting from differences in thermal expansion and stress [113].

3.5   Work of Adhesion and Surface Energy Components

Surface energy component values were completed using initial contact angle quantities obtained using the sessile drop technique with implementation of axisymmetric drop shape analysis method. Initial contact angles of probe test liquids diiodomethane, distilled water, and ethylene glycol, were obtained for varying blends of HPC:PEG substrate thin film. Distilled water and ethylene glycol contact angles generally decreased with

increasing PEG concentration; however at higher concentrations of PEG (135 μ L of PEG) the observed contact angle of ethylene glycol on polymer film suddenly increased in value by 179%. Distilled water, at 135 μ L of additional PEG into the film composition, also experienced an increase of approximately 165% in contact angle measurement. Diiodomethane generally experienced increases in contact angle with increasing PEG concentration with minor fluctuation. Contact angles of ethylene glycol and distilled water remained relatively close in value and the greatest difference in contact angles were observed according to $C_2H_6O_2$ ($\theta = 23.255$) > H_2O ($\theta = 22.435$) > CH_2I_2 ($\theta = 20.46$) implying that both the polar and dispersal elements of the surface energy are similarly affected by increases in PEG volume [114, 115].

A more robust and quantitative analysis of the substrate polymer blends was done utilizing Van Oss methods to calculate surface energy components. Fig 16 details the surface energy components of polymer blend substrate films.
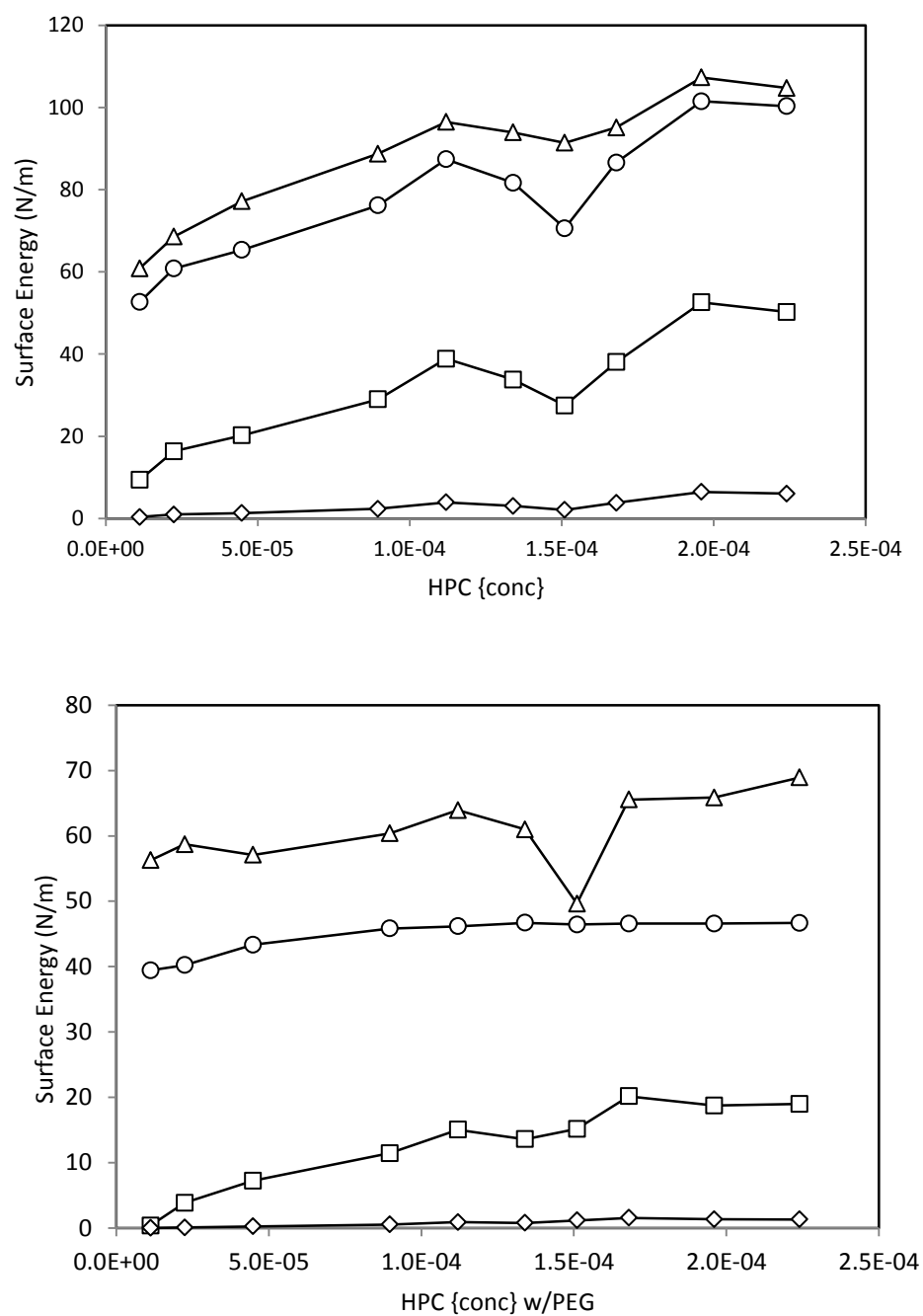
Fig 16 Surface energy components of parameters of polymer and polymers blend films Δ ○ □ ◇

With increasing volume fraction of PEG the overall surface energy γ_S remains relatively constant, increasing from approximately 39.42 mJ/m^2 to 46.67 mJ/m^2. Established literature reports surface energy values of HPC to be approximately 39-43 mJ/m^2 [116]. The Lifshitz - Van der Waals (LW) forces decreases from 39.08 mJ/m^2 to 27.05 mJ/m^2. In general the total Lewis Acid Base (AB) energies increase significantly from 0.3493 mJ/m^2 to 18.96 mJ/m^2. The positive component of AB ($\gamma+$) remains near constant and contributes little to the overall increase in AB forces. The negative AB($\gamma-$) component generally increases with increasing peg concentration; however at 135 μL of added PEG, the surface energy of the film decrease sharply. AB (negative component) surface energy is a measurement of the concentration of surface ether groups and decreases indicate a decrease in the hydrophilicity. Finite values of $\gamma+$ and $\gamma-$ indicate residual surface water present due to partial drying [85].

Important relationships are observed between the Lewis Acid Base forces and the Lifshitz Van der Waals forces. The graphs of these two components appear to be near non superimposable mirror images of each other with the distinction of compensating for each other during increases in PEG polymer concentration. These findings are in agreement with established data that report cellulose polymer films solubilized in water exhibit predominately electron-donicity [85] but diverge from the theory that the LW forces contribute the majority toward surface free energy while AB forces contribute only 5-10 % [85]. Literature reports that the γ LW forces are higher, as compared to other surface energy components, indicating that γ LW dominates the totals surface free energy of cellulose ethers [117]. In our study it was found that initially at low

concentration of PEG , AB forces were much smaller than LW force components; however, as the PEG concentration increases, the contribution of the LW forces declines while the contribution of the AB forces increase. It is likely that the addition of PEG as a plasticizer interferes with the internal molecular interactions between the electron donating and electron accepting sites [85]. HPC: PEG films solubilized in ethanol exhibit low energy with dominant forces changing from LW towards AB with increasing PEG volume. These findings suggest the LW forces are initially significant in the determination of adhesive properties. The addition of plasticizer PEG to the film solution results in significant increases in AB forces and suggests that in HPC:PEG blends AB interactions play a dominant role in advancing the work of adhesion[85]..

3.6   Thermal Analysis of HPC:PEG Films

Differential scanning calorimetry (DSC) analysis was performed using the Perkin Elmer DSC 7.. Experimental parameters included the following: sample weight: 10 mg of film substrate, 10 mg of polyethylene glycol 3350, 10 mg of hydroxypropyl cellulose, heating rate: 10 ºC/min, atmosphere: nitrogen. The samples were heated to 100 ºC to observe phase transitions of the HPC:PEG substrate. Figure 17 demonstrates the DSC curves of HPC, PEG MW400, and HPC:PEG (1:1 weight percentage ratio) substrate. Figure 18 displays DSC analysis of pure PEG of MW 1000, 1450, 1500 and 3350. The DSC results showed that the melting points for the virgin HPC, PEG MW 3350, and HPC:PEG substrate differed greatly. HPC powder, without the addition of plasticizers revealed a melting point greater than 100ºCSubstrate film HPC:PEG MW400 reflected a melting

point of approximately 100 °C. PEG MW 3350 began to melt at 41 °C.   Crystallization

for all substance was observed near 2 °C.
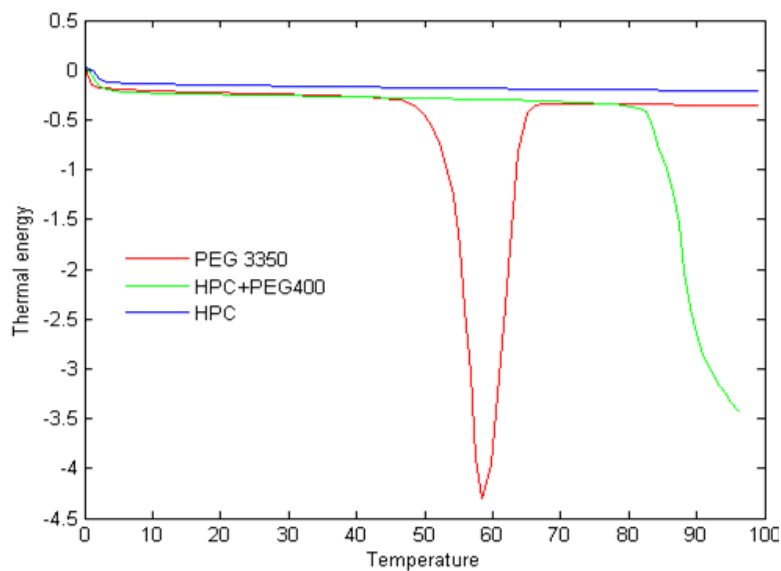
Figure 17 DSC Plot of PEG, HPC, and polymer blend
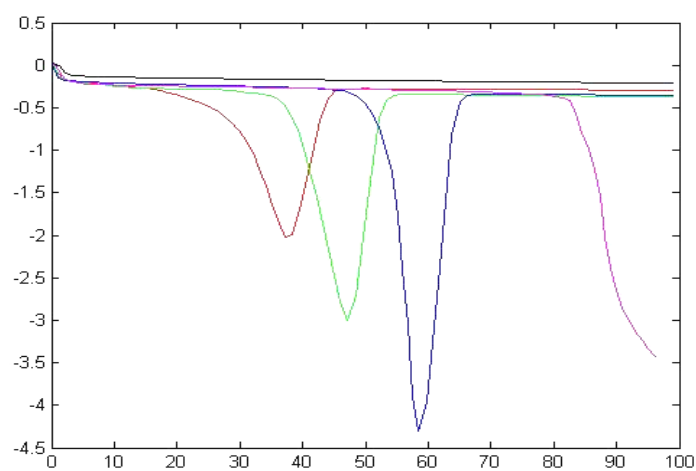
Figure 18 DSC analysis of PEG MW 1000, 1500, and 3350

3.7   Temperature Effects on Thin HPC Film

Hydroxypropyl cellulose (HPC) forms liquid crystal structures when immersed in water solutions. The behavior and characteristics of the solution are strongly dependent upon the lyotrophic nature of the cellulosic crystals [118]. In bulk solutions of HPC a liquid crystal mesophase is formed consisting of ordered crystal molecules that are capable of fluid flow. These properties give liquid crystals unique behaviors observed at the outermost boundaries of interfaces or surfaces [119] and are significantly important in creation of polymer blend thin films.

Due to the complex morphology of HPC as a liquid crystal thermal characteristics have been studied to understand the effect temperature will have on HPC film. Contact angles of PEG MW1000 were obtained in a temperature regulated environment. PEG MW1000 was placed onto a thin film coating of polymer HPC and a glass support using the sessile drop technique. The relationship observed is displayed in   Figure   19:   Variation   of Contact Angle of Printed PEG 1000 droplets on glass ($\triangle$) and HPC ($\bigcirc$) substrates as function of the temperature. Contact angles of PEG MW1000 on glass and on the HPC film decreased with increasing temperature.
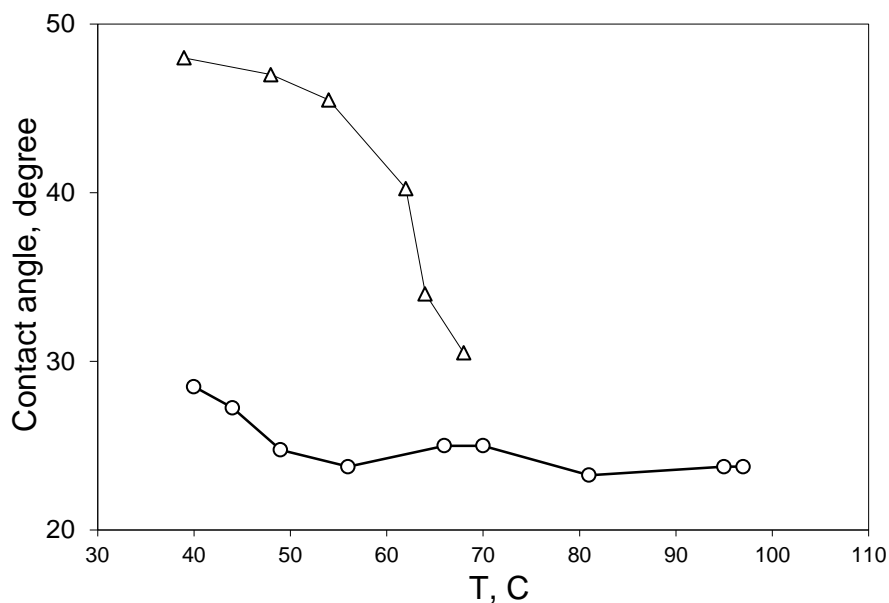
Figure 19: Variation of Contact Angle of Printed PEG 1000 droplets on glass (△) and HPC (○) substrates as function of the temperature

From the chart we observe that contact angles of PEG 1000 on HPC films were initially 20 ° smaller than those for glass substrate. The plateaus observed indicate the point at which the glass support and HPC film substrate underwent phase transition. At this point the thermal energy supplied to the system melts the polymer and; therefore, the temperature of the entire system remains steady. Without a change in temperature the observed contact angles remained relatively steady. At the point in which phase transition is complete the heat flow is increased and contact angle measurements drop according. In addition DSC analysis shows that PEG undergoes melting at approximately 43 °C. Surface tension analysis shows that with the exception of van der Waal forces surface energy components increases with increasing Peg concentration. Van der Waal forces result in spontaneous dewetting in thin films and as the presence of these forces is decreased the film resists destabilization. Increasing the temperature resulted in

increased miscibility and a decrease in the probability of phase segregation due to spinodal decomposition.

3.8   HPC:PEG Film Stability

Stability of evaporating thin films is challenging due to the coupling between heat transfer, mass diffusion, dynamics, and its inherent non steady state [120]. Non-equilibrium thin films on material support can undergo complete rupture with the emergence of a three phase contact line or undergo morphological phase separation [121]. Thick and thin films were formed from free casting and spin coating techniques. Film was placed on either glass or polystyrene (PS) for support material. Films formed on PS were thicker than those formed on glass and did not exhibit a phase separation between the HPC and PEG polymers. Film placed on glass substrates formed through free casting techniques was found to be highly unstable. After a period of approximately 24 hours phase separation was observed. Larger concentration of initial PEG volume resulted in larger structures formed during morphological phase separation. Figure 20

displays an example of morphological phase separation. The top images are 1% PEG concentration on PS and glass respectively. The bottom images are 2% PEG concentration on PS and glass.
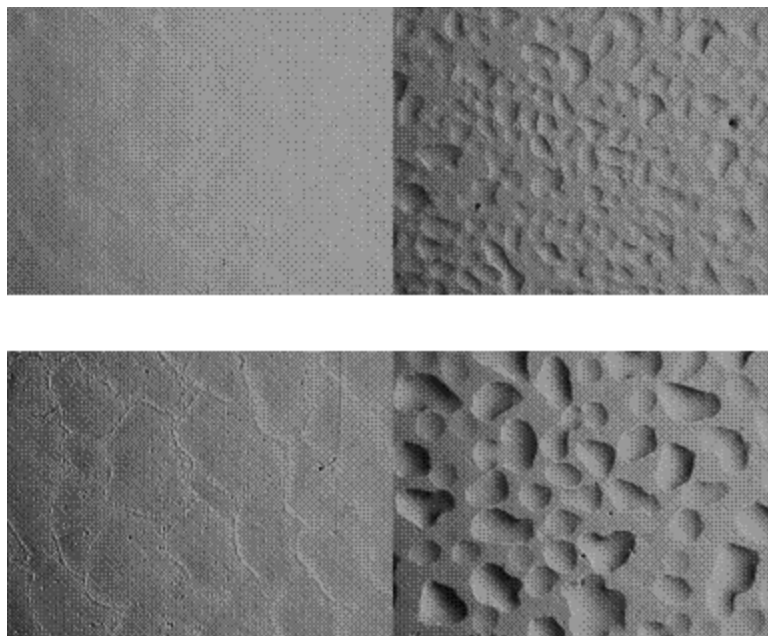
Figure 20: Breakdown of casted polymer blend film stability on PS and glass support

Film stability is dependent on the support material as well as the composition of the polymer blend film. Films with increasing volumes of PEG content were more likely to initially resist destabilization resulting in slower phase separation with larger morphological structures. Sakellariou and coworkers [100] reported that the concentration of the plasticizer directly affects the plasticizing efficiency. He also observed the movement of the plasticizer to the film surface when PEG_{400} content in HPMC films exceeded 15% by weight [100]. The energy created from stress arising from tension among surface energy components is large and if the support (glass in our systems) and the polymer substrate (HPC thin film) have sufficient wettability, phase segregation will occur. Obtained data indicate that initial contact angle measurements of PEG taken on glass support were generally lower than those taken on HPC film substrate for PEG 400. This finding supports the theory that glass and PEG400 exhibit greater

affinity and underscores the significance of miscibility in phase segregation and strength of adhesion between the polymer blend substrate and other polymers.

A homogeneous, stable binary mixture can undergo phase separation when quenched from a stable one-phase system to an a region of thermodynamic instability below the coexistence curve on the phase diagram [122]. Phase decomposition occurs due to the mechanism of long range diffusion [123]. If the mixture is quenched into a metastable region, nucleational growth will occur [123]. In the case where there is a preferential segregation of one element over the other, infinite fluctuations can occur in the composition field and the decomposition occurs without the nucleation barrier [122, 123]. The separation of the two immiscible phases is described by the Cahn-Hilliard equation [124]

$$\frac{\partial \varphi}{\partial t} = \nabla \frac{\alpha \lambda}{\varepsilon^2} \nabla \Psi \tag{21}$$

where φ is the phase field variable, the volume fractions of the components of the fluid are $(1+\varphi)/2$ and $(1-\varphi)/2$. The variable α is the mobility, λ is the mixing energy density, and ε is the capillary width [125].

The capillary length ε and energy density λ can be used to define the surface tension:

$$\gamma = \frac{\sqrt{8}}{3} \frac{\lambda}{\varepsilon} \tag{22}$$

A governing equation for Ψ function can be written in the form:

$$\Psi = -\nabla \varepsilon^2 \nabla \varphi + (\varphi^2 - 1)\varphi \tag{23}$$

The components are represented by a phase field function φ, and are considered pure when $\varphi = \pm 1$. The initial mixture is created by putting φ equal to a random number with zero mean and a standard deviation of 0.05. The initial random perturbation initiates the separation into pure phases.

A contact angle is imposed on the boundaries and this was the only variable used in simulation. Figure 21 shows the evolution of the phase field variable representing phase separation.

A
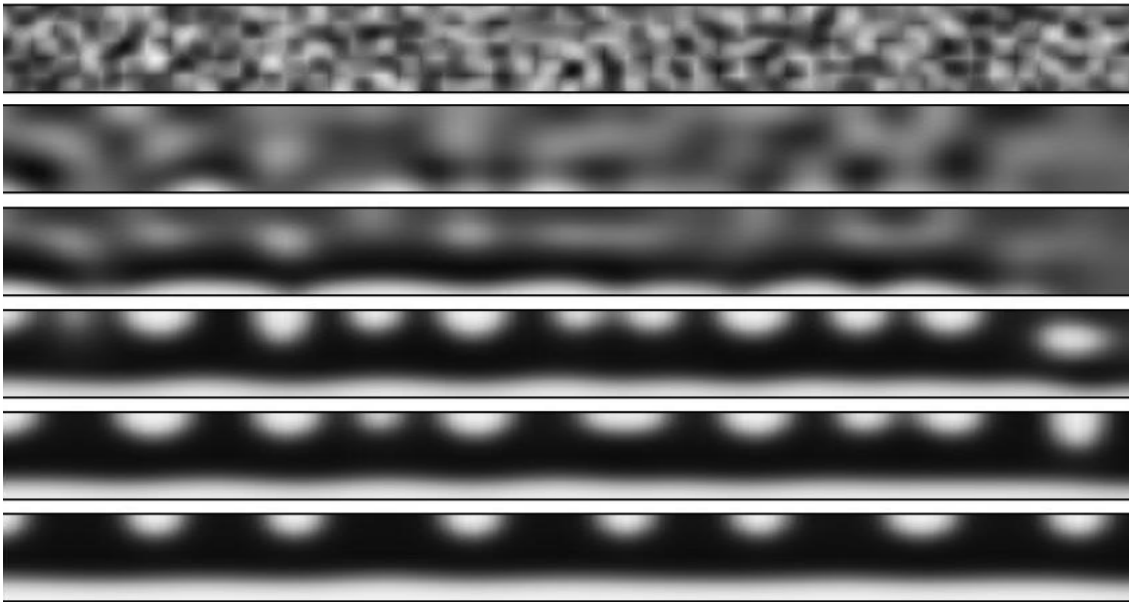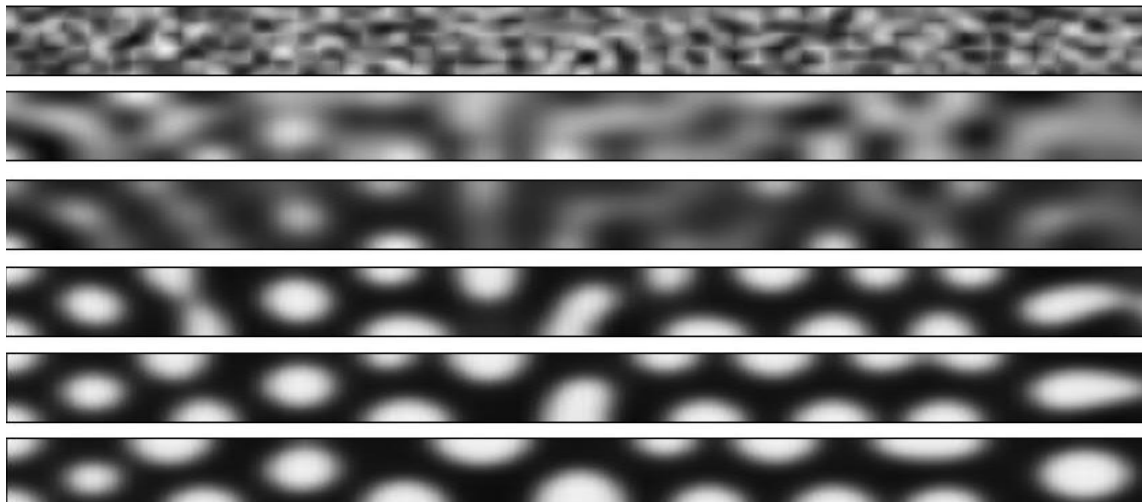
Figure 21: Plot of phase field variable at different time steps. The two fluids tend to separate into distinct phases.

Initially, the two phases are completely mixed except for a random perturbation around φ = 0 . By t = 4 the phases have started to separate. At t = 20, pure phases have started to form, and two seconds later only pure phases exist. After t = 40, the pure phases begin to coalesce to form large phase domains

3.9 Lateral Force Adhesion

Smooth films without observed spinodal decomposition exhibit very good adhesive properties. Even cleavage of the deposited and solidified droplet does not cause detachment. Films on the glass substrate that are subject or more likely to undergo spinodal decomposition (see Figure 22: Printed PEG 3350 droplets on (A) PS substrate and (B)) have much weaker ability to hold printed PEG droplets despite high affinity towards deposited material. As clearly seen in Figure 22: Printed PEG 3350 droplets on (A) PS substrate and (B) solidified droplets delaminate due to surface inhomogeneity caused as result of phase separation.
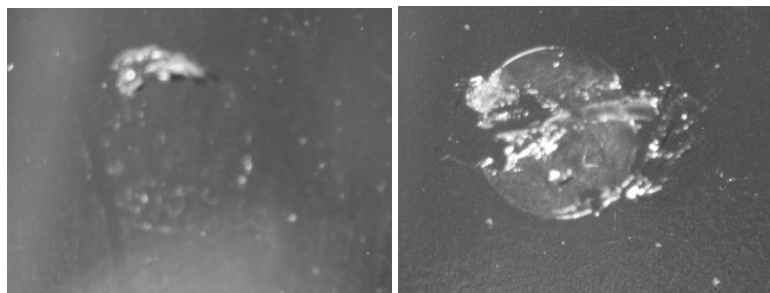
Figure 22: Printed PEG 3350 droplets on (A) PS substrate and (B) Glass

Adhesion strength of polymer blend films was determined using modified lateral force adhesion test [126]. Droplets of melted PEG were placed onto the thin polymer films and allowed to solidify.   The droplets were then moved through constant lateral force and the distance moved was measured. PEG3350 droplets placed onto film blends of PEG400 and HPC bonded with the film and were difficult to move through lateral force. Increased force was necessary to move the droplet and as the PEG concentration in the film increased the bond strength between the film and the droplet increased accordingly. In samples containing greater than 100 µL of PEG the droplets were unable to be moved without destruction of the sample. At lower concentrations of liquid PEG in the film adhesion was very weak and the solidified PEG_{3350} droplet could be moved with force and little or no destruction of the substrate film. At higher concentrations the PEG droplet required greater force to be moved and destruction of both the sample and the film were observed.

As an example of the applicability of the HPC:PEG films for the development of new dosage forms via drop-on-demand technology we have printed several pharmaceutical

formulations in form of melt consisting of drug and excipient (PEG_{3350}) mixture. Results are presented in Figure 23.
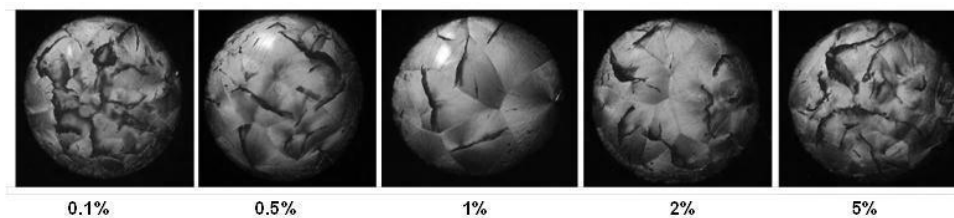
Figure 23: Printed griseofulvin:PEG droplets onto HPC:PEG substrate.

4 EFFECT OF SUBSTRATE SURFACE ENERGY ON DROPLET EVAPORATION, SPREADING, AND MORPHOLOGY

4.1 Solidification

Solidification phenomena are significantly vital in many industrial processes, including material science, chemical, and pharmaceutical industries. Physical and chemical properties are determined by solidification growth and the properties of the final solidified material. In order to sufficiently manufacture materials, i.e. soft drug delivery devices, it is important to gain fundamental comprehension of solidification processes as to predict and manipulate interfacial dynamics. Solidification of pure unmixed substances grows at a rate determined by the diffusion of latent heat released at the solid/liquid interface. The growth rate of mixed substances is controlled by heat and solute diffusion [110, 127].

In liquid form the atomic motion is randomly disordered. As the energy in the liquid system decreases toward the freezing point movement of atoms is restricted enabling increased probability of atoms to form lattices. At the freezing point kinetic energy of the liquid and solid state are the same; however there exists a potential difference due to distance between atoms. This potential between solid matter and liquid matter is the latent heat of fusion.

Solidification progression entails solidification, crystallization, and nucleation growth. Crystallization is the point at which liquid material undergoes transition to the solid state. In order for crystal growth to begin nucleation must occur prior. Nucleation is the onset of phase transition in a small distinct region of the material and it occurs if the material

exists at a point sufficiently below the freezing point or, for non-pure substances, when the concentration of a solute in a solvent exceeds its equilibrium solubility. During nucleation nuclei appear spontaneously throughout the liquid. As time progresses and the temperature continues to fall nuclei continue to spontaneously occur and grow. A nucleation site that has become fully solidified is referred to as a crystal or grain. Crystal growth continues and new and existing crystals begin to attach themselves to each other due to attraction of atoms from the liquid into the lattice space. Solidification of the material occurs at the point where all crystals have completed growth and maintained boundaries. [128, 129] The rate and manner at which the material solidifies is specific to material type and environmental factors [128].

The solidification of pure substances conducted through mathematical phase field models demonstrate that the model equations reduce to the free boundary equations when the width of the boundary decreases to zero [127]. Interface growth velocity is determined by Δ which can be calculated by

$$\Delta = c_p (T_m - T_\infty) / L \tag{24}$$

, where cp is the specific heat, T_∞ is temperature and T_m is the equilibrium melting temperature; L is the latent heat of fusion.

4.2 Substrate Surface Analysis

Substrate film was prepared and composed of the pharmaceutically relevant compounds HPC and HPMC. Film concentrations of 0.0975% HPC and HPMC, 2% HPC, and 5%

HPC were created. Glass was also used as a substrate for droplet deposition. Increases in concentration resulted in film with increased thickness and irregularities.
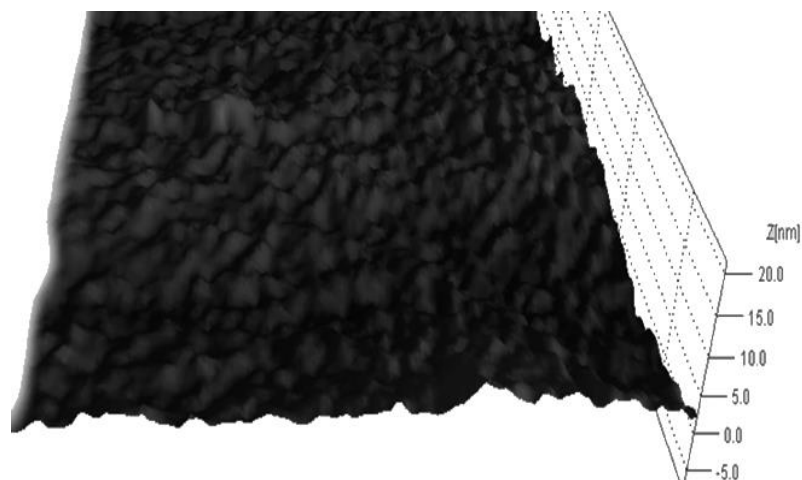
Figure 24: AFM of 5% HPC Film

Atomic Force Microscopy details the differences in surface roughness for 5% HPC film and glass. As expected, the 5% film appears rough, inconsistent, and porous. Glass has a more uniform smooth look as compared to that of HPC film.
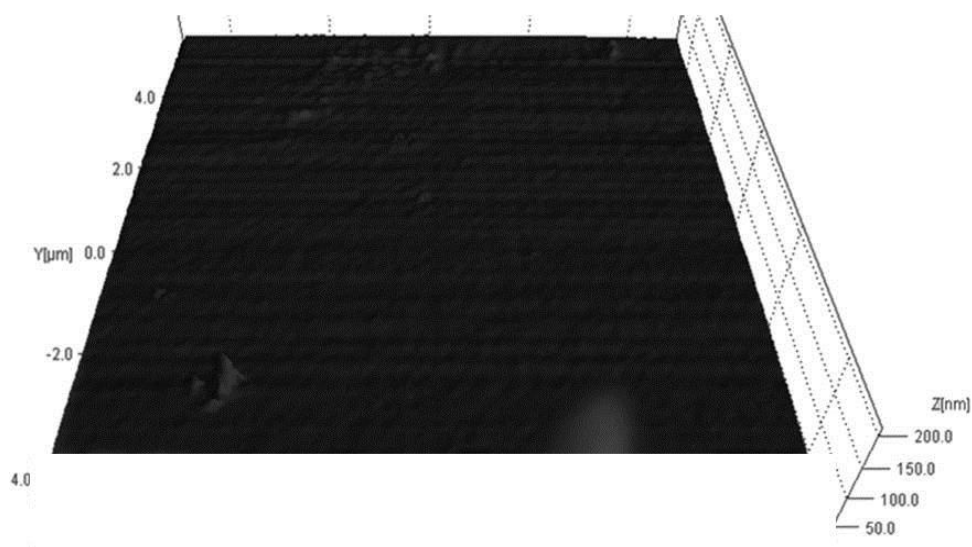
Figure 25: AFM of Glass Slide

4.3   Wetting Behavior

After a drop is deposited on a on a solid substrate [130] the behavior of the drop is determined by inertial, viscous, and surface forces [131]. Vital parameters include initial droplet radius, properties of the API solution, roughness and contamination of the substrate film, and impact velocity [131, 132]. In general, after the drop impacts the solid surface spreading occurs. The kinetic energy of the drop dissipates to overcome viscous forces and to create new surface area [132]. The surface tension of the substrate counters the dispersal of the drops and acts at the interfaces initiating recoiling [133]. Drop height decreases due to inertial flow until the point where all the kinetic energy is converted into potential energy [128, 131].

To investigate the solidification of dopamine hydrochloride, droplets were deposited onto solid substrates. Experiments conducted provided evaporation rates for dopamine on substrates with varying wettability. It was found that substrates with increased wettability had higher surface energy and resulted in droplet evaporation that occurred more rapidly. Research has shown that upon drop deposition a thin liquid film forms and its behavioral properties are determined by surface tension forces [134, 135]. The wetting phenomena is an important factor in the determination of the spreading of the film, and ultimately in the solidification and possibility of crystallization of the film.

Initial wetting phenomena indicate important details about substrate surface energy but dynamic and kinetic changes during evaporation affect the solidification of the droplet

and the adhesion between drug and substrate [30, 136, 137]. It is generally accepted that sessile drops of liquid disappear due to evaporation flux over its exposed liquid vapor surface. This evaporation leads to shrinking of the drop and a decreasing contact radius and height. However; during evaporation, Bourges-Monnie et al found that an increased evaporation rate exists near the contact line and phenomena related to wetting hysteresis resulting in deviation from the Young equilibrium contact angle contribute to kinetic changes of the triple line [138].

At some point during the evaporation it appears that the contact angle line becomes pinned or stuck. During this phase evaporation continues and contact angle and height decreases but the base radius remains constant. After pinning the drop recedes resulting in an actual increase in height and contact angle towards the equilibrium value. During this phase the base radius of the drop decreases. Sticking and receding of the drop continue throughout the evaporation process [138].

In addition to the slip-stick phenomena, we also observed a complex between the dopamine and the hydroxypropyl cellulose substrate. This complex altered the behavior of the drug during evaporation and solidification. We explain this behavior in three stages: Initial, Secondary, and Tertiary.

Initial stage

 Dopamine exists in solution until a concentration of approximately 0.6 g/ml. At and above this concentration dopamine is not soluble in water.

Second Stage

Evaporation of the sessile drop in dry air occurs due to a concentration gradient between the surrounding air and the drop. The basic processes involved in evaporation include (1) diffusion liquid molecules from the drop surface into the surrounding environment and (2) flow of the liquid molecules from inside of the drop to the exterior of the drop's surface [139]. The evaporation of water from the drop and the convection of the liquid molecules results in layers rich in dopamine. The dopamine molecules migrate toward the bottom of the drop toward the substrate surface driven by Van der Waal forces. Adsorption of the dopamine onto the surface of the molecules occurs due to the attractive forces between the hydrophobic regions of the substrate and the dopamine receptors.

The Langmuir Adsorption Theory explains that the rate of attachment to a surface is proportional to concentration of the API in the fluid multiplied by a surface area. The amount of dopamine molecules that will attach to the film's surface can be explained through the Langmuir Theory:

$$\varepsilon = \frac{\alpha C}{1 + \alpha C} \tag{25}$$

ε : Fractional surface covered, α : Langmuir adsorption constant and C : Concentration .

Additionally, the adsorption of any molecule onto a solid substrate can be further explained by van der Waals interactions and the Hamaker Theory which describes the interactions between two molecules.

Third Stage

In addition to the diffusive and hydrodynamic regimes the dopamine droplet deposited onto the film substrate HPC exhibited complex 'viscoelastic phase behavior' similar to a

"transient gel" [140]. Here the domain morphology is dependent on the elastic force balance [141-143]. This transient gel is so defined because the network exists where the deformation rate of the volume is faster than the stress relaxation rate [140, 143].

A transitory polymer network is formed by strong attractive interactions [140]. It is thought that this network is formed by the strong dopamine self-polymerization that involves the oxidation of molecules and the subsequent polymerization of comparable compounds [144]. In poor solvent conditions this network shrinks causing the interaction energy to lower. This is the driving force for the phase separation. In a transient gel polymer network, the connectivity prevents shrinking and generates mechanical stresses [143, 144].

4.4 Droplet Evaporation

While the initial contact line is important in determining surface energies and wetting phenomena, a sessile drop undergoing evaporation and changes in its geometry due to mass loss, significantly contribute to final drop structure and API migration. Figure 26 shows the progression of the contact radius, R, with time t, for dopamine hydrochloride drops of volume 20 nL on the substrates of glass, HPC, and HPMC. Figure 27 displays the optical images of droplet changes over time. Drops that were deposited onto hydrophobic substrates, i.e., 2% and 5 % HPC, exhibited initial contact angle values greater than 65 degrees and an increased drop base radius. Drops deposited onto slightly hydrophobic substrates experienced contact angles ranging from 30-45 degrees and smaller base radii as compared to hydrophobic surfaces. Drop deposition onto hydrophilic surfaces resulted in contact angles less than 30 degrees and had the smallest

drop base radius. As expected the evaporation rate of the drops appeared to be linear regardless of the surface type; however, the rate at which evaporation occurred was substrate dependent. While not completely understood, simple linear prediction models explaining the dependence between time and contact angle indicate that evaporation rates for drops deposited on 5% HPC, 2% HPC, and 0.0975% HPMC are $2.53*10^{-2} \frac{\deg}{\sec}$, $2.39*10^{-2} \frac{\deg}{\sec}$ and $2.37*10^{-2} \frac{\deg}{\sec}$ respectively. Drops deposited on 0.0975 % HPC evaporated at a rate of $1.56*10^{-2} \frac{\deg}{\sec}$. The rate of decrease may be obscured due to receding and pinning of the triple line during evaporation; particularly for higher hydrophobic substrates. Dopamine drops on hydrophobic surfaces resulted in a substrate: drug complex which altered the triple line. In addition it was found that for hydrophobic surfaces the initial contact angle remains relatively constant for a time period of t <1000 seconds and then decreases rapidly. For this reason it is proposed that the evaporation involves complex processes and a simple linear model cannot be used to predict evaporation rates.

In addition to hydrophobic dynamics, we found that humidity conditions also affect the evaporation rate of an API droplet. As visible from the evaporation images in Figure 27 and Figure 26 displaying the base radius evolution as a function of time, drops deposited onto HPC at humidity levels between 20-30% was $1.56*10^{-2} \frac{\deg}{\sec}$. At higher humidity levels, between 60-70%, the rate of evaporation decreased to $9.4*10^{-3} \frac{\deg}{\sec}$. To correct

for this humidity factor care was taken to ensure that the evaporation experiments were conducted at humidity levels between 20-30%.
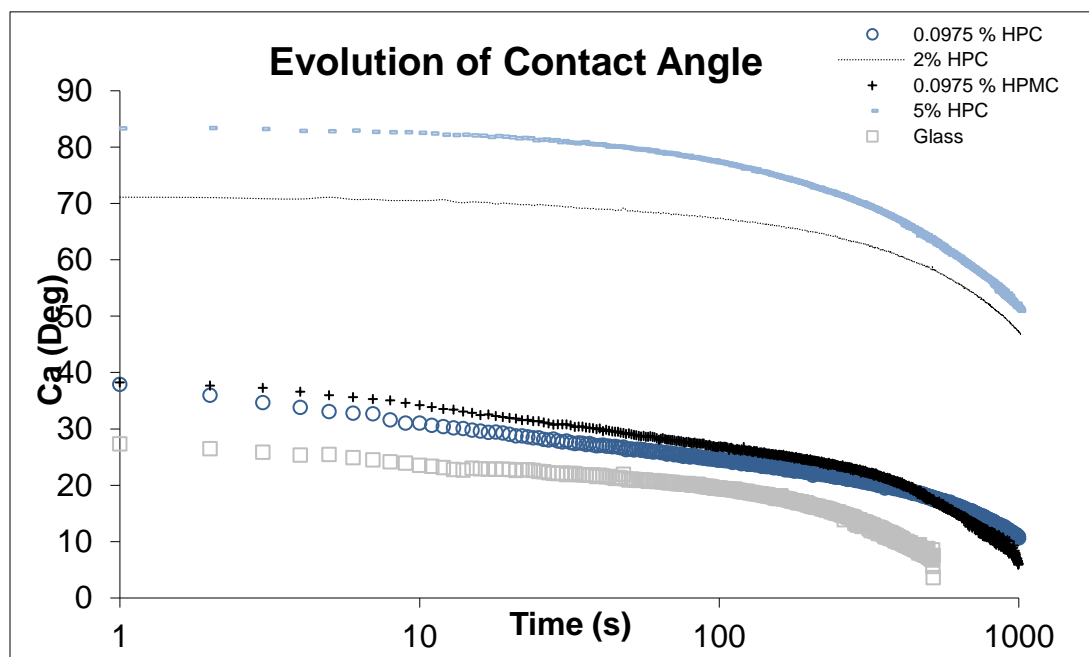

Figure 26: Evolution of Contact Angle on Varying Substrates
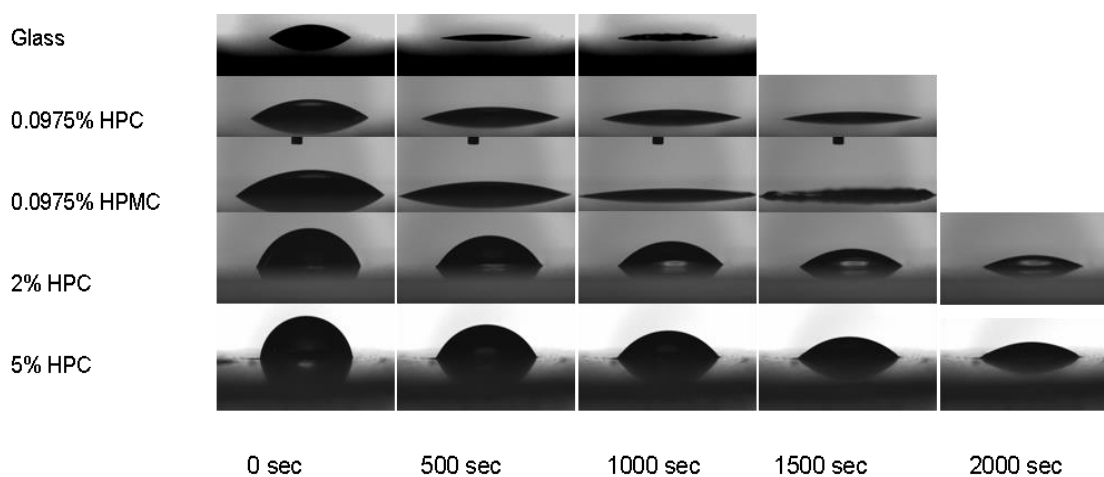
Figure 27: Optical Images of a profile of evaporating drops on hydrophilic and hydrophobic substrates

Figure 28 shows top-down images of dopamine droplets were taken during its evaporation process on 5% HPC and glass. On 5% HPC the images clearly show the

progression of the drop geometry from a spherical droplet with increased height to a flat splat with raised thick ridges existing on the boundaries of the drop. The droplet deposited onto glass undergoes a transition from a liquid droplet to an intermediate crystalline structure rapidly. The droplet remains in liquid form for approximately 1 minute, nucleation occurs spontaneously, and within an additional 5 seconds crystallization is complete. It should also be noted that total evaporation times for the solidification process are dependent on properties of the wettable substrate. On 5% HPC the solidification process takes approximately 7 minutes and on 2% HPC solidification of a dopamine droplet, of the same volume, takes little more than 1 minute.

Many of the differences observed between solidification processes on hydrophilic and hydrophobic surfaces can be explained by analysis of triple line motion and evaporation kinetics. In the top down images of solidification (Figure 30) and the plot profiles (Figure 29) we note that the intensity level for a specific area on the drop decreases with increases in time. We also note that at a time above 210 seconds the plot profiles seem similar despite the continuance of solvent evaporation. Two phenomena for this behavior are explained. Firstly, evaporation on hydrophilic and hydrophobic surfaces occurs differently. As evidenced in the images, evaporation on hydrophilic surfaces occurs linearly due to a constant evaporation flux over the exposed liquid/vapor surface. Printing on hydrophobic surfaces induces phase separation and evaporation on in two stages. The first stage involves evaporation of solvent from the edges and the formation of a thick ridge of concentrated dopamine around the periphery of the drop. The second stage involves the continuous evaporation of the solvent in the center of the drop with the exclusion of dopamine. The second phenomenon observed is the pinning and later

sticking of the triple line. Initially evaporation occurs from the edges and due to the migration and dense concentration of dopamine in this layer ridges occur. The triple line is now fixed and does not later recede; although, evaporation of the solvent continues.

A third contributor to the final shape and structure of the splat is the possibility of interaction between the dopamine and the HPC film. Studies show that on hydrophobic surfaces a complex exists between molecules of similar lipophilicity and these molecules are attracted to each other. In our experiment, it is likely that hydrophobic molecules in the dopamine attached to hydrophobic molecules in the HPC creating an enriched dopamine layer at the base and around the edges of the splat.
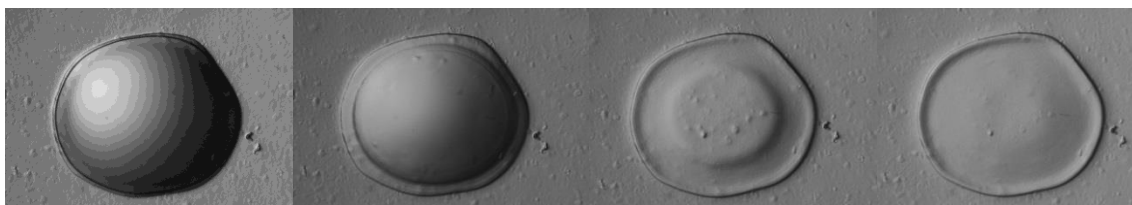
Dopamine On hydrophobic c surface (5% HPC)
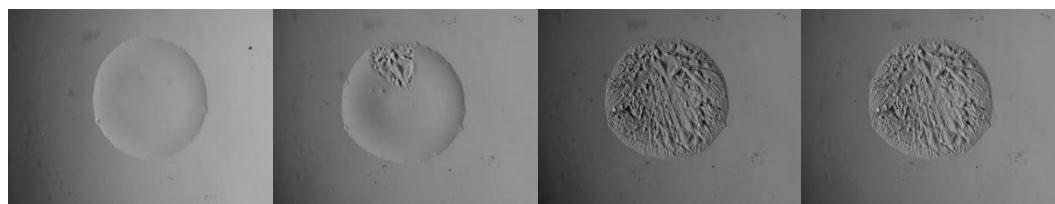
Figure 28: Dopamine Droplet on 5% HPC (Top) and on Glass(Bottom)
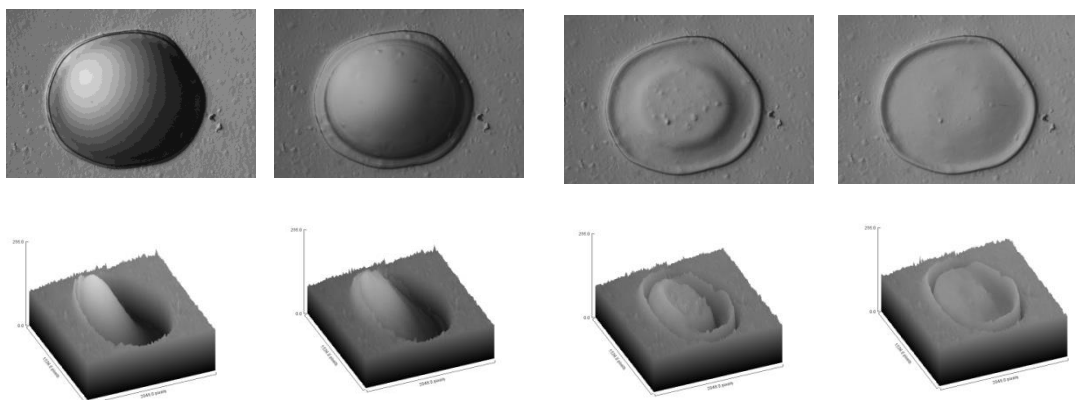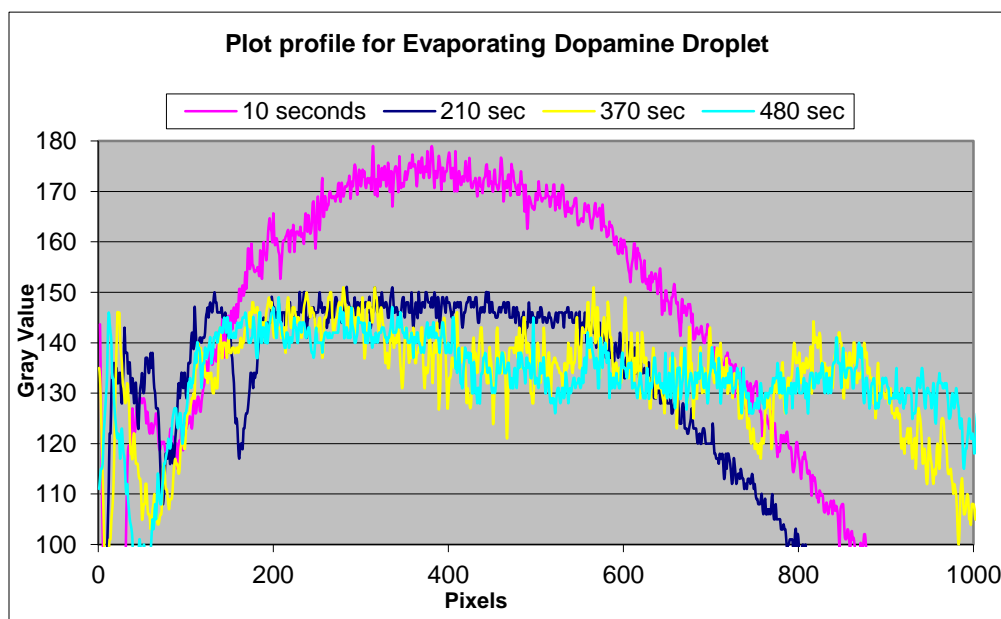
Figure 30: Top down images of evaporating drop with intensity

4.5 Mass Flux

Drops of API solutions were deposited onto substrates with varying wettability. An automated drop on demand (DoD) platform was used to control the pressure, open valve time, and spacing of the droplets. Pressure was held constant at 2psi and the valve

opening time was 1 ms. Normalized weight measurements show that drops deposited onto surfaces with higher hydrophobicity have slower evaporation rates as compared to the evaporation that occurs on hydrophilic materials. In our experiment it was shown that the bulk of the solvent evaporated fastest on glass, followed by 0.0975% HPMC, and lastly 5% HPC. This is due to the differences in initial height of the drop upon impingement. Droplets on hydrophobic materials had higher initial heights and evaporation occurs differently as compared to hydrophilic materials.
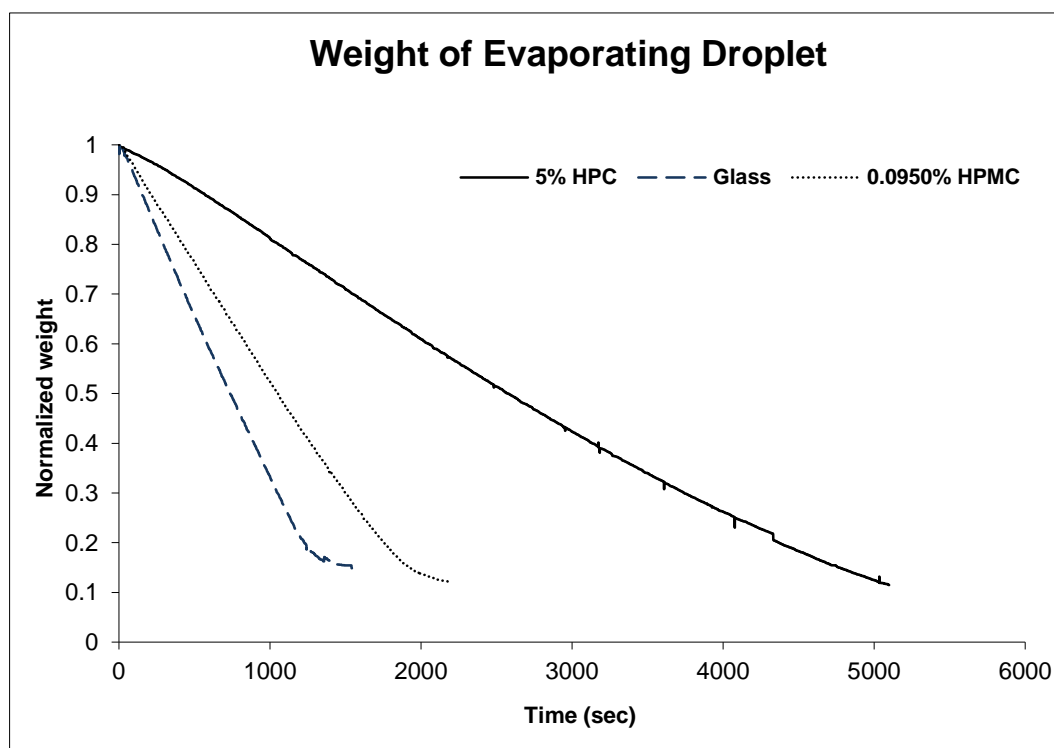
Figure 31: Plot of Mass Loss of Evaporating Drop

Droplet evaporation onto solid substrates has been studied extensively because comprehension of this phenomenon is useful in agricultural and other industrial applications that may utilize ink-jet printing [1]. The general theory of droplet

evaporation can be explained through the analysis of mass rate of change of water droplet in a steady state vapor field and is given by [2]

$$\frac{dm}{dt} = \frac{4\pi D_v^* M}{R} \left(\frac{p_\infty}{T_\infty} - \frac{p_{sat}}{T_a} \right)$$

(26)

where T_∞ is temperature in the ambient, a is the droplet radius, T_a is the temperature of the drop, m represents the mass of the droplet, R is gas constant, M is the molar mass of water droplet, P_∞ is the partial pressure of water, p_{sat} is the water equilibrium vapor pressure, and D_V^* is the gas phase diffusion coefficient.

We can understand the evolution of the contact angle during evaporation by examining the drops as a spherical cap geometry during the evaporation process [145]. Research has concluded that evaporation of a spherical drop can occur in 3 distinct modes as shown in Figure 32 [146, 147]: (1) constant contact area (CCA), (2) constant contact radius (CCR) [148], and (3) a mixed process where the contact angle and area change with droplet mass loss [138, 146]. In addition research has also detailed that the height and contact angles vary with time for initial contact angles less than 90 degrees while the contact area remains constant. In agreement with the results of our proposed hypothesis, our experimental results shows that for initial contact angles of > 90 degrees contact angle remained relatively constant until it reached a critical time which point the contact angle and height will decrease sharply in a linear fashion. Initial contact angles of 90 degrees or less exhibited linear decreases in height and contact angle.
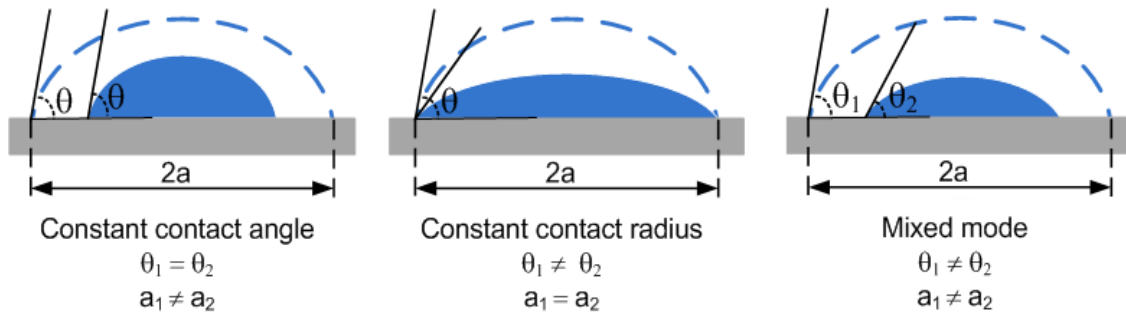
Figure 32: Schematic Illustration of three modes of evaporation. [146, 147, 149].

Liquid deposited onto the surface a solid substrate will maintain its spherical droplet geometry. The size of initial contact angle that forms between the interface is dependent on the liquid wetting behavior on the substrate [150]. The magnitude of the initial contact angle determines the shape geometry and is a significant variable in droplet evaporation [150]. The evaporation of droplet or mass loss with time, is defined as

$$\text{rate} = -\frac{dm}{dt} = -\left(\rho\frac{dv}{dt}\right) \qquad (27)$$

, where m is the droplet mass, V is the volume, p is the density , and t represents the time [150].

The extent of the initial contact angle was measured and found to be dependent on substrate type and wettability (independent of drop volume). Initial contact angles were 83.4, 38.7, and 28.8 degrees for the 5% HPC, 0.0975% HPC, and glass respectively. Hydrophilic conditions give an initial contact angle of closer to zero and hydrophobic conditions resulted in initial contact angles that approached 90.

4.6   Optical Microscopy of Solidified API Droplets

Optical microscopy displays the affect that substrate wettability will have on the solidification and final form of the API droplet solution.   Results show that hydrophobicity of the substrate dictates the growth of amorphous structures or crystalline regions.

Figure 33 demonstrate images of dopamine solution in a 1:10 (w/w) API:water ratio deposited onto substrates of varying hydrophobicity including glass, 0.0975% (w/w) HPMC and HPC, 2% HPC, and 5% HPC. Analysis of the data show that initial contact angle upon impingement can be used to predict the final structures. Depending on the initial contact angle three types of structures were identified: amorphous, semi-crystalline, and crystalline structures. The splat formed crystalline regions due to the higher concentrations of the API migrating towards the center of the drop when deposited onto hydrophilic substrates. On intermediate substrates where initial contact angles between 20 degrees and 60 degrees were observed for droplet impingement, final splat structures appeared to have semi- crystalline regions toward the periphery. Hydrophobic substrates, where initial contact angles lines measured above 65 degrees produced completely amorphous structures with no evidence of drug crystallinity. Furthermore, drops deposited onto highly hydrophobic substrates with contact angles greater than 65 degrees resulted in amorphous structures where a ridge forms towards the periphery of the drop.
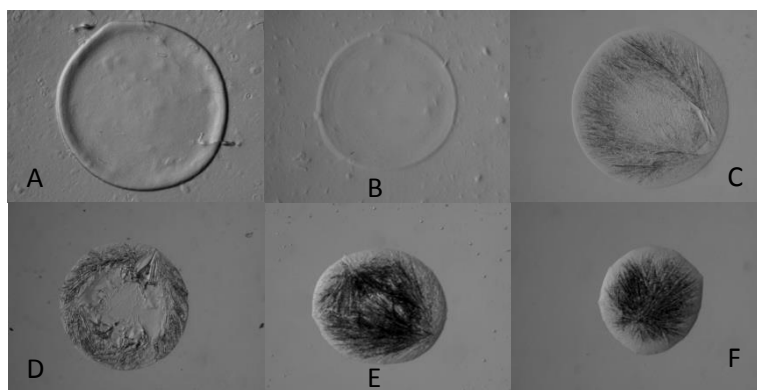
Figure 33: Drops of dopamine hydrochloride deposited onto (A) 5% HPC, (B) 2% HPC, (C) 0.0975% HPMC, (D) 0.0975 % HPC, (E) VWR Glass, (F) Corning Glass

4.7 Surface Energy Effects on Droplet Crystallinity

Surface energies of the substrates were obtained. Data indicate that substrate surface energies range from approximately from 30 mN/m to 50 mN/m. Surfaces with lower surface energies at or below 35 mN/m resulted in amorphous structures after solidification. Intermediate semi-crystalline structures resulted from surface substrates with surface energy between 35 mN/m and 40 mN/m. Substrates with surface energies greater than 40 mN/m produced ordered structures with crystalline API in the center of the splat. From optical microscopy and surface energy analysis it appears that there exists a progression from amorphous to crystalline stage and at some critical point, determined by surface and wettability properties of the substrate and surface tension of the API liquid droplet, the structure will change form and migration of the API crystals towards the peripheries or the center of the drop will result. Figure 34 displays the relationship between final splat structure and surface energy of the substrate.
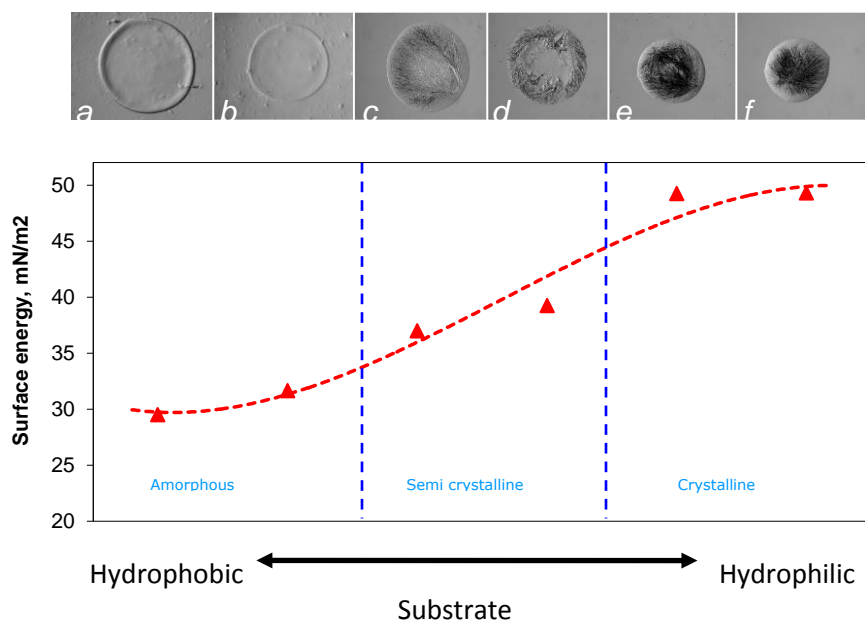
Figure 34: Surface Energy of Substrates

5 DOD AS MANUFACTURING PLATFORM FOR NOVEL ORAL AND TRANSDERMAL SYSTEMS

5.1 Drop on Demand Automation

($^($Section 5.1 is summarized from my previous work ""Automated Drop-on-Demand System with Real-Time Gravimetric Control for Precise Dosage Formulation")

The dispensing system is comprised of a pressurized fluid [68] reservoir (Ultra^{TM} Dispensing system, EFD,) that is connected to a pressure-regulated gas source using a barrel adapter assembly and to the VHS micro dispensing unit[68] (The Lee Co., CT). There are three ways the dispensed volume can be changed [68]:

• The MINSTAC dispensing nozzle can be changed. Using larger or smaller orifice sizes will increase or decrease the dispensed volume respectively.

• The inlet pressure can be changed. The inlet pressure directly affects the volume dispensed. If the pressure is increased, the dispensed volume increases proportionately. A typical starting pressure is 5 psi (at the valve)

• The on-time of the valve can be changed.

The variables can be modified to find the optimum dispensing point for a specific fluid.
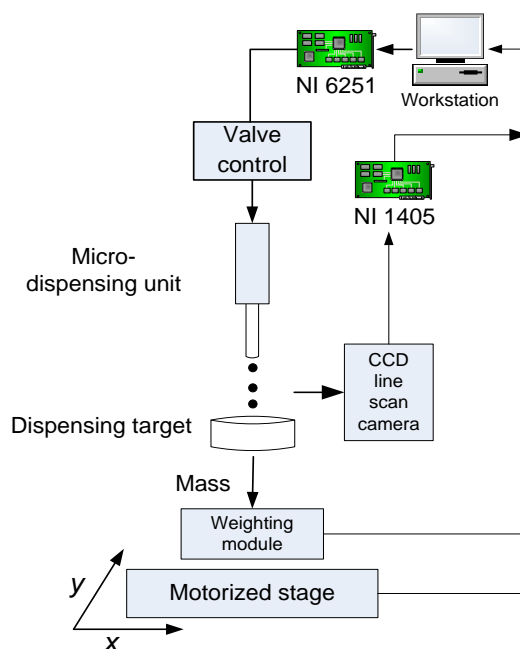
Figure 35 Schematic representation of Drop-on-Demand System.

Below the valve a weighting module, (Mettler Toledo) interfaced with the computer for automatic recording of weight, is placed on top of a motorized stage (OptiScan ES 103) which can be moved in the X & Y directions. The stage can be operated manually, using a joystick, or by Labview though a serial interface. An in line camera is focused on the system which is also automatically controlled through Labview. The weighting module and dispensing system are located inside an acrylic box to minimize the effect of environmental variables that can negatively impact the operating performance of the system [68]. All the electronics are mounted outside. Based on need the system can be operated in two modes: filling and printing [68].

5.1.1   Validation of Drop-on-Demand System

To test the reliability of the system API droplets were deposited onto the weighing module to observe the correlation between opening time of the valve (t) and fluid mass dispensed after 100 cycles From Figure 36 we see that the valve opening time is linearly related to the mass of the drop. The time the valve remains open is a critical parameter in the design of a dosage form [68]. The system can dispense a wide array of fluid volumes with the suitable arrangement of cycles and opening time of the valve [68].
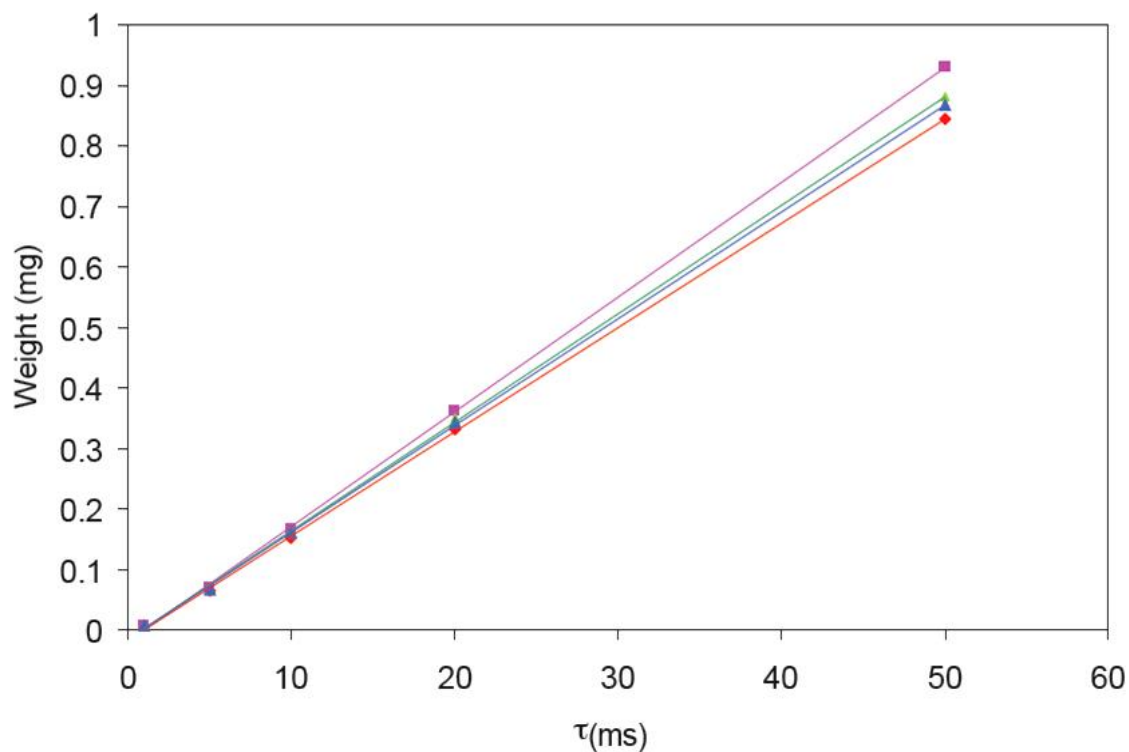
Figure 36 Validation of Drop-on-Demand System

5.1.2   Flexible Dosage Formation/Printing of Single Drug Delivery System

In printing mode, the API solution is ejected as a single droplet form and is 'printed' on a substrate [68]. The system parameters such as opening time of valve (tau), column and

row distance, and pressure are manipulated to obtain printed drops of drug solution with the desired release properties [68] . Using the weighing module the actual mass of droplet can also be monitored in line.

The capability of the system to print precise and reproducible volumes drug solutions onto varying substrates is evaluated This ability is necessary in the design of DDS which entail precision dosing, time-dependent dosing, or other advanced delivery modes, e.g. matrix drug delivery in controlled TDDS [68]. In printing mode the system parameters such as opening time of valve (tau), column and row distance, and pressure are manipulated to obtain printed drops of drug solution of desired specifications. In order to ensure that the desired product is obtained it is critical that all system parameters are accurate and easily controlled [68].

Variation of key system parameters enables the production of printed solutions and DDS with desired properties [68]. In some instances reproducibility and accuracy are desired while in other applications droplets with varying properties are produced [68]. Figure 37 and Figure 38 depict drug printing with variations in impingement substrate and/or process parameters [68].
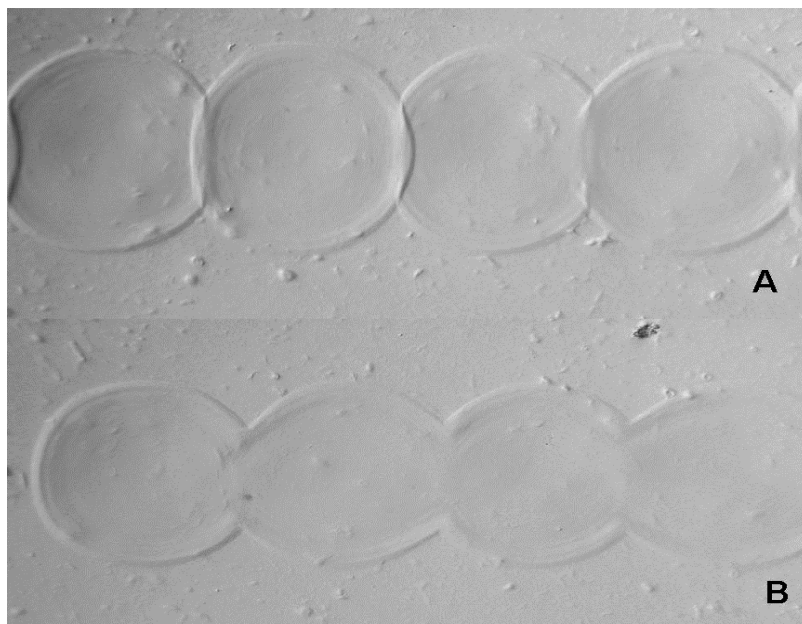
Figure 37: DI Water droplet printed onto 5% HPC Film.

Water droplets were printed onto 5% HPC Film. The top layer (A) was printed consecutively without allowing the water in the drops to evaporate. The bottom layer B was printed with a built in delay of 40 seconds.
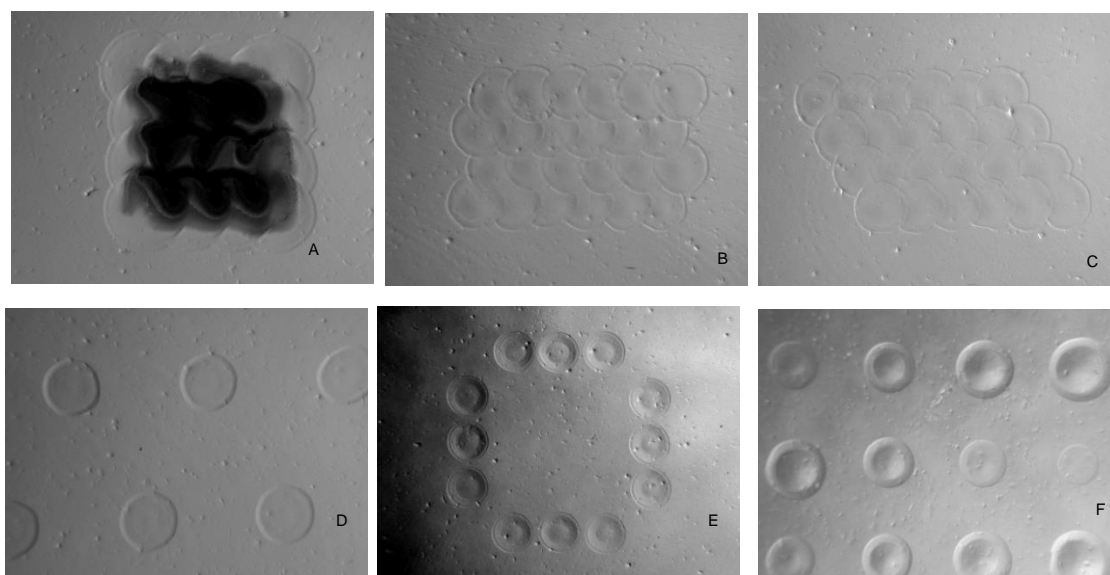
Drops of Dopamine Hydrochloride printed into various patterns through manipulation of key process parameters. (A) Overlap pattern of dopamine printed at max drug solubility, (B) Fish scale pattern, (C) Overlap pattern, (D) Array pattern, (E) O ring, (F) Ramp of variable tau.

Figure 38: Dopamine Hydrochloride printed into various patterns

In printing mode the system is robust, precise, and accurate [68]. It enables for the production of advanced drug delivery systems through automation [68]. Varying types of drops utilizing different drug solutions are able to be printed within exact range. Furthermore the system provides increased efficiency and allows for easy adaptation in the printing of different types of drug patterns, droplet diameters, and drug type.

5.2 Poly Pharmacy/ Printing of Multiple Drug Delivery System

In the design of printing dosage multi-drug dosage forms we incorporated the use of multiple syringes. Each syringe is independently controlled through its own valve control and a Labview program is utilized to specify the timing, count, and valve opening time of each valve independently. The motorized stage can be programmed to move prior to the drop deposition increasing spatial accuracy and allowing the end-user to determine the drop location of each syringe. In this manner two drugs, for example nicotine and haloperidol, could be delivered orally or through the skin (transdermal) on the same dosage form. This enables printing of drug dosage forms for combination therapy and poly-pharmacy. This is important because it allows accurate deposition and dispensing of two or more drug into one dosage at specific volumes and concentrations. This increases patient compliance and potential bioavailability, particularly for patients of mental illness of those patients taking combination therapy of different drugs to combat diseases such as AIDS or cancer.
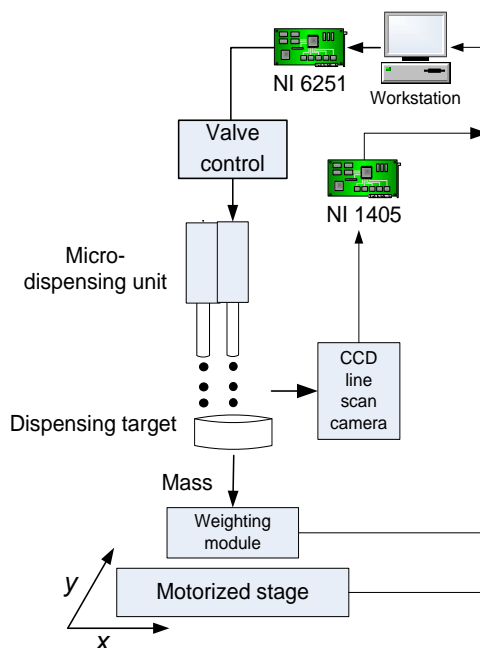
Figure 39: Schematic of Drop of Demand System for Multi-Drug and Poly pharmacy Designs

Printing of Transdermal Dosage Form

Transdermal dosage forms were created by utilizing multiple syringes where each syringe is attached to a reservoir containing either drug A, drug B, or an adhesive. Figure 40 and Figure 41 display the schematic of the drop-on-demand set up for multi-drug printing and the experimental transdermal dosage form.
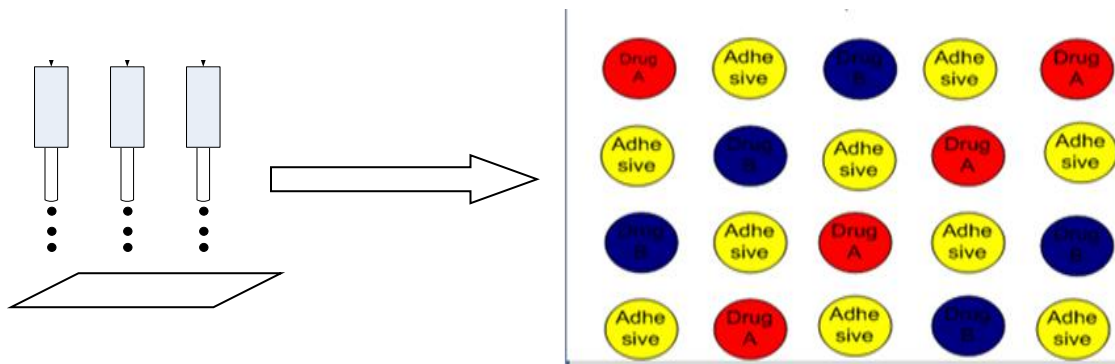
Figure 40: Schematic representation of Set-Up for Printing two different drugs and an adhesive
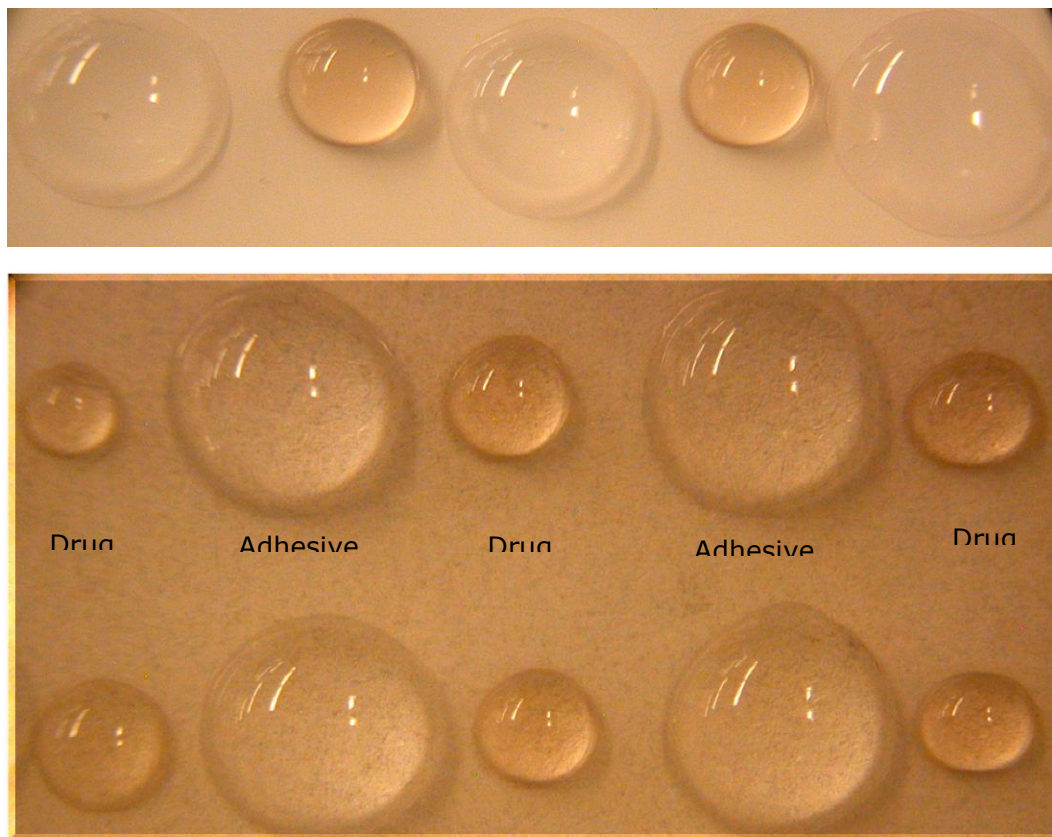
Figure 41: Optical images of Printed Transdermal Dosage Form Consisting of Drug Nicotine, Haloperidol, and PMMA

6 API DISSOLUTION FROM BIOPOLYMERIC FILM

6.1 Dissolution as a Thermodynamic Process

Enhancement of patient compliance and greater control of drug release rates in vivo have been the driving force behind the advancement of novel oral and transdermal drug delivery systems. The ability to predict the bioavailability of a drug in vivo is a necessary condition for any successful drug delivery system. Methods to create drug delivery systems that rapidly disintegrate or delay the release of drug are of particular interest because they can result in situations where patient compliance is increased due to the ease of disintegration or the alleviation of additional medication due to the controlled release.

Dissolution can occur either spontaneously or non-spontaneously depending on the net charge of the Gibbs free energy for the incorporation of a solute into a solvent [151]. The Gibbs free energy or ΔG, is given by

$$\Delta G = \Delta H - T\Delta S \tag{28}$$

where ΔH and ΔS represent the change in enthalpy and entropy due to mixing. The free energy for dissolution of a solute is

$$\Delta G = -RT \ln K \tag{29}$$

,where K is the equilibrium constant that characterizes the equilibrium of the solute in the solution phase and solute in the bulk phase. Increased solubility and probability of dissolution is represented with increasing values of $-\Delta G$. Block points out that ΔS is typically positive because solute molecules are more randomly or chaotically dispersed

than in the pure solid or liquid bulk phase. Furthermore, ΔH, can be either positive or negative. In this manner dissolution can be examined as a process defined entropically as opposed to an enthalpically driven process [151]. A mixture of solute and solvent results in varied microstates that each have individual specific arrangements of solute and solvent components. Given that the solution contains n_1 particles and n_2 particles of solute, the number of microstates available is

$$\frac{\left(n_1 + n_2\right)}{n_1! n_2!} \tag{30}$$

The configurational entropy of the mixture is defined as

$$Scf = \ln \frac{(n1 + n2)}{(n1! n2!)} \cdot \frac{R}{No} \tag{31}$$

, where R is the molar gas constant and No is Avogadro's number. From these equations we observe that the solute concentration, on a molar basis, compared to the configurational entropy of a mixture becomes very large as the mole fraction decreases. The thermodynamic aspects of dissolution are significant to the characterization of dissolution and should be analyzed during dosage form design [151]. In dissolution there are generally three energy changes that occur.

6.2 Controlled Delivery and Dosage Form Disintegration

In addition to thermodynamic aspects of the dissolution process, other factors such as the dosage pattern, droplet form (amorphous or crystalline) and drug type also greatly influence the dissolution process and potential bioavailability of a drug. Specifically we have found that manipulation of patterns can enhance or delay dissolution rates. Assuming that the drug form remains the same, we have proven that API sessile droplets printed as matrix patterns show dissolution rates dependent on the inter-droplet distance between the center of droplet radii, droplet radii size, and a dimensionless time τ. This is due to the defined diffusion zone areas where we have: (1) no overlap of the concentration fields from the individual printed droplets, (2) expanding concentration fields with partial overlaps (3) and complete coverage of the entire printed surface by the diffusion zones

Crystalline, amorphous, or solution forms of drugs have varying mechanical, physical, and chemical properties [152]. These different properties can affect the overall process-ability, stability, dissolution, and directly affect bioavailability in vivo [152]. Pharmaceutical scientists are interested in selecting preferred forms of drug materials to use in formulation because critical parameters such as morphology and solubility vary greatly between different physical forms [153]. The selection of a particular solid state form enables a manner in which to manipulate API dissolution properties during formulation stage[152]. Engineering of drugs forms can be applied to materials to solve problems of poor solubility, dissolution rate, and bioavailability [154]. Crystal engineering, as defined by Blagden et al, is the design of molecular solids with the goal

of engineering specific physio-chemical properties [154]. Blagden further points out, that the ability to engineer materials that have suitable chemical and physical stability with desirable dissolution properties offers a strong incentive for the utilization of these new applications to drug delivery and dosage form design [154]. This research utilizes engineering and thermodynamic principles to create amorphous and crystalline drug forms to manipulate drug delivery rates, disintegration properties, and dissolution.

Amorphous Drug Structure

An amorphous structure exists as a structure where the molecules, ions, or atoms are random. Molecules do not repeat and, in general, have localized order near their individual structural units. Generally speaking, amorphous drug forms enable enhanced dissolution, solubility, and wettability. The amorphous state of the drug represents a higher energy state as compared to the crystalline drug form [152] and; therefore, is less stable, prone to degradation and crystallization, and represents greater risk due to its metastable form. Dissolution of amorphous materials occurs rapidly as compared to crystalline structures. DDS systems present as amorphous structures will dissolve readily and can have a solubility advantage of at least 10 to 1600 fold higher than that of the crystalline structure [153]. It should be noted that; although materials are much more soluble in the amorphous state v crystalline form, the experimental solubility is usually less than the predicted solubility form thermodynamic considerations [153]. This is likely due to the solubility advantage that is immediately diminished as the amorphous form begins the transform to the more stable crystalline form once water is introduced to the amorphous API [152]. Despite this, research has shown that the calculated thermodynamic values can provide a useful indication of the theoretical maximum

solubility for initial dissolution rate of amorphous materials [153]. Additionally, calculated and measured values, even for partially amorphous materials, show that there is an increase in solubility that is significant for clinical relevance [153]. The amorphous structures can be applied to situations where increased disintegration or dissolution is highly desired.

<u>Crystalline Drug Structure</u>

Crystalline structures exist as ordered arrangements in fixed geometric patterns. The molecules are arranged in a manner to maximize the occupied space, where the smallest unit, the unit cell, repeats itself. The three-dimensional pattern of repeating atoms, ions, or molecules occurs over long atomic distances or long range order. Crystalline structures are more thermodynamically stable than amorphous structures. They present greater long-term stability, decreased risk, and lower solubility. Crystalline structures have decreased solubility and can be utilized for controlled or delayed drug release dissolution in vivo.

6.3   Dopamine Hydrochloride Dosage Form

6.3.1   HPC Biopolymeric Film

Films composed of 2% hydroxypropyl cellulose films were formed using free-casting techniques. Hydroxypropyl cellulose was dissolved into water at a material to water ratio of 1g:50 ml. 6 ml of HPC solution was deposited into sterile 15*60 mm VWR polystyrene petri dishes. The dishes were then placed under vacuum pressure for a period of 24 hours and subsequently put in an oven for 48 hours at a temperature of 30 degrees Celsius until dry.

Dopamine hydrochloride solutions were formed by dissolving 1 gram of drug powder into 10 ml of distilled water.

6.3.2 Printing of API droplets onto Biopolymeric Film

A DoD printer automated through Labview Programming was utilized to deposit droplets of drug solution onto hydroxypropyl cellulose film. The API droplet was deposited as single drops, array, multi-layered drops, or overlap patterns. All patterns were created such that the total volume and the total amount of drug deposited onto the film were consistent for all samples. The calculated total volume was approximately 0.25 ml and the total amount of drug deposited onto the film was 2.28 mg. For the single drop pattern a volume equal to 0.25 ml was deposited onto the film. The droplet was then allowed to solidify. Both amorphous and crystalline structures were formed by manipulating surface tension properties of the substrate. In the simple array patterns an 8*5 array of droplets were deposited onto the film and allowed to dry. Crystalline and amorphous splat structures were formed depending on the substrate surface energy properties. The overlap pattern an 8*5 array was also created but the droplets were deposited such that half the diameter of one droplet overlapped the other by approximately ¾ mm. The multi-layer patterns were formed by creating one array where 40 drops were deposited directly onto each other. For each location in the array a drop was deposited directly onto another every 30 seconds. All films with drug deposited were cut from the petri dishes for dissolution testing.

The drop on demand system is capable of printing a variety of patterns and matrices. In addition, we can use system parameters such as time and rop to drop proximate radial

distance to formulate crystalline or amorphous patterns. In the following group of images we display the versatility and capability of the system. In all cases the 10% dopamine hydrochloride droplets were printed on a low surface energy substrate such as 2% hydroxypropyl cellulose. Figure 42 shows the evolution of a desposited drop as it solidifies. Figure 43 shows the diversity of the capability of the DoD system to print both amorphous and crystalline structures. In image A we printed droplets of varying volumes and diameter size by increasing the amount of time the valve remained opened. Printed diamters ranged from ~1.0 mm – 2 mm. Image B a large droplet is printed of both amorphous and crystalline morphology. In Image C (top row) a "fischscale overlap pattern was formed by overlapping the droplet diameters by ~250 microns and introducing a delay of 120 seconds between depositions (amorphous and crystalline patterns) The increased time between the droplets enabled droplet evaporation to occur and the partial solidification of the initial droplet prior to the next droplet. This resulted in a fishscale pattern where all droplets remained amorphous. In image C (bottom row) an overlap pattern is observed where the overlap printing distance remains at 250 microns but the delay between each drop deposition is decreased to approxiamtely 10 seconds. This printing pattern permitted the droplets to spread into other droplets at greater lengths and result in the the convection of water towards the center of the overall structure. The dopamine contained within the water was carried towards the center of the overall structure resulting in a mixed morphology where the pattern remains crystalline in the center and amorphous at the periphery. It should be noted that there are a variety of the factors that influence the phase transition from amorphous to crystalline regions. These

factors include size of droplet, initial loading of API concentration, substrate wettability, droplet pattern and spacing, and time.
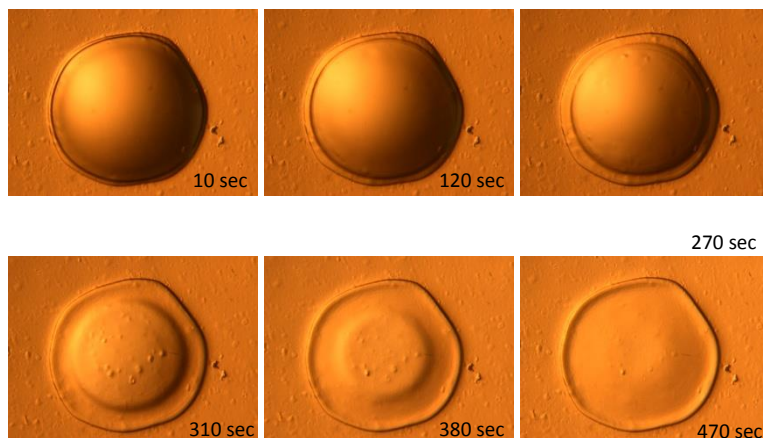
Figure 42:Evolution of Dopamine Hydrochloride printed on low surface energy substrate
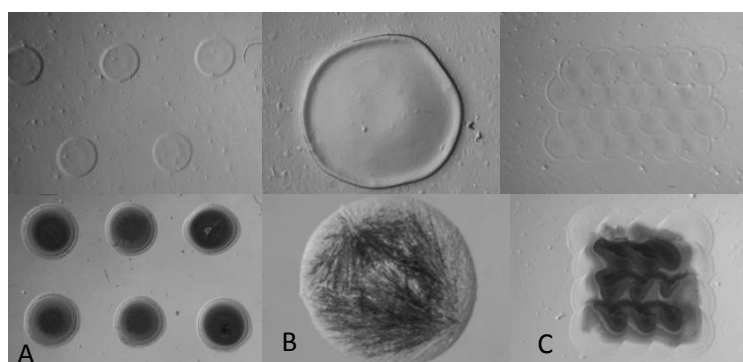
Figure 43: Printed Dopamine Droplets (A) Array, (B) Large Droplet, (C) Overlap Patterns. Top: Amorphous & Bottom: Crystalline

6.4 Drug Load in the Printed Array Dosage Form

To determine actual parameters of the printed dosage form, we start with the representation of the sessile droplet as ½ of a sphere in Figure 44.
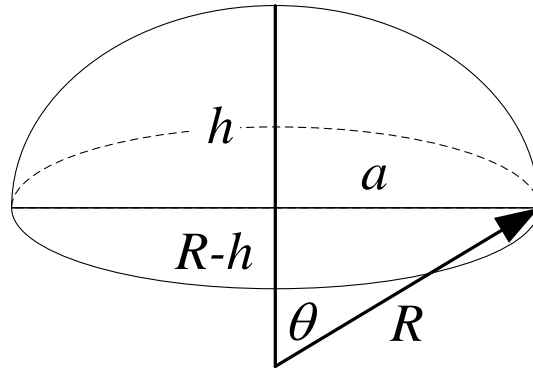
Figure 44 Schematic representation of the printed sessile droplet

Non-evaporating stable printed droplet can be represented as a spherical cap with the radius R. The volume V_{sd} of a sessile droplet of height h and base radius a is given by the following equation [155]:

$$V_{sd} = \frac{1}{6}\pi h\left(3a^2 + h^2\right)$$ (32)

Taking into account that radius of the base circle of the sessile droplet is:

$$a = \sqrt{(2R-h)h}$$ (33)

and plugging this into (32) gives us the equivalent formula:

$$V_{sd} = \frac{1}{3}\pi h\left(3R - h\right)$$ (34)

Let us introduce an α - the angle between the normal to the sphere at the bottom of the cap and the base plane. From simple geometrical considerations:

$$\alpha = \arcsin\left(\frac{R-h}{R}\right) \tag{35}$$

Now (34) can be written as follow:

$$V_{sd} = \frac{1}{3}\pi R^3 \left(2 - 3\sin\alpha + \sin^3\alpha\right) \tag{36}$$

We have two parameters that predetermined by the DoD system and substrate: r - radius of the droplet generated by the printing device and θ - contact angle formed at three-phase interface of the API solution and substrate.

Now angle α can be calculated from the contact angle:

$$\alpha = \frac{\pi}{2} - \theta \tag{37}$$

Substituting (37) into(36), and using mass conservation principle, we can find the radius of the sessile droplet according to:

$$R = \left[\frac{4}{\left(2 - 3\cos\theta + \cos^3\theta\right)}\right]^{\frac{1}{3}} r \tag{38}$$

Putting (38) into (35) and taking into account(37), we can determine height of the sessile droplet:

$$h = \frac{\left[4\left(2 - 3\cos\theta + \cos^3\theta\right)^2\right]^{\frac{1}{3}}}{2 - \cos\theta - \cos^2\theta} r \tag{39}$$

Substitution of (38) and (39) into (33) results in quite complex transcendental equation that can be simplified by means of Taylor series expansion:

$$a = \sqrt{\frac{2 \cdot 2^{\frac{1}{3}} \left[\left(\cos\theta+2\right)^2 \left(\cos\theta-1\right)^4 \right]^{\frac{2}{3}} \left(\cos\theta+1\right)}{\left(\cos^2\theta - \cos\theta - 2\right)^2 \left(1-\cos\theta\right)}} \, r \qquad (40)$$

Taking into account that θ is much smaller than 1, after some rearrangements, we can simplify expression(40):

$$a \approx \beta \theta^{-\frac{2}{3}} r \qquad (41)$$

where β = 11.53799657. Computed ratio between droplet footprint and radius as function of the contact angle is depicted in Figure 45.
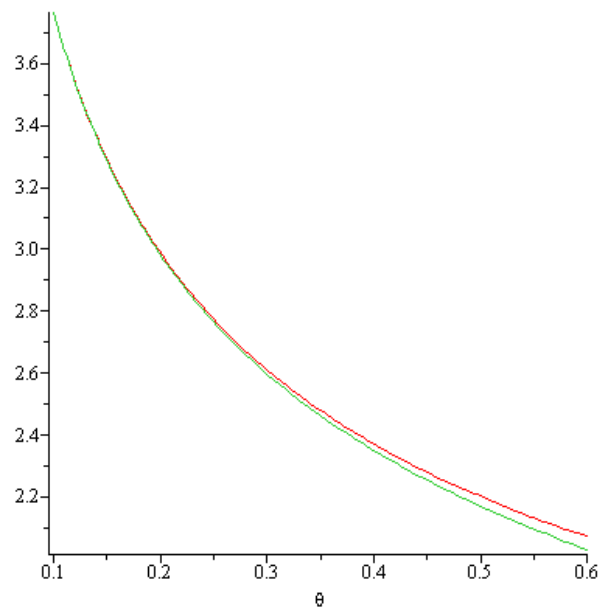
Figure 45: Calculation of β (red simplified, green exact solution)

Mass of the dosage form in the single droplet can be calculated from the following expression:

$$m_d = \frac{4}{3}\pi r^3 \rho_d \tag{42}$$

Thus one printed dosage of radius a will contain $m_d \chi_d$ of the API. Total API load can be predicted as following. Dosage is printed as equidistant array of droplets with the interdroplet distance d. Therefore, required substrate area $S = nd^2$ covered by the array will contain $nm_d \chi_d$ of API, and surface coverage can be described as:

$$\varphi = \frac{nd^2 \theta^{\frac{4}{3}}}{\pi \beta^2 r^2} \tag{43}$$

Consider first one disk-shaped printed droplet on non-absorbing substrate as depicted in Figure 46
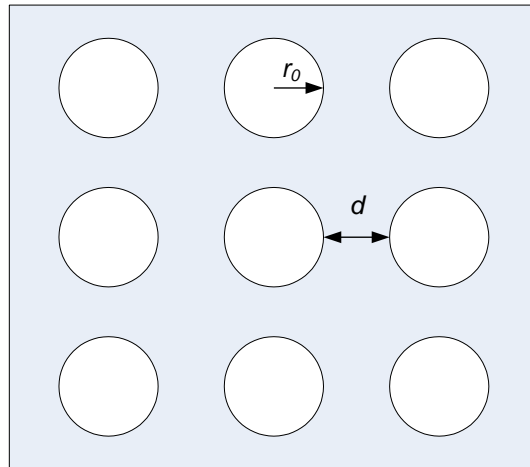
Figure 46 Printed API dosage: array of uniformly distributed droplets

Because of the hemispherical symmetry, diffusion from the API print can be calculated from:

$$\pi r_0^2 J_s(t) = -\pi r_0^2 D \frac{dC}{dr}\bigg|_{r=r_0} \tag{44}$$

where $\pi r_0^2 J_s(t)$ is the total amount of material diffusing from the surface of the dissolving drug. For a printed disk of small dimensions, the condition $r_0 > \sqrt{\pi D t}$ will be valid for sufficiently long times and therefore equation (44) after use of Laplace transform can be written in the following form:

$$\pi r_0^2 J_s(t) = \pi r_0 DC - \frac{\pi r_0^2 DC}{\sqrt{\pi D t}} \tag{45}$$

So that the amount of material $\pi r_0^2 J_s(t)$ diffusing from the surface of an isolated printed droplet reaches a steady state.

In considering diffusion from the dissolving array of printed droplets we examine hemispherical diffusion zones adjacent to the individual API printed droplets [156]. Close to the drop, droplet diffusion will retain spherical symmetry; however, as the distance is increased and tends toward the inter-droplet separation distance, the hemispherical concentration fields interact [156]. Comprehension of the effect of the overlapping concentration fields is complex [156] . The equations that describe this phenomenon can be simplified if we convert the three-dimensional equations that represent the growth of the diffusion-induced concentration fields to a two-dimensional calculation [156].

The equivalent region of the plane surface, πr_d^2 where $r_d(t)$ -radius of the diffusing zone, results in the same amount of material diffusing through its surface as the amount that diffuses from a printed droplet through radial diffusion. In semi-infinite linear and complete diffusion [156], mass transport can be defined through well-known Cottrell-type equation:

$$\pi r_d^2 J_p(t) = -\frac{\pi r_d^2 DC}{\sqrt{\pi Dt}}$$
(46)

where $J_p(t)$ is normal to the plane mass flux of the dissolving drug in the z direction.

The radius of the equivalent diffusion zone, $r_d(t)$, can be calculated by comparing the mass quantity of API that is diffusing radially to the printed droplet (45), to the quantity that is diffusing linearly to $r_d(t)$ [156]. This is determined by equation (46):

$$r_d^2 = \pi r_0 - \frac{\pi r_0^2}{\sqrt{\pi Dt}}$$
(47)

The equivalent diffusion zone area is now calculated as [156]:

$$S = \pi r_d^2 = \pi r_0 \sqrt{\pi Dt} + \pi r_0^2$$
(48)

The overlap of the equivalent diffusion zones is now utilized to calculate the diffusion spherical to planar transition of the printed array of droplets [156]. Without loss of generality, we consider a square lattice array with uniform droplet distribution and inter-

droplet distance, d. Following equation (48), the diffusion zone coverage of the droplet array is given by:

$$S = \frac{\pi r_0 \sqrt{\pi D t} + \pi r_0^2}{d} \tag{49}$$

The number of printed drops in a given area n, is correlated to the inter-droplet distance d, as $n = d^{-2}$ [156]. Substituting it into (49) give us:

$$S = \pi n \left(r_0 \sqrt{\pi D t} + r_0^2 \right) \tag{50}$$

Let us introduce a dimensionless time τ as the following:

$$\tau = n r_0 \sqrt{\pi D t} \tag{51}$$

The fraction of the diffusion zone area compared to that of the printed array is:

$$S = \pi \left(\tau + n r_0^2 \right) \Big|_{r_d = \frac{d}{2}} = \frac{\pi}{4} \tag{52}$$

Now we can classify three distinct types of diffusion zones: no overlap of the concentration fields from the individual printed droplets, expanding concentration fields with partial overlaps, and complete coverage of the entire printed surface by the diffusion zones [156]:

i) $r_d < d/2$, with no intersection of diffusion zones. As follows from (52), there will be intersection or overlap of diffusion zones for times such that $0 < \tau < \frac{1}{4} - n r_0^2$. For the

small τ determined by (51), the mass flux density current to the array is determined by the diffusion current from the drug print of fractional area S [156]:

$$J_p(t) = nC\left(\pi r_0 + \frac{\pi r_0^2}{\sqrt{\pi Dt}}\right)$$

(53)

If we state equation (52) in units normal to the current single printed droplet we obtain:

$$\frac{J_p(t)}{\pi n r_0 DC} = 1 + \frac{n r_0^2}{\tau}$$

(54)

ii) Partial overlap of diffusion zones that occurs at time interval defined as $d/2 < r_d < d/\sqrt{2}$ [156]. During the interval $\frac{1}{4} - n r_0^2 < \tau < \frac{1}{2} - n r_0^2$, calculation of the mass flux must include consideration of the overlap of diffusion zones. The flux current is given, in normalized units, by:

$$\frac{J_p(t)}{\pi n r_0 DC} = \frac{1}{\pi \tau}\left[\sqrt{4\left(\tau + n r_0^2\right) - 1} + 4\left(\tau + n r_0^2\right)\left(\frac{\pi}{4} - \arctan\sqrt{4\left(\tau + n r_0^2\right) - 1}\right)\right]$$

(55)

iii) For printed drug array completely covered by the diffusion zones ($r_d > d/\sqrt{2}$) and for times such that $\tau > \frac{1}{2} - n r_0^2$ the entire surface of the printed dosage is completely covered by diffusion zones [156] and the mass transport of the dissolved drug from the array is given by:

$$\frac{J_p(t)}{\pi n r_0 DC} = \frac{1}{\pi \tau}$$

(56)

7   RESULTS - DOPAMINE HYDROCHLORIDE DOSAGE FORM

7.1   Raman Spectra of API Dosage Form

Raman Spectra data show that both the amorphous and crystalline droplets have similar spectra. See Figure 56. Sharp peaks are seen at the 200-300 band region, 600 band region, around the 975-1025, and near the 28500 band region for both the amorphous and crystalline dopamine droplets. The most intense band is seen in the spectral range between 2800-2900 cm^{-1}. Examination of all three spectra show that the crystalline drop and the amorphous droplet have very similar fingerprints and are dopamine hydrochloride.
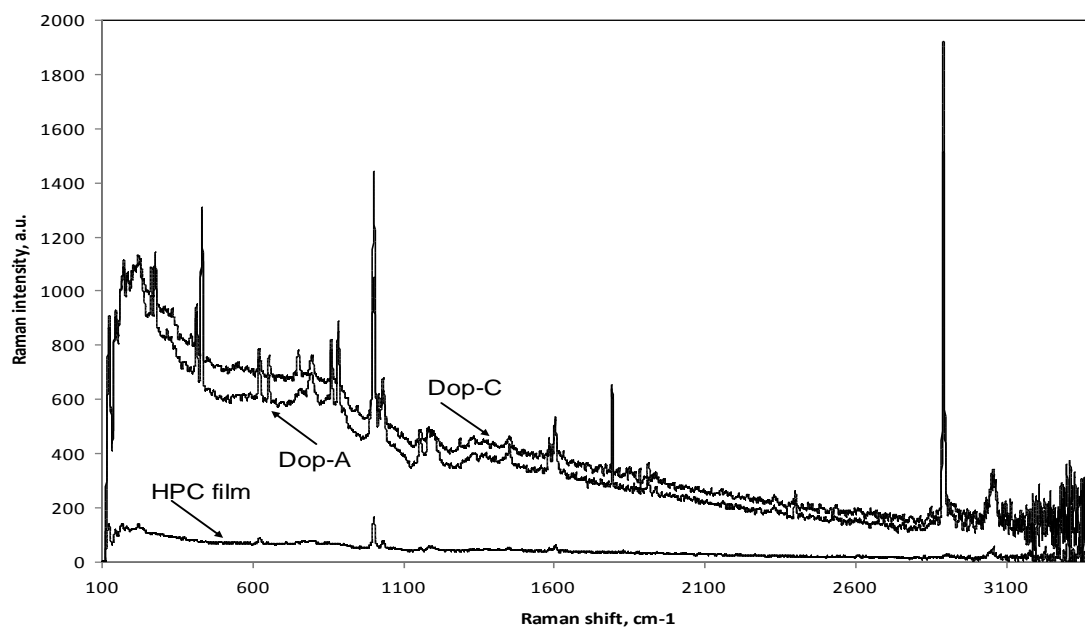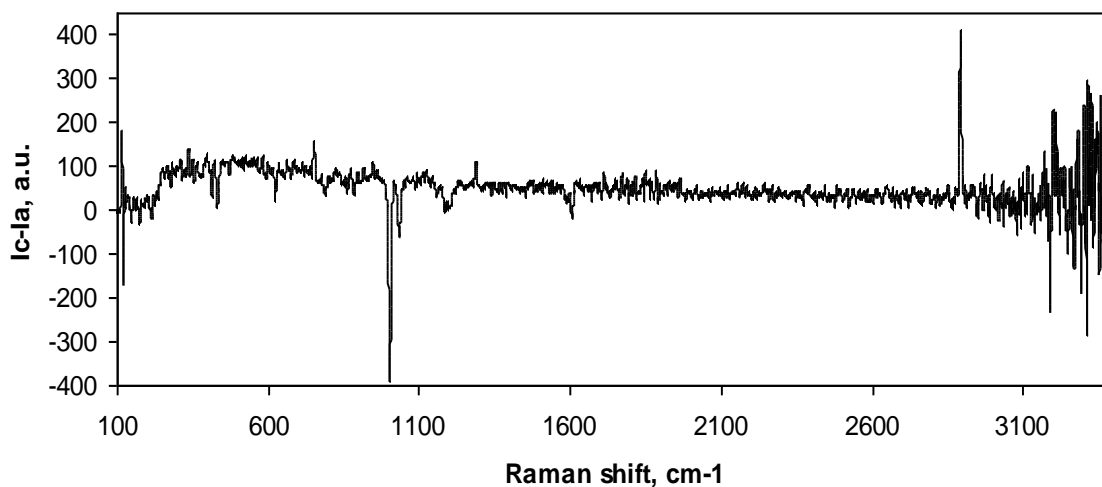
Figure 47 Raman Spectra of Dopamine Crystal Droplet, Amorphous Droplet, and HPC film.

7.2   X -Ray Diffraction of Dopamine Hydrochloride Dosage Form

Samples of the printed dopamine droplets were analyzed utilizing XRD analysis to determine the final morphology as either crystalline or amorphous and to identify any structural variations. XRD analysis revealed that larger droplets printed onto 2% HPC crystallized within hours while smaller droplets containing less amount of drug remained amorphous for a time period exceeding 48 hours. Figure 48 shows that the amorphous sample has broad peaks indicating large amorphous regions. The large sharp peaks shown in the x-ray diffraction pattern signify crystalline regions.
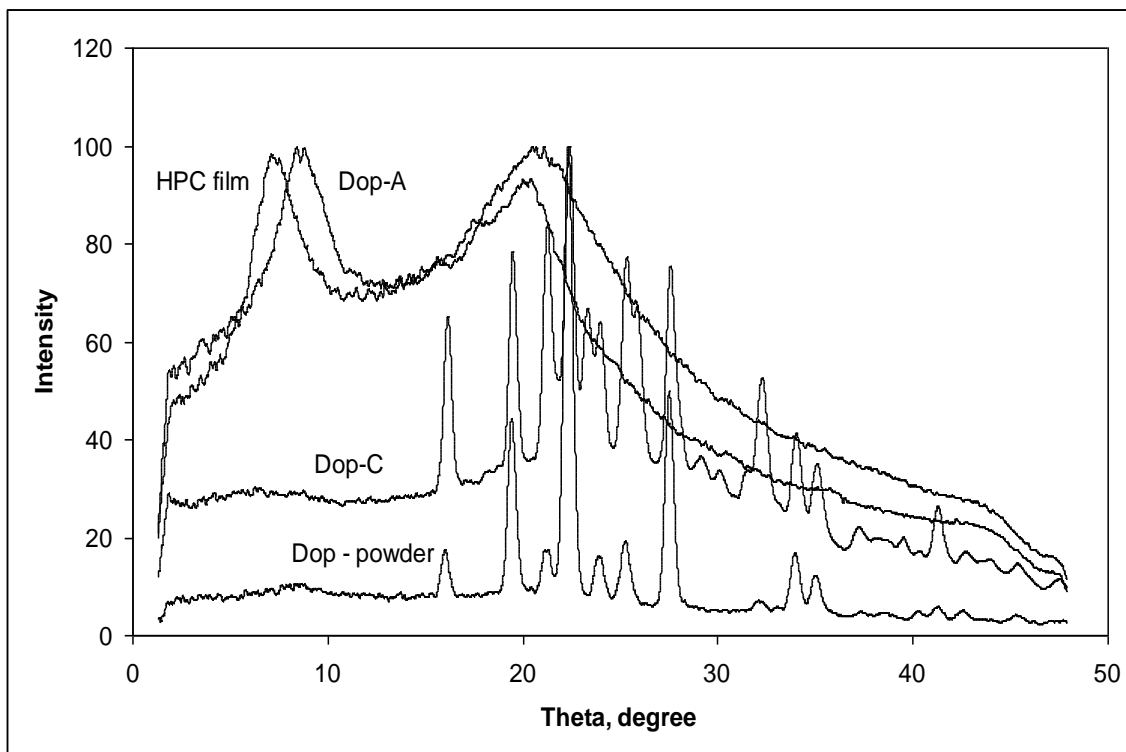
Figure 48: X Ray diffraction patterns of Dopamine droplets on film

The droplets were then compared to the XRD pattern of the pure dopamine hydrochloride powder. Both the HPC film and the dopamine droplet in the amorphous form report similar peaks and broad spectrums. This indicates that while the dopamine exists in the solution drop its atoms are not arranged and the structure is different as compared to the crystalline powder.

The printed dopamine droplet that appeared to be crystalline from optical microscopy is compared to the standard of pure dopamine hydrochloride powder. From Figure 48, we observe that the printed dopamine droplet and powder dopamine diffraction patterns are similar in peak location and d spacing. From this we conclude that the printed dopamine droplet is crystalline.

7.3   Thermal Analysis of Dopamine Hydrochloride Dosage Form

Thermal analysis of the samples was conducted for the pure dopamine crystal powder, the amorphous dopamine droplet, the crystalline dopamine droplet, and HPC film. See Figure 49. The plot of heat flow versus temperature shows that pure dopamine hydrochloride powder has a melting point of approximately 250 C. The crystal droplet printed onto HPC film experiences glass transition at approximately 260 C and almost immediately the heat flow drops indication melting of the crystal droplet. The amorphous droplet experiences a decrease in heat flow around 250 C indicating melting and then increases towards 300 C. This can indicate an initial melting and resultant glass transition. The 2% HPC film, similar to the amorphous droplet, does not experience a large sharp drop but smaller drops indicating melting between 200 -250 C.
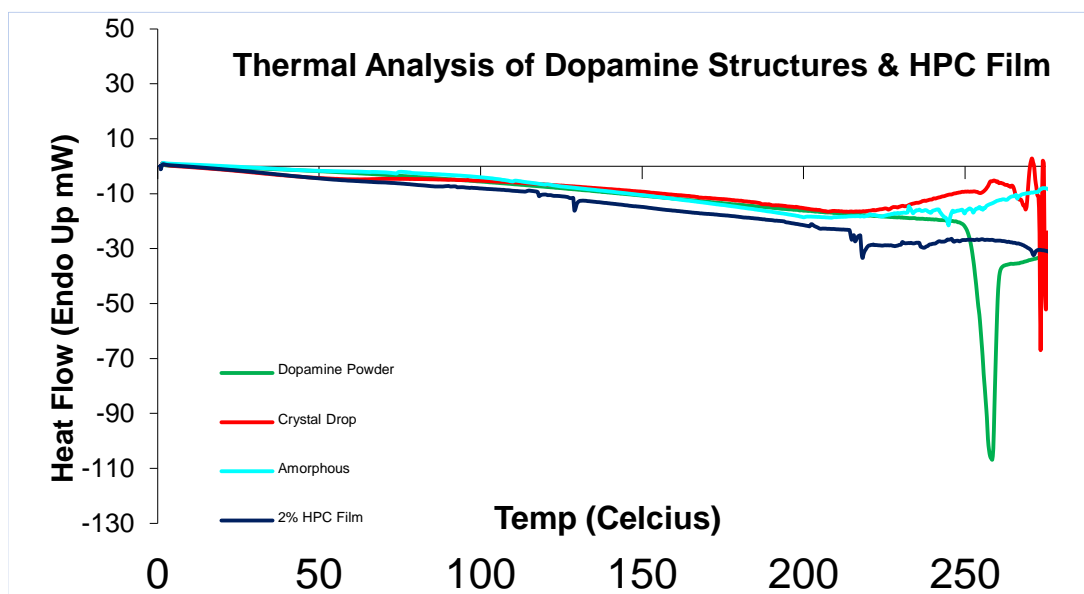
Figure 49: Thermal Analysis of dopamine droplet on HPC films

7.4   Rapid Release In-Vitro Dissolution Models

7.4.1   Traditional Models

To examine in vitro release profiles of the film loaded with dopamine and to compare existing models with our model several standard dissolution models were utilized [157]. These models include:

Zero Order Model: (Ravelli & Rossi): This model assumes a constant drug release rate that is independent of API concentration [157-159].

$$\frac{M_t}{M_\infty} = kt \tag{57}$$

M_t is the quantity of API released during a specified period and M_∞ is the total amount of API at infinity .

First Order Model.   The concentration of API in the donor is based on exponential decline and the release rate is relative to the concentration [157, 160].

$$\frac{M_t}{M_\infty} = 1 - \exp^{-kt} \tag{58}$$

Higuchi model. This model explains the API release rate through a matrix based upon Fick's equation [9, 161].

$$\frac{M_t}{M_\infty} = kt^{\frac{1}{2}} \tag{59}$$

Hixson and Crowell cube-root equation model.   In this model dissolution is limited due to differences in the available surface and particle size of the API [157,161,162].

$$\left(\frac{1-M_t}{M_\infty}\right)^{1/3} = 1 - kt \tag{60}$$

Korsmeyer and Peppas model: This model explains the simple drug release from a polymer system. The type of drug release is established by plotting and fitting the release data [161,163, 164].

$$M_t / M_\infty = kt^n \tag{61}$$

where n characterizes different release mechanisms for cylindrical shapes.

7.5 Drug-Release Dissolution Studies

The dopamine loaded films were subject to dissolution testing. The five standard models were used to plot the dissolution data. Plots included the zero order model, first order, Higuchi model, Korsmeyer (Log Cumulative % vs. Time), and the cubic root of remaining percentage of drug in the vehicle vs. time. See Figure 50: Higuchi Plot of Dopamine Hydrochloride – Crystal and Amorphous Array dissolution profiles.
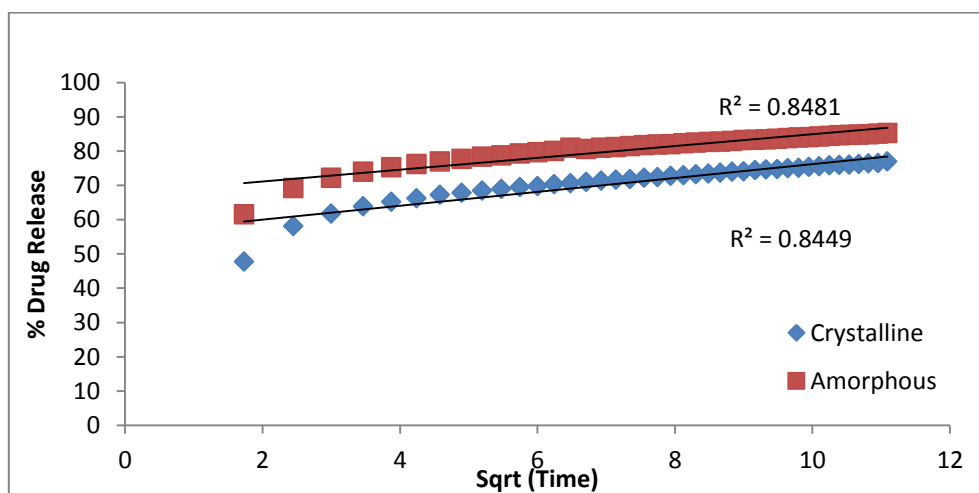
Figure 50: Higuchi Plot of Dopamine Hydrochloride – Crystal and Amorphous Array dissolution profiles.
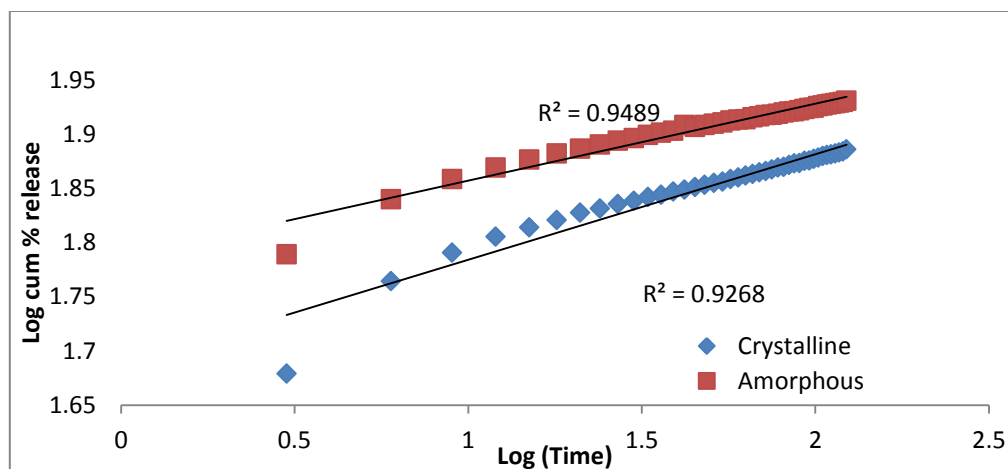
Figure 51: Korsmeyer Plots of Dopamine Hydrochloride Crystal and Amorphous Array dissolution profiles.

Our drug dosage form consists of crystalline and amorphous droplets deposited onto HPC film. This type of dosage form should follow the steps as outlines by [161] and [165]. Initially penetration of the dissolution solvent into the film occurs due to hydration. Secondly the film swells and the erosion of the polymer matrix occurs. Lastly the dissolved API is transported from the hydrated matrix into the surrounding dissolution medium [161]. Dopamine hydrochloride experiences an initial rapid release rate of approximately $1.3484\dfrac{mg}{min}$ and $1.7329\dfrac{mg}{min}$ for the crystalline and amorphous droplets, respectively. During the first 10 minutes 74% of the amorphous drug has been released and 61% of the drug in the crystalline form. After approximately 10 minutes the release rate changes due to the concentration of the dopamine in the dissolved medium. To predict the overall completion of the dissolution rate profile we plot the dissolution as concentration (mg/L) vs. Time (minutes). The best fit straight line indicates a first order model utilizing the Korsmeyer & Peppas model [164]. Linear regression of the data gives the equation c=.071t+1.786 with R^2 equal to 0.9489 for the amorphous droplet and c=.0975t + 1.6866 with R^2 equal to 0.9268 for the crystalline droplet.

The R^2 values and correlation coefficients of different kinetic models can be seen in Table 5. Good correlation was found with the Higuchi and Korsmeyer models achieving R^2 values of .85 and .95 respectively. It is important to note that we do not reach values R^2 above .95 due to the type of release profile. Dopamine is very soluble in water and as a result, our drug model consists of an initial rapid linear release during the first 10 minutes of dissolution followed by a second slower phase that can be characterized accurately by the Higuchi or Korsmeyer models.

Amorphous Structure									
Zero Order		First Order		Higuchi		Hixson-Crowell		Korsmeyer-Peppas	
R^2	k	R^2	k	R^2	k	R^2	k	R^2	k
0.3205	0.2608	0.8367	-0.0023	0.8481	1.718	0.7995	-0.0015	0.9489	0.071
Crystalline Structure									
Zero Order		First Order		Higuchi		Hixson-Crowell		Korsmeyer-Peppas	
R^2	k	R^2	k	R^2	k	R^2	k	R^2	k
0.395	0.2656	0.8278	-0.019	0.8449	2.3024	0.794	-0.014	0.9268	0.097

Table 5: R squared and k values of Dissolution Plots

7.5.1 Modified Drug-Release Dissolution Studies

Dissolution experiments showed that the dissolution profile of our dosage forms do not fit the traditional dissolution models. We believe that the dissolution of the dopamine hydrochloride from the polymer matrix occurs in two distinct steps. Initially the dissolution rate is inversely proportional to the non-dimensional time constant, τ. Once

mass released from the matrix is approximately 65-70% of the initial drug load, the dissolution rate is limited due to the concentration gradient and the dissolution rate is proportional to the natural log of time. The relationship is due to the water-soluble dopamine dissolving from the porous HPC matrix [166, 167].

A plot of cumulative API M vs. time (Figure 52) and $\dfrac{dM}{dt}$ (Figure 53) show that the highest initial rate of dissolution occurs in the larger size droplets of approximately 3 mm in diameter. The multi-layer droplets, crystal and amorphous array, and overlap patterns have initial dissolution rates less than the larger droplets. After approximately 15-20 minutes the derivative plot shows that the dissolution rates began to converge towards 0 where the rate is constant. Figure 52 shows that the cumulative API release rate is highest for the largest droplet (3mm diameter), followed by the 1.50 mm diameter droplets of the array. The overlap and multi-layer droplets (1.50 mm) have the smallest total cumulative dissolution rate. It is important to note that two factors of the dosage form contribute to the dissolution rates and subsequent profiles: droplet volume/size and droplet patterning & inter-droplet spacing. The largest volume droplets have higher initial dissolution and total cumulative mass. This finding was true for both the amorphous and crystalline forms. The array patterns with inter-droplet spacing of ~750 microns had intermediate dissolution rates. Lastly the overlap and multi-layer droplets had the lowest overall dissolution rate and cumulative dissolution. It is important to note that the overlap patterns resulted in a dosage form that was crystalline in the center and amorphous towards the peripheries. The multi-layer droplet was crystalline. In all cases, with the exception of the large droplet, the droplet dosage forms that were amorphous or

semi-amorphous in form had cumulative dissolution rates greater than the crystalline form. In all cases the larger individual droplets had larger total cumulative dissolution as compared to the smaller droplets.
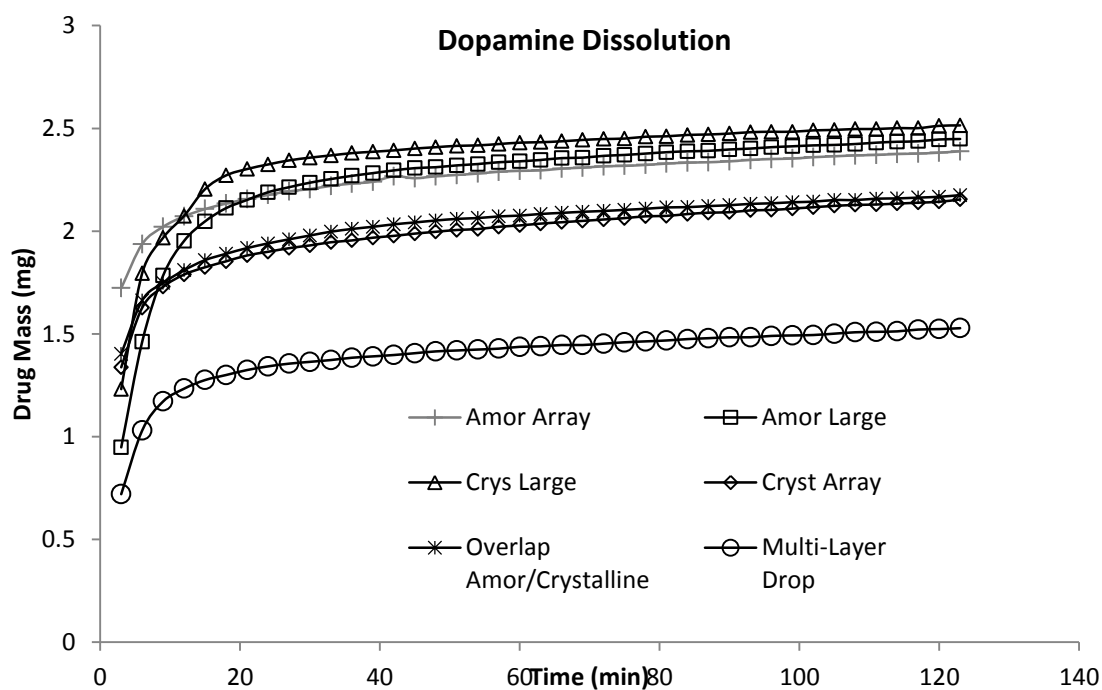
Figure 52: Dopamine Dissolution Profile (Cumulative Mass (g) versus Time)
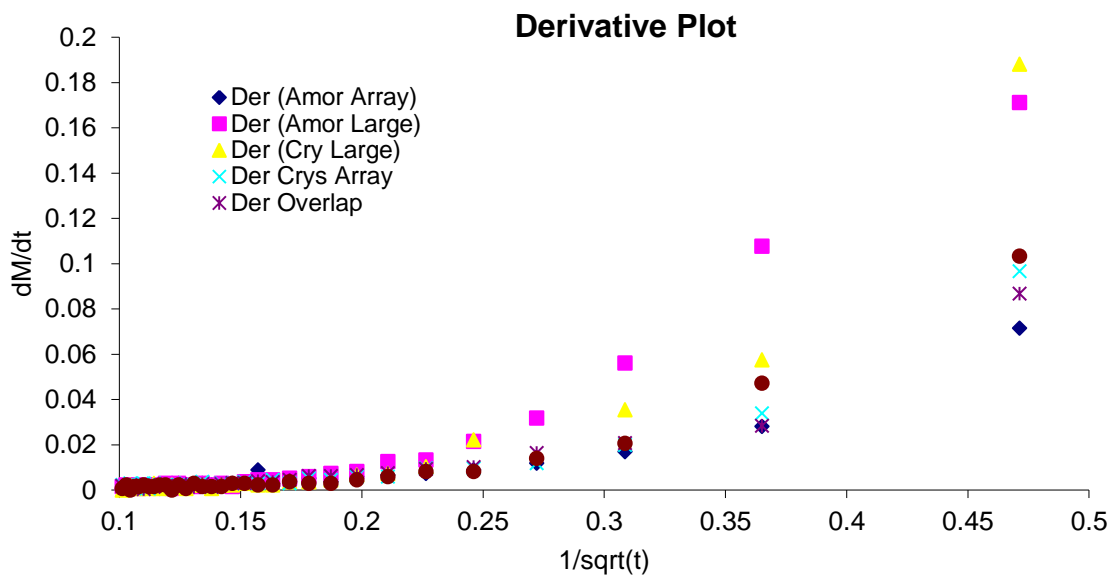
Figure 53: Derivative Plot of Dissolution Profiles

The cumulative data was plotted and fit according to two models. As previously explained, our dissolution data do not fit into the traditional models. We hypothesized that during the initial rapid dissolution the data fit our model of $\frac{J_p(t)}{\pi n r_0 DC} = 1 + \frac{n r_0^2}{\tau}$.

After the initial dissolution the data can be fit according to a first order model $J_t = k\ln(t) + C$. Plots A-F of Figure 54 show that we are able to obtain fits with R^2 values ≥ 0.99.
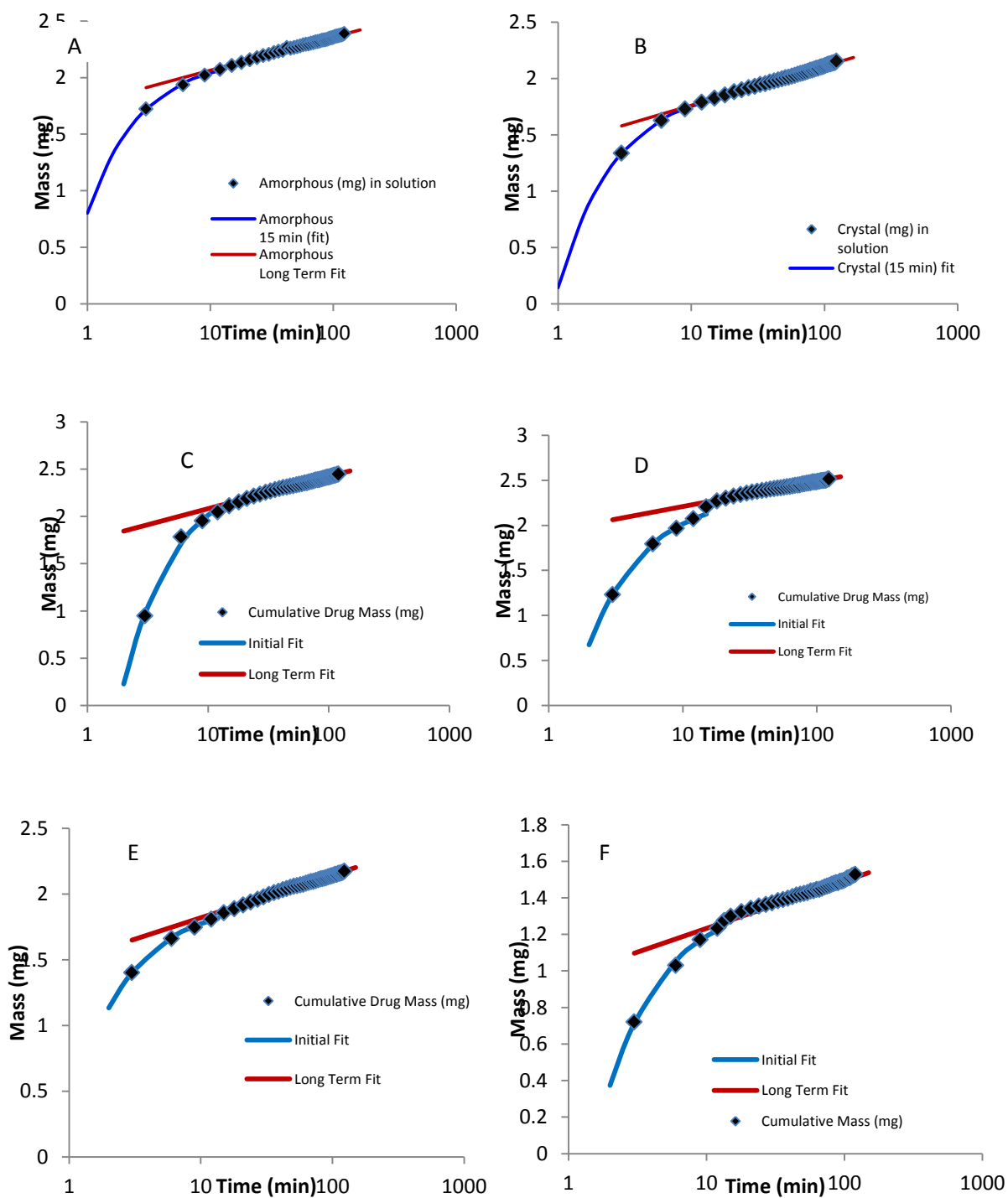
Figure 54: Fitting Data for Dopamine Dissolution Profiles (A-F). A: Amorphous Array, B:Crystal Array, C:Amorphous 3 mm Drop, D: Crystal 3mm Drop, E: Overlap Pattern, F: Multi-Layer (Pillar Droplet)

8   NOVEL TRANSDERMAL DOSAGE FORMS

Commercially there are three primary types of simple patch designs. These include the drug in adhesive, monolithic (drug in polymer matrix), and the drug reservoir designs. These simple designs are usually referred to as first generation patches [49,168,169]. To enhance diffusion of the API through the stratum corneum 2nd generation patches can be utilized [170]. 2nd Generation TDDs enhance the delivery of drugs through the stratum corneum by temporarily interrupting skin function and/or by creating a driving force to move the API through the epidermis [170].   These include chemical enhancers, iontophoresis, and applied heat [49]. Third generation enhancers, such as electroporation or micro-needles, transiently open up "pore-like" pathways in the barrier layer allowing larger and /or polar compounds to pass through[171].

Nicotine replacement therapy (NRT) gradually replaces the majority of the nicotine contained in cigarettes [73]. The goal of NRT is to reduce the incentive and cravings to smoke as well as reduce the nicotine withdrawal symptoms [73, 173]. The utilization of transdermal pathways for the delivery of nicotine for smoking cessation has been widely applied. Treatment of tobacco use can be difficult and long-term due to low patient compliance issues and the refractory attitude many patients have regarding therapy [174]. Schizophrenic patients have increased rates of smoking and decreased patient compliance; however there has not been significant research which studies the effects of dosage forms which contain both nicotine and anti-psychotic medications to deter smoking [175]. Additionally, many of the current design of transdermal systems require the use of an adhesive that the drug must diffuse through prior to reaching the skin. This,

in turn, increases the time from drug application to delivery at site of action, increases the amount of API needed, and increase the overall cost of the dosage form for the patient..

To alleviate some of the issues observed with traditional transdermal drug delivery we propose utilizing Drop-on-Demand technology to fabricate a novel dosage form where two or more drugs (nicotine and the anti-psychotic haloperidol used in the treatment of Tourette's syndromes) [176, 177] were printed onto the same layer to achieve desired efficacy effects. From data, we observed the effect of printing the adhesive adjacent to the dosage form and predicted the forms which would have the greatest and lowest drug release profiles. We created distinct transdermal dosage forms where (1) the adhesive is printed adjacent to the API droplet (2) the inter-droplet distance and volume of the API droplet is varied, and (3) two different drugs are printed onto the same layer.

8.1   Diffusion Model: Adhesive Patch

Mathematical models that can be used to calculate the API flux and movement of solute concentration are significant to scientist, biomedical engineers, and other health care professionals, because these models can predict the API mass transport to the intended target site [178]. Further, these models can provide insight into design optimization of drug delivery dosage forms to achieve the desired results. See Figure 55.
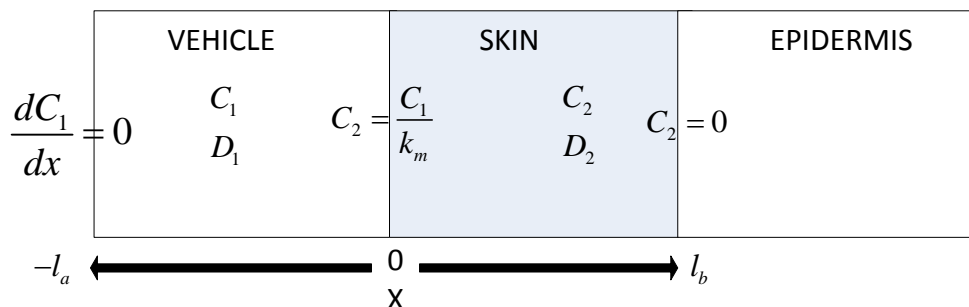
Figure 55: Simple Transdermal Diffusion Model [179].

A mathematical model using partial differential equations was utilized to examine the flux of a drug through the layers of a traditional transdermal patch compared to the modified patch developed using Drop on Demand technology. The standard transdermal model using Fick's 2nd law of diffusion describes the API concentration in the dosage form, C_1 , and in the skin, C_2 [179]. D_1 and D_2 describe the API diffusivity in the dosage form and in the skin [180]. If there is no drug in the skin initially and uniform distribution of the drug, we utilize the following initial equations[179]:

$$Q = \sqrt{(2C_0 - C_s)(C_s - Dt)} \tag{62}$$

This equation taken from Higuchi's result [9, 178] is based upon Q equaling the total amount of drug absorbed, C_0 is the initial drug loading and C_s is the drug solubility [178]. D is the diffusivity or diffusion coefficient of the drug.

 Yin explains that this model relies on the "pseudo-steady state" assumption where there is a linear concentration profile in the diffusion regime. [178]. In this model C_0 must be greater than C_s so that diffusion is controlled resulting in managed drug release rates [178]. If we assume perfect sink conditions, than we imply that the drug is removed or

absorbed immediately upon diffusing from the carrier [178]. This model is explained in Figure 56.
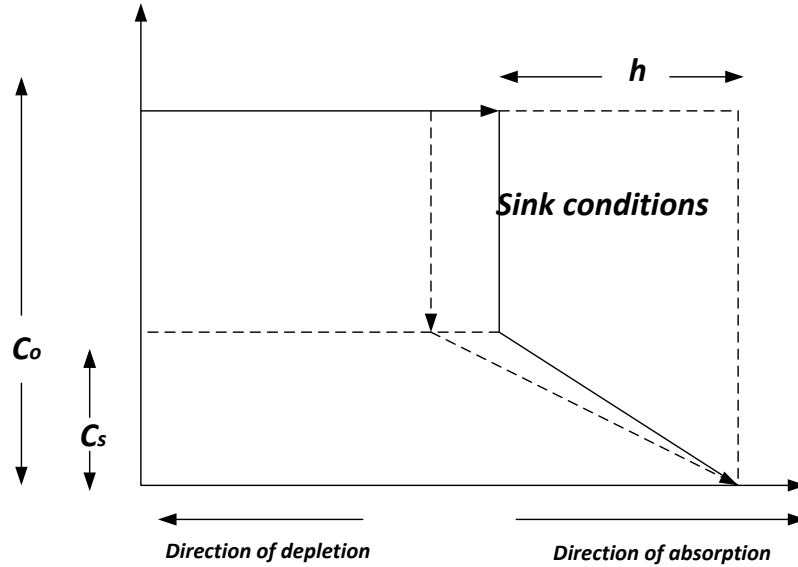
Figure 56: Pseudo steady state diffusion model. [178]

If we examine the release of drug from a granular matrix in a planar system Higuchi [9] expands his equation to

$$Q = \sqrt{\frac{D\varepsilon}{\tau}(2C_0 - C_s)(C_s - Dt}$$

(63)

where τ is the tortuosity factor and ε is the porosity of the matrix. ε or tortuosity is introduced to correct the granular matrix effect [178].

From Equation(62) we can obtain the drug release only using the parameters of the drug release system and time. The result here will align with experimental data where $C_0 \gg$ C_s and [178] diffusion controls the drug release. If C_0 approaches C_s, mass transport

can become significant [178]. In this case Paul and McSpaden [178, 181] simplified and applied the Stefan model to drug release processed from laminated and planar matrix[179]. From Fick's 2nd law we have:

$$\frac{\delta C}{\delta t} = D\frac{\partial^2 C}{\partial x^2}$$

(64)

Equation (64) is utilized as the principal equation in the diffusion between 0 and S(t) [178]. We utilize the following initial conditions [181]:

$$C(x,t) = 0, \ t = 0$$

(65)

$$C(x,t) = 0, \ x = 0$$

(66)

$$C(x,t) = 0, \ x = S(t)$$

(67)

Figure 57 displays the phenomenon where mass transport is the significant factor in the drug diffusion rate.
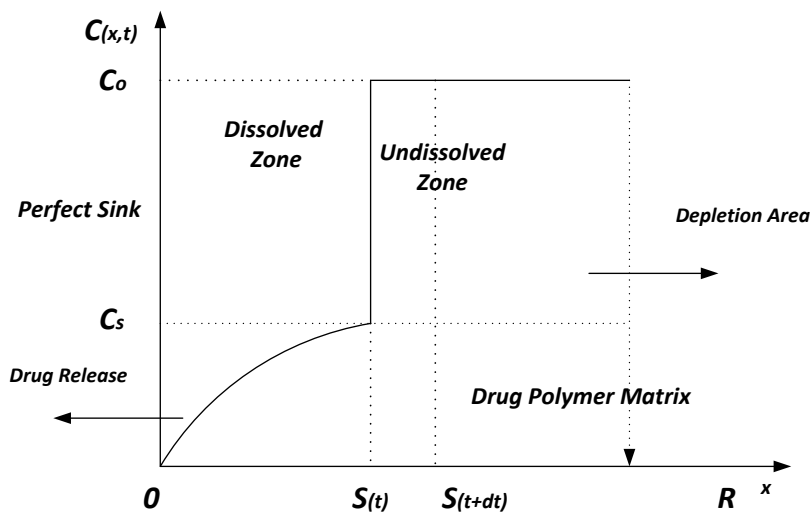
Figure 57: Mass Transfer dominated diffusion model. [178]

To examine the significance of printing the adhesive as a droplet adjacent to the API droplet, we solve the following partial differential equation using Matlab to visualize the differences in the diffusion. We found that the flux of the drug in our modified transdermal patch, where the adhesive layer was printed as drops and the diffusive pathway was separate from the drug layer, was much greater as compared to a traditional patch where the drug was immersed in adhesive (drug in adhesive patch). See

Figure 58. We utilize the following equation:

$$\frac{\partial C}{\partial t} = -\nabla\left(D\nabla c\right) = Q \tag{68}$$
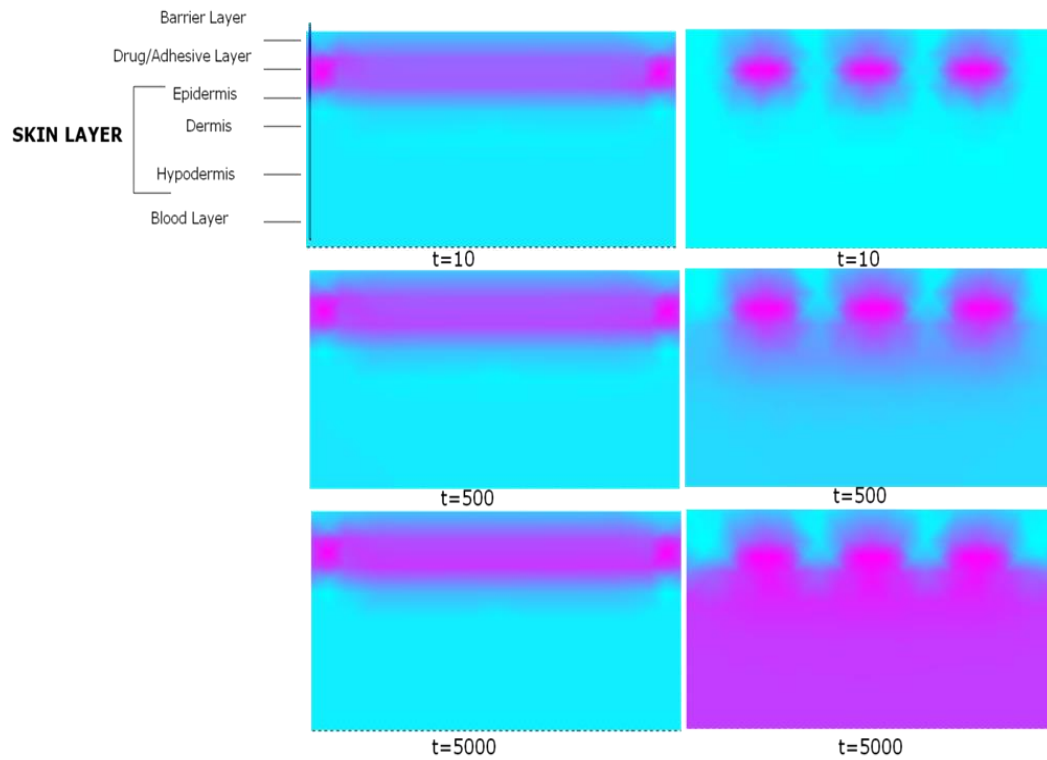
Figure 58: Drug Flux 2D Plot of Solution to Diffusion Equation

C is the drug concentration. D is the diffusion coefficient and Q is the volume source. The boundary conditions are defined as a general Neumann type where the flux is determined according to:

$$n(D\nabla(c)) + qc = g \tag{69}$$

Here q is the transfer coefficient and g is the flux. The solution for the partial differential equation for (1) traditional adhesive transdermal model where the drug is dispersed

throughout and (2) the novel system where the adhesive is printed adjacent to the API

droplet were plotted at select time points. See Figure 59.

Time=500   Color: c

Time=500   Color: c

Time=1500   Color: c

Time=1500   Color: c

Time=2500   Color: c

Time=2500   Color: c
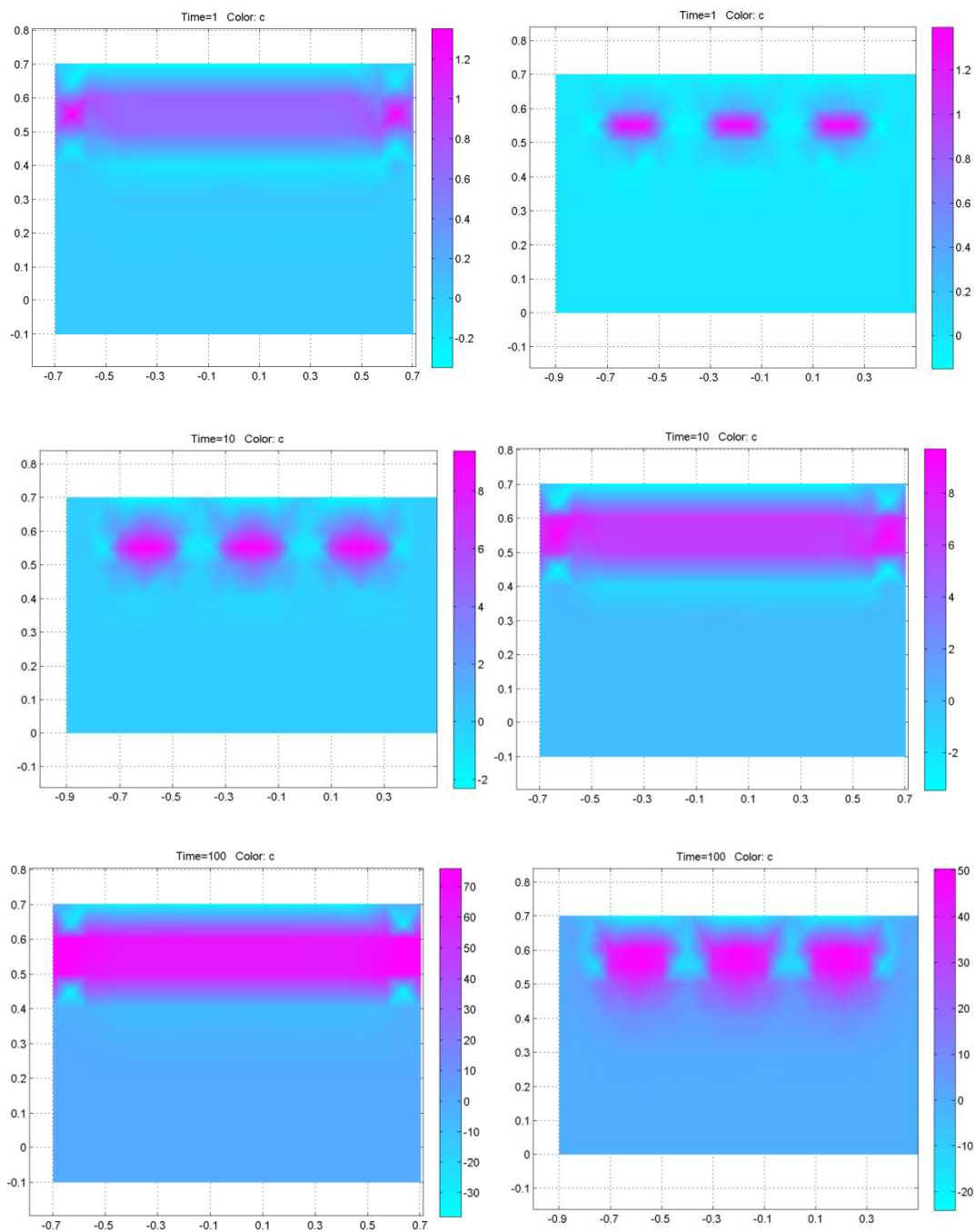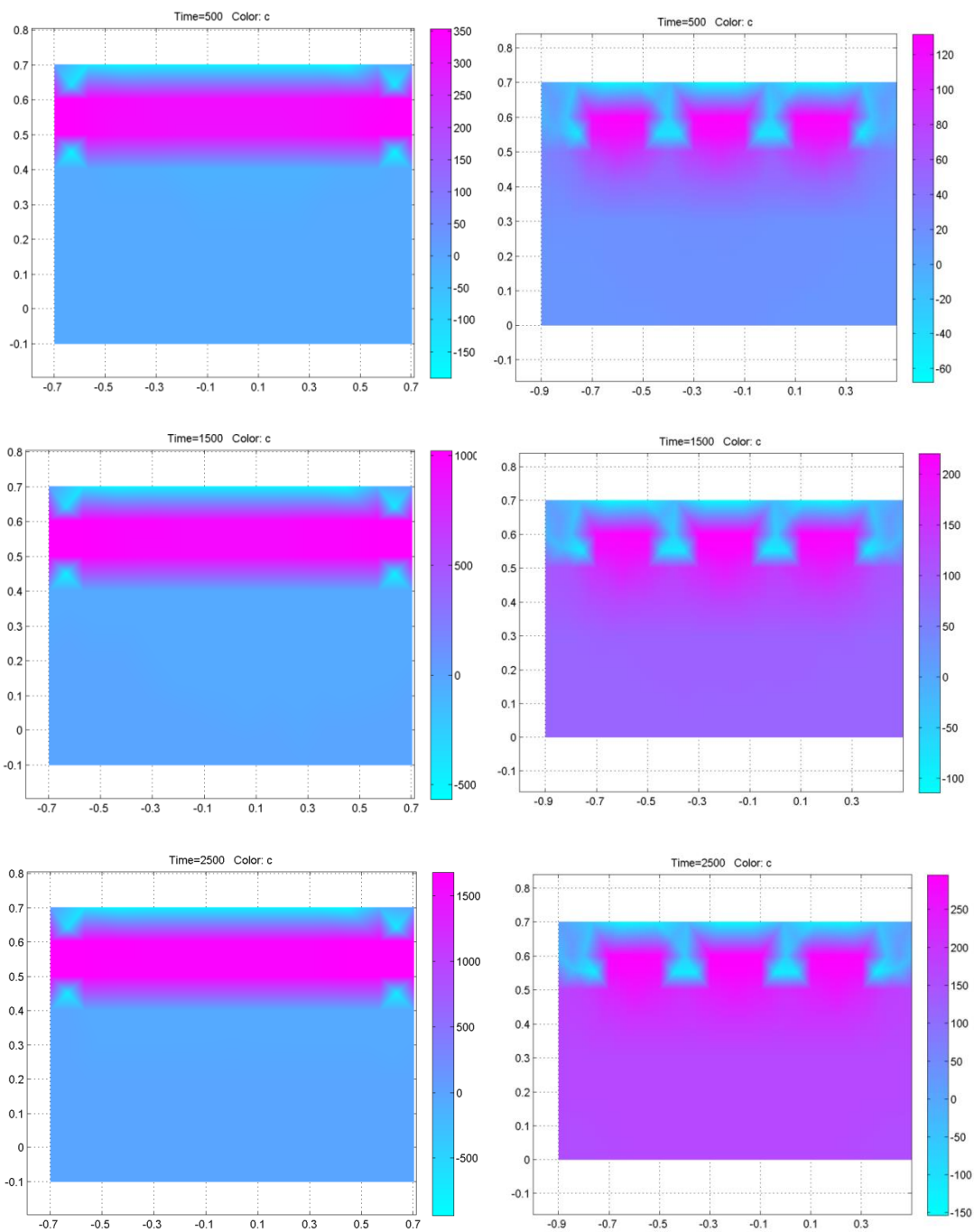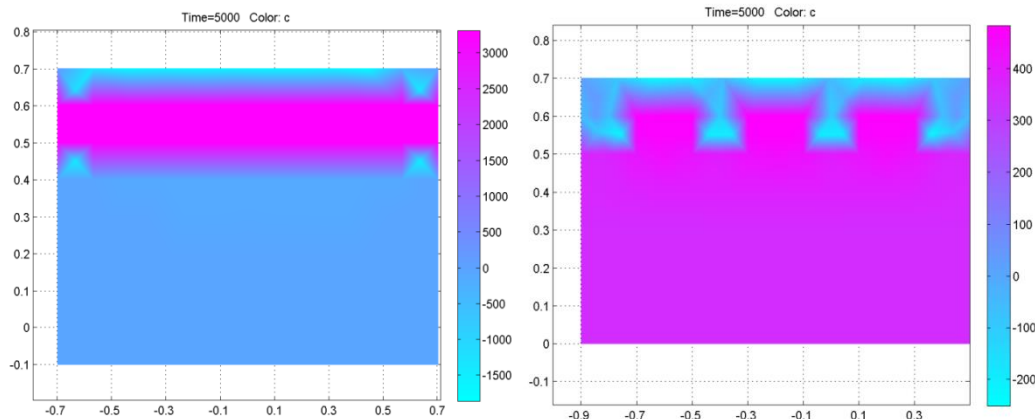
Figure 59: Plots of cumulative concentration over time for Traditional adhesive layer and Novel Adhesive Dosage Form

From Figure 59 we see that the flux in our transdermal system is larger as compared to the traditional system. The plots over time (t=10:5000) show that the cumulative concentration of drug is the traditional system slightly increases over time but does not fully traverse into the systemic circulation. The modified system has printed droplets where the diffusion coefficient ,D can up to 10-100 times greater as opposed to the traditional system, and the total penetration of the drug (represented by the darker purple color) cross into the systemic circulation as early at t=1500.

8.2 Drug Delivery Model Dosage Forms

In order to fabricate a feasible transdermal dosage form the following tasks were completed: (1)Deposition of API droplets onto polymer films to characterize the evaporation kinetics, droplet spreading, and final splat morphology, (2) Fabrication of a transdermal dosage form,(3) API dissolution of polymer from film, (4) Relationship of the dissolution rate of the drug with the structure of the biocompatible film, (5) the development of a foundation for the design dosage forms to obtain desired drug release rates, and (6) API diffusion of drug though PVDF membrane.

The transdermal drug dosage forms were created utilizing the Drop on Demand System Transdermal models formed were based upon the current commercial forms now available. The 4 basic models included: adhesive transdermal system (drug dispersed in adhesive), monolithic transdermal system (rate controlling membrane containing drug), reservoir drug system, and our model system where the adhesive and drug is printed (see Figure 60).
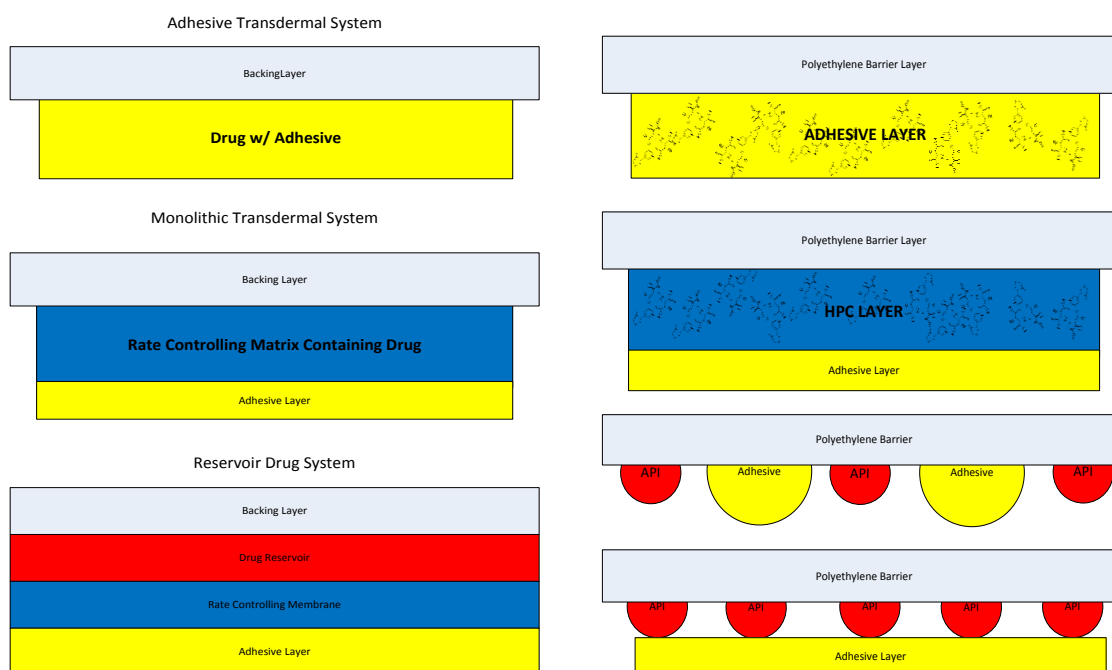
Figure 60: Schematic Representation on Experimental Transdermal Dosage Forms

A total of 0.5 mg of Nicotine was contained within each film. Current therapies of transdermal patches contain between 7 and 21 mg/day with patch sizes ranging from 3.5 – 30 cm^2. See Table 6 [43]. The formulation developed by our group contains a maximum 0.5 mg of nicotine due to the limitation of 19.62 mm (the area of the donor orifice) for diffusion studies. On larger film created for dissolution studies

(approximately 75*25 mm), the average dosage form contains approximately 20 mg of nicotine.

Drug molecular weight, melting point	Product Names	Main Use(s)	Available Strengths (dosing rates)	Customary duration of wear	Available sizes cm^2
Nicotine 162.2; liquid	Harbitrol	Assist in smoking cessation	7, 14, 21	16-24 hr	10,20,30
	Nicoderm		7, 14, 21		Unspecified
	Nicotrol		15		Unspecified
	Prostep		11, 22 mg/day		3.5, 7

Table 6 Adhesive Drug Delivery Systems [43]

8.3   Results – Nicotine Ditartrate Transdermal Forms

8.3.1   Optical Microscopy of Nicotine Ditartrate

Optical examination of the transdermal dosage forms was done immediately after printing occurred (See Figure 61) and after a time period of approximately 24 hrs. Examination of the optical images shows us that nicotine ditartrate and PMMA were successfully printed onto the polymer PE backing. The top images are of a 20% nicotine: water solution. The bottom images are of droplets of 20% (w:v) of nicotine solution with a thin layer (20 μL) of PMMA layered on top of the droplets. The drops of nicotine appear to be amorphous after drying; however the PMMA appears to have crystallized.
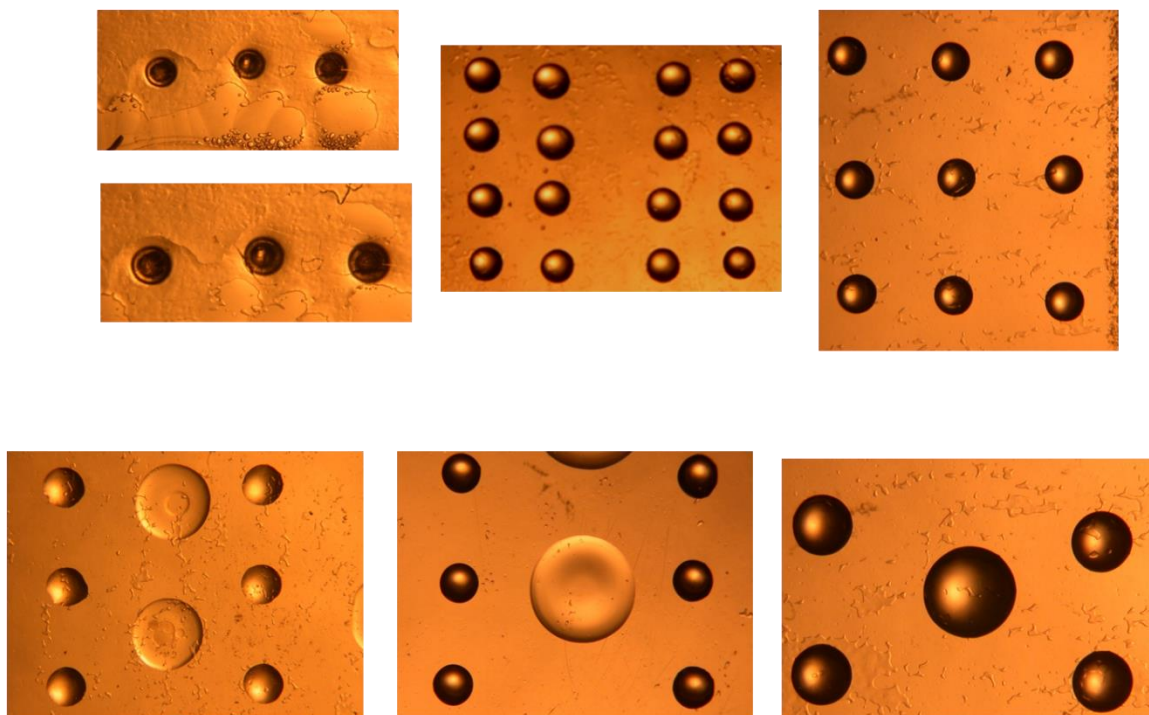
Figure 61: Top: Nicotine Ditartrate printed onto PE. Bottom: Nicotine ditartrate and PMMA printed onto PE.

8.3.2   XRD of Nicotine Droplets

X-ray diffraction analysis was done for the experimental nicotine transdermal dosage forms. Figure 62 shows the diffraction patterns for the pure nicotine and the nicotine embedded in HPC.
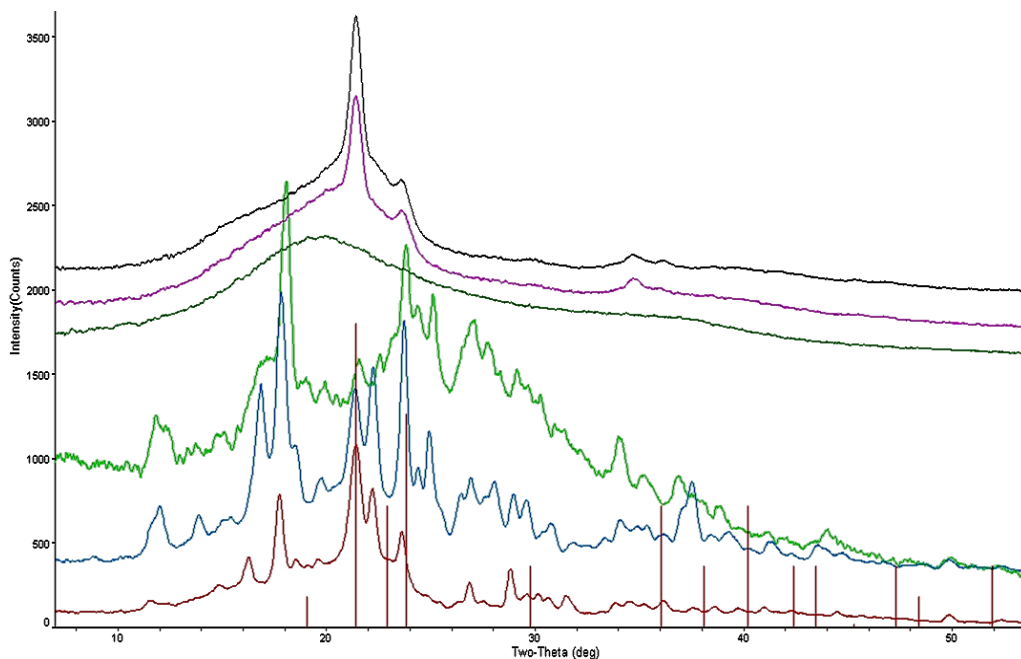
Figure 62: XRD of Nicotine Droplets on Poly Ethylene

"Nicotine drops" (on film or by themselves in a capillary) did not diffract and appear to be amorphous. "HPC imbedded w/ nicotine" sample also did not diffract (only the adhesive pattern is significant. Figure 63 shows the diffraction pattern of nicotine that has been layered with the adhesive PMMA.
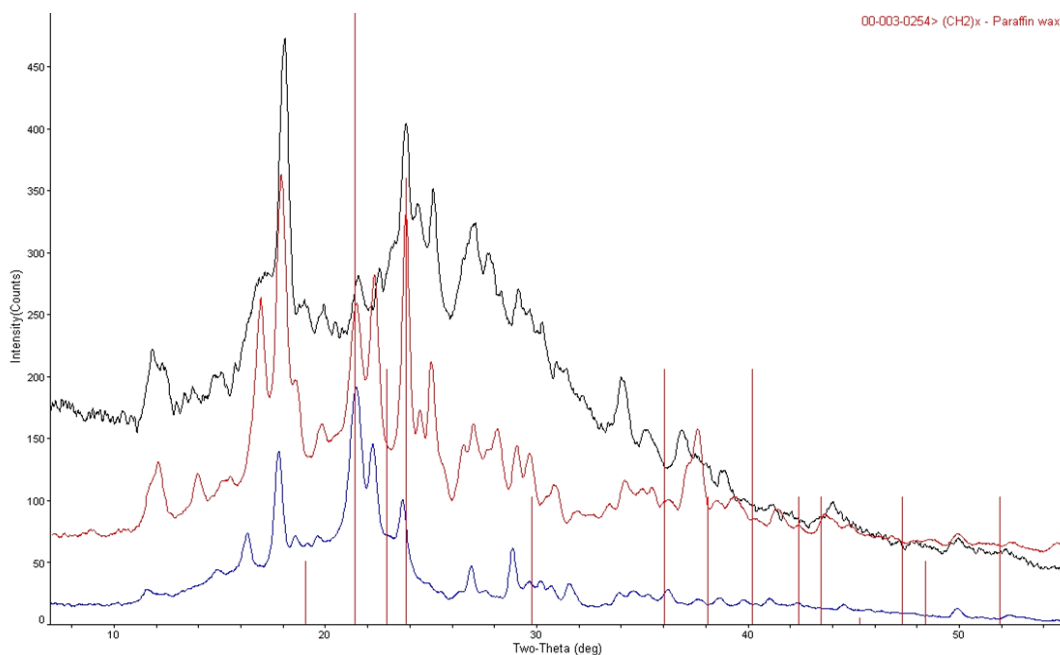
Figure 63: Nicotine Droplets layered with PMMA adhesive on Poly Ethylene

The nicotine drops w/ adhesive layer sample matches well with "nicotine ditartrate" powder. The nicotine imbedded in PMMA" sample is not identical to "nicotine drops w/ adhesive" sample, but could be a hydrated or dehydrated version of "nicotine drops w/ adhesive". The remaining samples (PVDF transfer membrane, PMMA on PE film, PE did not help to identify diffraction features in the other samples, mostly because the diffraction of these polymers is too diffuse. More could be done in the area of identifying the polymer in the films if desired, including different types of small-angle x-ray diffraction analyses.

8.3.3   Nicotine Patch Dissolution Studies

Dissolution tests of nicotine droplets were performed utilizing the HP Agilent/ Varian VK 7000 / 7010 Dissolution Apparatus. A total of 10 mg of nicotine was deposited onto

25* 6.25 mm PE films. The transdermal nicotine dosage forms consisted of the following specifications:

- o   80 5-microliter droplets of Nicotine dissolved in water
- o   125 microliter droplet of Nicotine embed in PMMA
- o   125 microliter droplet of Nicotine embedded in 2% HPC/water mixture layered with PMMA
- o   80 5-microliter droplets of Nicotine dissolved in water and layered with PMMA

The droplets were allowed to dry for 48 hours prior to being subjected to dissolution testing. Dissolution profiles for the 4 configuration profiles on PE film were plotted in Figure 64. The films were placed into rotating baskets at a speed of 250 rpm in 500 ml of distilled water.   The wavelength spectrum was set 259 and sample time point measurements will occurred every 10 minutes up to 24 hours.
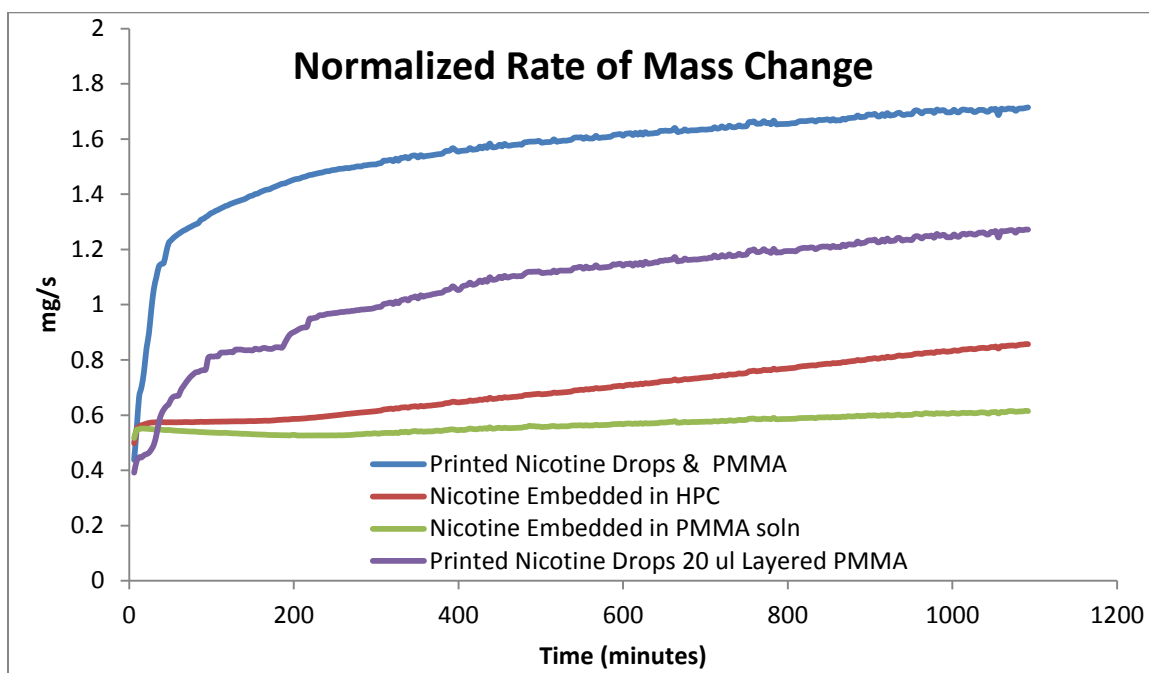
Figure 64: Nicotine Dissolution Studies

The plot shows that nicotine dissolution of samples embedded in PMMA and HPMC have a smaller normalized rate of mass change as compared to the printed nicotine drops. Overall, embedded nicotine had a smaller amount of drug released. The printed drops w/ printed adhesive layer had the greater overall release of nicotine.

8.3.4 Multi-Drug Dosage Form Dissolution Studies

To verify the ability of the DoD system to print multi-drug dosage forms, a dosage form containing the drug haloperidol and nicotine was created utilizing Drop-on-Demand-Technology. Alternating drops of nicotine and haloperidol solution were deposited onto PE film. A total of 5 mg and 3.75 mg of nicotine and haloperidol were deposited onto each patch, respectively. After printing dissolution experiments were done utilizing the USP Dissolution Apparatus I.

Mixtures of Haloperidol and Nicotine were done to obtain the calibration curve. See Plots in Figure 65.
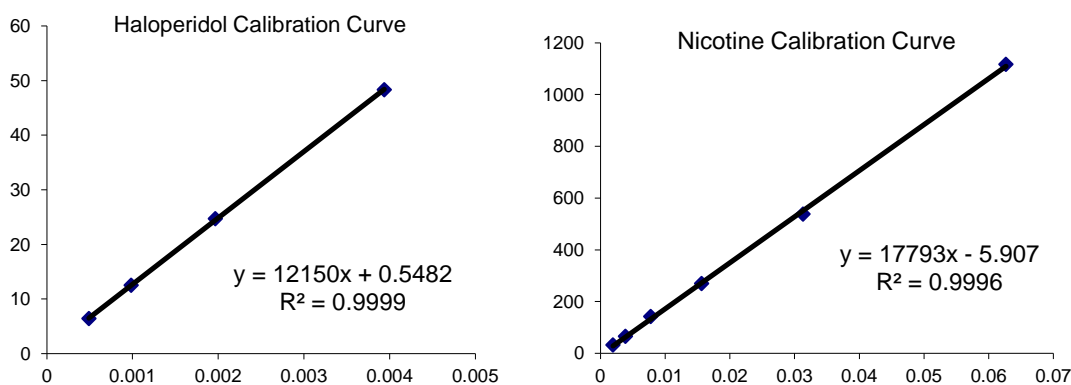
Figure 65: Nicotine Ditartrate and Haloperidol calibration curves

After the calibration fitting curve was complete, a mixed standard of nicotine and haloperidol was created by "spiking" the drug standards of nicotine with haloperidol. This calibration curve for the mixture is plotted in Figure 66.
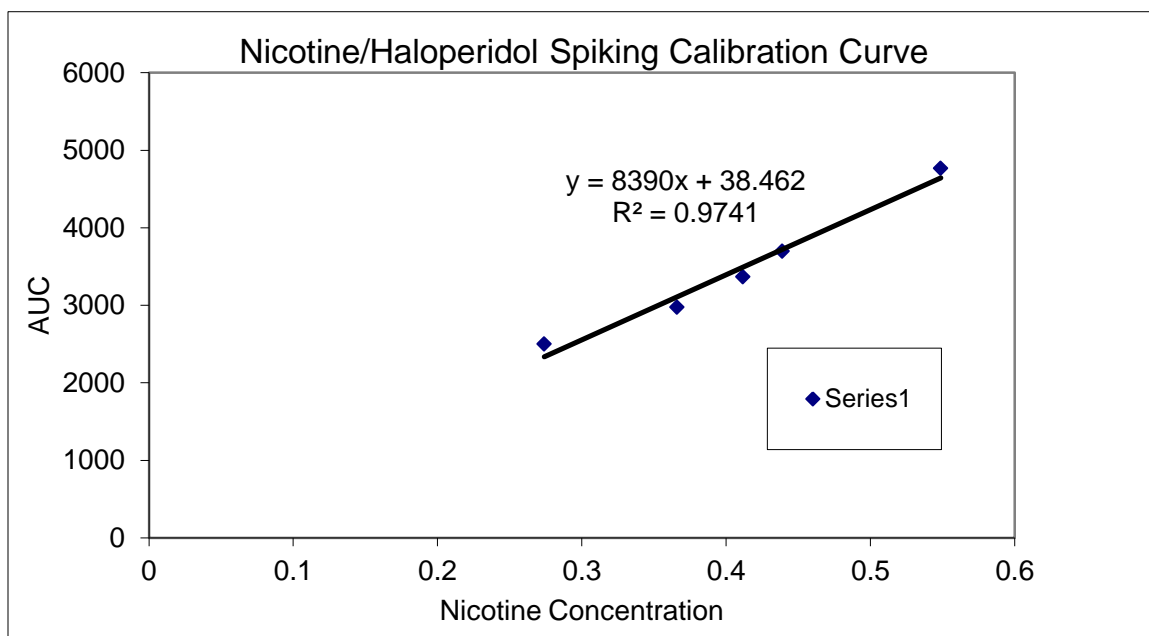
Figure 66: Calibration curve for Haloperidol and Nicotine as single dosage form

From the Haloperidol plot (Figure 67) we note that the majority of the drug is dissolved out of the dosage form within the first 5-20 minute time frame. It should be noted; however, that the haloperidol analysis was done utilizing HPLC. The UV detection limit was set at 230 nm and 259 for nicotine. Prior to performing HPLC analysis and determining the detection wavelength UV scans were done using the dissolution apparatus to determine the HPLC assay. It was found that nicotine has minute small peak around 230 nm. Haloperidol has peaks and 230 nm and peaks significantly at the detection wavelength for nicotine (259 nm). Attempts were made to decouple the

nicotine dissolution results from the haloperidol interference; however, we were not able to successfully perform this task. From the data we have gathered to date, we were able successfully print two dosage forms with the Drop-on-Demand systems and gather HPLC results indicating the presence of both drugs on one dosage form.
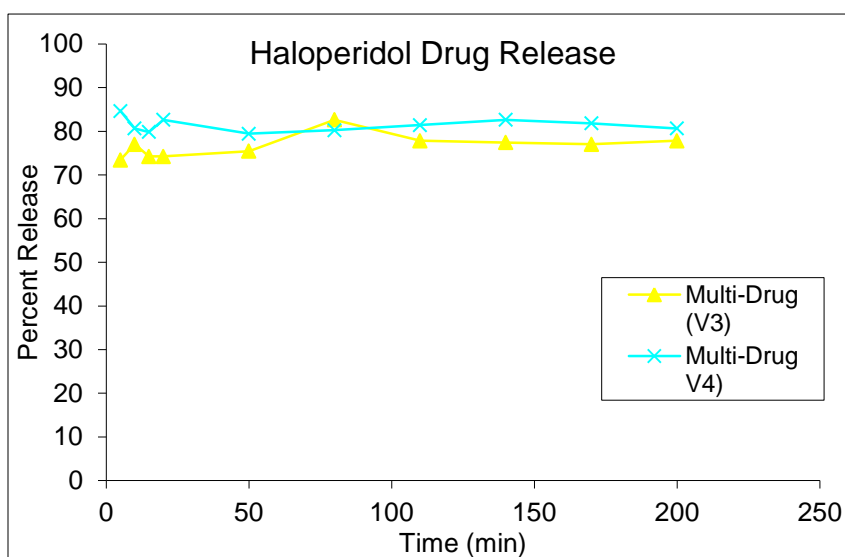
Figure 67: Haloperidol Release from Multi-Drug Dosage Form

8.3.5   Nicotine Franz Diffusion Cell Studies

Measurement of the amount of nicotine that crossed the membrane at short time intervals and the total amount of API that crossed the membrane over time of 24 hours were analyzed. Samples were prepared as described in the Materials & Methods Section. The tested samples included a 2*2 matrix, 2*2 matrix with layered adhesive, and a 3*2 matrix. The total amount of drug contained in each dosage form was 0.5 mg.
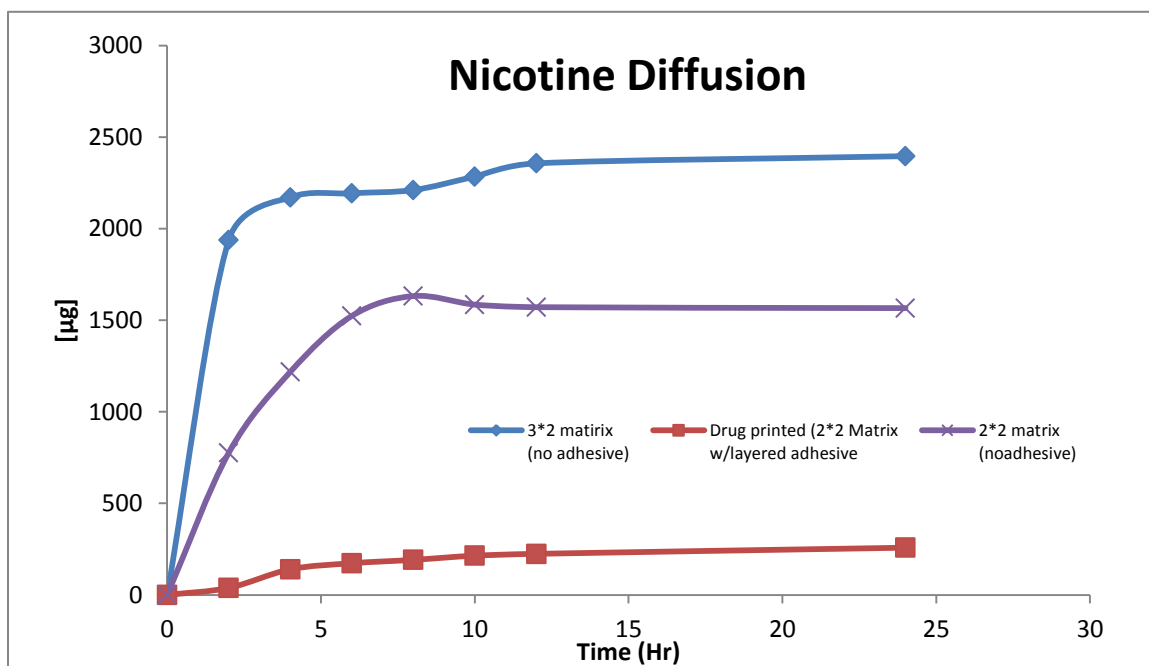
Figure 68: Nicotine Diffusion

The data shows that the engineered drug delivery systems where the drug was printed adjacent to the adhesive as an individual droplet experienced drug release totals that were up to four times greater than the dosage form that was layered with an adhesive. This is due to the fact that the diffusion pathway to the skin was shorter and was not impeded by an adhesive which can be difficult for the drug molecules to cross. The experimental results are in accordance with the theoretical computed Matlab results that show the modified transdermal system where the drug/adhesive is printed has an overall greater diffusion rate significantly greater than the traditional transdermal adhesive system.

9   CONCLUSION

We have successfully designed and implemented a mini manufacturing platform capable of printing drugs onto biopolymeric substrates. Utilizing ink Jet printing (IJP) our Drop on Demand (DoD) system prints drugs with greater precision and accuracy as compared to batch operation procedures. It is highly adaptable and can be used to print drug delivery systems with tunable properties. In addition it can be used to create DDS consisting of complex three-dimensional architecture which support controlled delivery useful in DDS such as transdermal drug delivery.

Our work details the interactions and spreading phenomena of the drug splat upon impingement onto varying substrates [182]. We have found that process parameters such as drug concentration, surface tension of drug solvent, and surface energy of substrate have a direct effect on spreading diameter and wetting phenomena[182]. In addition, we also have established that surface properties of the substrates can be manipulated to produce amorphous or crystalline structures, where drug accumulation can occur on the peripheries of the structure or in the center, upon droplet impingement [182]. Utilizing a DoD platform we deposited drops of dopamine solution onto the substrates glass, 0.0975% HPC, 0.0975% HPMC, and 2% HPC film. Substrate energy of edible substrate and surface tension of liquids have a direct impact on drug pattern. It was concluded that the surface energy of the substrate film is responsible for controlling the crystallinity of the final drug pattern. As surface tension increases crystals tend to form more readily in the drop upon impingement. Lower surface energy results in amorphous structures.

Edible thin films consisting of hydroxypropyl cellulose and polyethylene glycol were prepared and investigated for identification of adhesion mechanism type. SPM analysis of film surface morphology revealed porous irregular structures in which fluid could enter; however, the measured diameters were too small to permit capillary forces to contribute to adhesion. DSC and surface tension analysis determined the probable mechanism of adhesion was bonding through van der Waals interactions with L AB forces advancing of the work of adhesion.

Experimental data show that there is a direct correlation between both the concentration of HPC and PEG with surface energy parameters. The concentration of PEG in the polymer blend altered the surface energy parameters of the films compared to the pure HPC films that contained no PEG. In the films where PEG was present, increased concentrations resulted in increased Lewis Acid Base forces and decreased the LW interaction energies. Furthermore, a direct relationship was also found between PEG molecular weight and adhesion strength. Higher MW PEG and higher PEG concentration in the film produced stronger bonding between melted PEG droplets and the film substrate. These finding allow us to predict adhesion and surface energy characteristics facilitating the construction of polymer blend substrates with desired adhesion properties

Analysis of the data demonstrated that wettability properties of the substrates have a direct effect on the final structure of the splat and, in fact, determine spreading phenomena, evaporation kinetics, phase transition, crystallinity, and amorphous structure

The findings presented here are significant because they provide pharmaceutical manufacturers and drug compounders with a straightforward methodology to achieve controlled delivery using the surface adhesive properties of polymers. Drug sponsors and compounders can explore the use of HPC and PEG as modified biopolymeric substrates to increase the accuracy and control of dosage formulation while simultaneously attaining the desired adhesion properties. The fabrication of a DDS utilizing drop-on-demand technology in which both the dosage form and the rate of delivery can be manipulated through adhesive properties can provide a viable alternative to existing drug delivery mechanisms. This so-called drop-on-demand technology, applied to the manufacture of novel DDS(s), is convenient, precise, and offers enhanced cost effectiveness as compared to the current methodologies used in oral dosage drug delivery and formulation.

Dissolution

Deposition of drug solution via Ink Jet Technology can be used to predict and manipulate final drug structure resulting in control of the disintegration of the drug delivery system and API dissolution and bioavailability in vivo. Drop-On-Demand systems and other Ink Jet Printing avenues have recently emerged as a significant technology in the fabrication as templates for micro needles, microarrays for biomaterials, colloidal particles, and SEM devices [183, 184]. In these applications the ability to control the thickness and spatial arrangement of deposited solutes onto the thin film after the evaporation of the sessile drop is crucial. [184]. We have shown that utilizing drop on demand technology (DoD) and manipulating substrate properties we can control the morphology of the API droplet splat and obtain regimes ranging from amorphous to crystalline structures.

Our data indicates that the dissolution rate can be controlled by droplet volume/size, inter-droplet pattern spacing, and crystalline or amorphous droplet morphology.   We have found that the dissolution rate of amorphous structures will exceed that of crystalline structures and, therefore; we predict that amorphous structures will result in increased drug bioavailability and crystalline structures will results in an initial delayed drug release and an overall decreased initial bioavailability. Additionally we indicate that the larger droplet sizes actually have greater dissolution rates and overall cumulative API mass as compared to smaller droplets. Early studies have shown that deposition rate and pattern strongly affect the evaporation kinetics and final structure of the drug formulation. These findings are significant because this phenomenon can be used to design formulations of the same drug, excipients, and carriers that result in drastically different dissolution rates. The key attribute of this type of system is that the dissolution can be manipulated using the exact same drug and additives without the need for changing carriers, drug concentration, or additives to achieve the desired result.

Diffusion

In addition, we were successful in creating two distinct innovative transdermal dosage form where (1) two drugs, nicotine ditartrate and haloperidol, were printed onto the same transdermal patch   and (2) the adhesive is printed as drops in desired pattern negating the need for a separate adhesive layer. It is our understanding that the creation of a multi-drug transdermal form and a reservoir design patch using Drop-on-Demand Technology has not accomplished in prior works. From the computerized Matlab model of the printed adhesive dosage form, we see that this results in localized diffusion regions for

the API and significantly increases the rate of delivery as compared to the traditional reservoir patch with an adhesive layer. Further we also note that the given the same total drug concentration on a strip, formulations with more droplets will result in greater diffusion rates due to increased surface area and local diffusion areas.

These findings have direct applicability towards transdermal and oral drug delivery applications and has the potential to increase efficiency, reduce material and time costs, and enhance the overall manufacturing processes of many oral and transdermal DDS

Limitations

A novel transdermal system was manufactured using drop on demand technology. Although the system was successfully fabricated and dissolution profiles and transdermal diffusion of the API were experimentally measured, the mechanism of drug release from the transdermal system was not thoroughly investigated. As previously discussed, one aspect of my work focused on creating a novel transdermal dosage form where the adhesive is printed adjacent to the API droplet. In the traditional system the drug may be dispersed homogeneously throughout the adhesive or the API is contained within a reservoir of some type and the drug must transvers through the complete adhesive layer prior to reaching the epidermis. The mechanism of drug release and the rate of the drug release are dependent on a variety of factors including polymer type and adhesive in the construction of the transdermal dosage form. In constructing the transdermal form 2%HPC was utilized as the polymer and PMMA was utilized as the adhesive. The effect of the type of adhesive, concentration of adhesive, and thickness of adhesive was not studied experimentally. Additionally, the polymer used for the construction of the rate

controlling membrane was 2% HPC. Other concentrations were not studied experimentally. For these reasons; although the overall mass flux of the drug across the membrane was calculated; how the drug diffused through the membrane and the mechanism of diffusion was not thoroughly explored.

My research focuses on the fabrication of a nicotine transdermal form and a dopamine hydrochloride dosage form. The drugs chosen were both highly soluble in water and an optimum choice for delivery through drop on demand. The manufactured transdermal form generated was simple and based on passive diffusion and was not able to control or enhance the moisture uptake from the skin through formulation.

Also, a large number of the complex formulations used in transdermal dosage delivery to control the delivery rate cannot be constructed using Drop-on-Demnad (i.e.hydrogels, matrix reservoir systems, drug dispersed throughout the adhesive); however my research has proven that DoD technology can be feasibly used in the manufacture of delivery systems and provide greater prediction of dissolution and diffusion through accurate spatial patterning, and control of final splat radii and morphology.

Future Work

Future work includes examination the utilization of the drop-on-demand system for complex drug delivery systems that do not rely simply on passive diffusion. The mechanism of drug diffusion and how the drop on demand system can be used to manipulate, develop, or influence current mechanisms of drug release should be explored. Additionally multipart and complex API(s) should be studied for use with the DoD

System. Mathematically, the effect of the inter-droplet distance examined in the dissolution of the API should be compared and applied to the transdermal dosage form to observe if any correlation exists.

REFERENCES

1. *The New Science of Personalized Medicine: Translating the Promise into Practice* 2009, Price Waterhouse Coopers.
2. Deakin, D., *Personalized Medicine.* 2011.
3. Jørgensen, J.T., *From blockbuster medicine to personalized medicine.* Personalized Medicine, 2007. **5**(1): p. 55-63.
4. Volgelson, *Advances in Drug Delivery.* Modern Drug Discovert, 2001. **4**: p. 49-52.
5. Florence, A.T.a.J.S., ed. *Modern Pharmaceutics: Applications and Advances*. Vol. 5. 2009, Informa Healthcare USA: New York, NY. 511.
6. Lee, T. and J. Robinson, *In Remington: The science and practice of pharmacy; Gennaro, Ed.* Lippincott Williams and Wilkins: Baltimore, 2000. **2**: p. 903-929.
7. Crank, J., ed. *The mathematics of Diffusion*. 1975, Clarendon Press: Oxford.
8. Fan, L.-t. and S.K. Singh, *Controlled release: A quantitative treatment*. 1989: Springer-Verlag Berlin.
9. Higuchi, T., *Rate of release of medicaments from ointment bases containing drugs in suspension.* Journal of Pharmaceutical Sciences, 1961. **50**(10): p. 874-875.
10. Siepmann, J. and F. Siepmann, *Mathematical modeling of drug delivery.* International Journal of Pharmaceutics, 2008. **364**(2): p. 328-343.
11. Tiwari, R. and P. Takhistov, *Nanotechnology-enabled delivery systems for food functionalization and fortification.* Nanotechnology research methods for foods and bioproducts. Wiley-Blackwell, Oxford, 2012: p. 55-101.
12. Kamath, K. and K. Park, *Biodegradable hydrogels in drug delivery.* Advance Drug Delivery Review, 1993: p. 59-84.
13. Linhardt, R.J., *Biodegradable polymers for controlled release of drugs.* Controlled Release of Drugs: Polymers and Aggregate Systems, edited by M. Rosoff, 1988: p. 53-95.
14. Aouada, F.A., et al., *Biodegradable hydrogel as delivery vehicle for the controlled release of pesticide.* Pesticides—formulations, effects, fate. CC BY-NC-SA, 2011.
15. Peppas, N.A. and Lowman, *Hydrogels encyclopedia of controlled drug delivery*, ed. E. Mathiowitz. 1999, Wiley.
16. Kaparissides, C., et al., *Recent advances in novel drug delivery systems.* Journal of Nanotechnology Online, 2006. **2**: p. 1-11.
17. Lee, e.a., *Trends and Future Perspectives in Peptides and Proteins Drug Delivery.* Harwood Chur, 1995.
18. Peppas, N.A., et al., *Hydrogels in pharmaceutical formulation.* European Journal of Pharmaceutics and Biopharmaceutics, 2000. **50**: p. 27-46.
19. Fix, J., A, *Oral controlled release technology for peptides: Status and future prospects.* Pharmaceutical Research, 1996. **13**: p. 1760-1764.
20. Plate, N., A., Valuev, L1., Starosel'tseva, L, K., Valueva, T, A., Vanchugova, L, V., UI'yanova, M, V., Valuev, I, L., Sytov, G, A., Ametov, A, S., Knyazhev, V, A, *Macromolecular systems containing insulin as related to the problem of diabetes.* Polymer Science, 1994. **36**: p. 1581-1585.

21. Kopece, J., Kopeckova, P., Omelyanenko, V, *Biorecognizable biomedical polymers: Advanced biomaterials. In Biomedical and Drug Delivery Systems*, in *Springer*, N. Ogata, Kim, S, W, Feijen, J., Okano, T, Editor. 1996: Tokyo. p. 91-95.

22. Paolino, D., et al., *Drug delivery systems.* Encyclopedia of Medical Devices and Instrumentation, 2006.

23. *Ansel 's Pharmaceutical Dosage Forms and Drug Delivery Systems, 9th Edition.* Journal of Pharmacy Technology, 2010. **26**(3): p. 167-168.

24. Zuo, Z. and V.H. Lee, *Pharmacokinetic Considerations: Methods and Systems of Controlled Drug Delivery.* Chemical Biology: Approaches to Drug Discovery and Development to Targeting Disease: p. 147-164.

25. Peer, D., et al., *Nanocarriers as an emerging platform for cancer therapy.* Nat Nano, 2007. **2**(12): p. 751-760.

26. Vogelhuber, W., et al., *Programmable biodegradable implants.* Journal of Controlled Release, 2001. **73**(1): p. 75-88.

27. Wu, J., G. Huang, and Z. Hu, *Interparticle potential and the phase behavior of temperature-sensitive microgel dispersions.* Macromolecules, 2003. **36**(2): p. 440-448.

28. Das, M., H. Zhang, and E. Kumacheva, *Microgels: old materials with new applications.* Annu. Rev. Mater. Res., 2006. **36**: p. 117-142.

29. Divyesh, P., et al., *Transdermal delivery System: An overview.* International Journal of Biopharmaceutical & Toxicological Research, 2011. **1**(1): p. 61-80.

30. Chandra, S. and C. Avedisian, *On the collision of a droplet with a solid surface.* Proceedings: Mathematical and Physical Sciences, 1991: p. 13-41.

31. Ranade, V.V. and J.B. Cannon, *Drug delivery systems*. 2011: CRC press.

32. Elias, P.M., *Epidermal lipids, membranes, and keratinization.* International journal of dermatology, 1981. **20**(1): p. 1-19.

33. Katz, M. and B.J. Poulsen, *Corticoid, vehicle and skin interaction in percutaneous absorption.* J Soc Cosmet Chem, 1972. **23**: p. 565-590.

34. Barr, M., *Percutaneous absorption.* Journal of Pharmaceutical Sciences, 1962. **51**(5): p. 395-409.

35. Ranade, V.V., *Drug delivery systems. 6. Transdermal drug delivery.* The Journal of Clinical Pharmacology, 1991. **31**(5): p. 401-418.

36. Chien, Y.W., ed. *Transdermal Controlled Systemic Medication*. Drugs and the Pharmaceutical Sciences, ed. J. Swarbrick. 1987: Chapel Hill.

37. Mikszta, J.A., et al., *Improved genetic immunization via micromechanical disruption of skin-barrier function and targeted epidermal delivery.* Nature medicine, 2002. **8**(4): p. 415-419.

38. Williams, A.C. and B.W. Barry, *Penetration enhancers.* Advanced drug delivery reviews, 2012.

39. Katstra, W.E., *Fabrication of complex oral drug delivery forms by Three Dimensional Printing (tm).* 2001, Massachusetts Institute of Technology.

40. Chien, Y.W., *Development of transdermal drug delivery systems.* Drug Development and Industrial Pharmacy, 1987. **13**(4-5): p. 589-651.

41. Sitruk-Ware, R., *Transdermal delivery of steroids.* contraception, 1989. **39**(1): p. 1-20.

42. Siepmann, J., R. Siegel, and F. Siepmann, *Diffusion Controlled Drug Delivery Systems*, in *Fundamentals and Applications of Controlled Release Drug Delivery*, J. Siepmann, R.A. Siegel, and M.J. Rathbone, Editors. 2012, Springer US. p. 127-152.

43. Flynn, G.L., *Cutaneous and transdermal delivery-processes and systems of delivery.* Modern pharmaceutics, 2002. **2**.

44. Williams, A., *Transdermal and topical drug delivery: from theory to clinical practice*. 2003: Pharmaceutical Press.

45. Gentile, F., et al., *A doublet mechanics model for the ultrasound characterization of malignant tissues.* Journal of Biomedical Science & Engineering, 2011. **4**(5).

46. Silver, F.H., *Mechanosensing and mechanochemical transduction in extracellular matrix: biological, chemical, engineering, and physiological aspects*. 2006: Springer.

47. Silver, F.H., *Microscopic and macroscopic structure of tissues.* Mechanosensing and Mechanochemical Transduction in Extracellular Matrix: Biological, Chemical, Engineering, and Physiological Aspects, 2006: p. 76-119.

48. Bronaugh, R.L. and H.I. Maibach, *Percutaneous Absorption: Drugs--Cosmetics--Mechanisms--Methodology: Drugs--Cosmetics--Mechanisms--Methodology*. 1999: Informa Healthcare.

49. Wilson, E.J., *Three Generations: The Past, Present, and Future of Transdermal Drug Delivery Systems.*

50. Scheuplein, R., *Blank, 1. H., Brauner, GJ and Mac Farlane, DJ, 1969, Percutaneous absorption of steroids.* J. Invest. Derrn. **52**: p. 63-70.

51. Scheuplein, R.J., *Mechanism of percutaneous absorption.* Journal of Investigative Dermatology, 1967. **48**(1): p. 79-88.

52. Anderson, R.L. and J.M. Cassidy, *Variations in physical dimensions and chemical composition of human stratum corneum.* Journal of Investigative Dermatology, 1973. **61**(1).

53. Elias, P.M., N.S. Mcnutt, and D.S. Friend, *Membrane alterations during cornification of mammalian squamous epithelia: A freeze‐fracture, tracer, and thin‐section study.* The Anatomical Record, 1977. **189**(4): p. 577-593.

54. Sun, Y.-M., et al., *Composite poly (2-hydroxyethyl methacrylate) membranes as rate-controlling barriers for transdermal applications.* Biomaterials, 1997. **18**(7): p. 527-533.

55. Ginsburg, G.S. and H.F. Willard, *Genomic and personalized medicine: foundations and applications.* Translational Research, 2009. **154**(6): p. 277-287.

56. Haselden, J.N. and A.W. Nicholls, *Personalized medicine progresses.* Nat Med, 2006. **12**(5): p. 510-511.

57. Springen, K., Underwood, Anne, *Medicine Tailored Just for You.* Newsweek, 2005. **145**(26A): p. 76-79.

58. Abrahams, E., G.S. Ginsburg, and M. Silver, *The Personalized Medicine Coalition.* American Journal of Pharmacogenomics, 2005. **5**(6): p. 345-355.

59. [cited 2013; Available from: www.picojet.com.

60. Cooley, P., D. Wallace, and B. Antohe, *Applicatons of ink-jet printing technology to BioMEMS and microfluidic systems.* Journal of the Association for Laboratory Automation, 2002. **7**(5): p. 33-39.

61.   WILLIAMS, C., *Ink-jet technology moves beyond paper.* Paintindia, 2006. **56**(10).

62.   Pardo, L., W.C. Wilson, and T. Boland, *Characterization of patterned self-assembled monolayers and protein arrays generated by the ink-jet method.* Langmuir, 2003. **19**(5): p. 1462-1466.

63.   Basaran, O.A., *Small-scale free surface flows with breakup: Drop formation and emerging applications.* AIChE Journal, 2002. **48**(9): p. 1842-1848.

64.   Onose, G., et al., *Recent advancements in biomaterials for spinal cord injury complex therapeutics.* Digest J Nanomater Biostruct, 2008. **2**(4): p. 307-314.

65.   Boland, T., et al., *Application of inkjet printing to tissue engineering.* Biotechnology journal, 2006. **1**(9): p. 910-917.

66.   Xu, T., et al., *Inkjet printing of viable mammalian cells.* Biomaterials, 2005. **26**(1): p. 93-99.

67.   Ganan-Calvo, A.M., et al., *Straightforward production of encoded microbeads by Flow Focusing: Potential applications for biomolecule detection.* International Journal of Pharmaceutics, 2006. **324**(1): p. 19-26.

68.   Sahay, A., et al., *Automated Drop-on-Demand System with Real-Time Gravimetric Control for Precise Dosage Formulation.* Journal of Laboratory Automation, 2013. **18**(2): p. 152-160.

69.   Umbanhowar, P.B., V. Prasad, and D.A. Weitz, *Monodisperse Emulsion Generation via Drop Break Off in a Coflowing Stream.* Langmuir, 2000. **16**(2): p. 347-351.

70.   Chen, A.U. and O.A. Basaran, *A new method for significantly reducing drop radius without reducing nozzle radius in drop-on-demand drop production.* Physics of Fluids, 2002. **14**(1): p. L1-L4.

71.   Stachowiak, J.C., et al., *Dynamic control of needle-free jet injection.* Journal of Controlled Release, 2009. **135**(2): p. 104-112.

72.   Sastry, S.V., J.R. Nyshadham, and J.A. Fix, *Recent technological advances in oral drug delivery–a review.* Pharmaceutical science & technology today, 2000. **3**(4): p. 138-145.

73.   ; Available from: www.ncbi.nim.nih.gov.

74.   Tarcha, P., et al., *The Application of Ink-Jet Technology for the Coating and Loading of Drug-Eluting Stents.* Annals of Biomedical Engineering, 2007. **35**(10): p. 1791-1799.

75.   Sastry, S.V., J.R. Nyshadham, and J.A. Fix, *Recent technological advances in oral drug delivery - a review.* Pharmaceutical Science & Technology Today, 2000. **3**(4): p. 138-145.

76.   Siddiqui, S.A., et al., *Vibrational dynamics and potential energy distribution of two well-known neurotransmitter receptors: tyramine and dopamine hydrochloride.* Journal of Theoretical and Computational Chemistry, 2009. **8**(03): p. 433-450.

77.   Reichmann, H., *Transdermal delivery of dopamine receptor agonists.* Parkinsonism & related disorders, 2009. **15**: p. S93-S96.

78.   Giuliano, F., et al., *Pro-erectile effect of systemic apomorphine: existence of a spinal site of action.* The Journal of urology, 2002. **167**(1): p. 402-406.

79. Giuliano, F., c. ois, and J. Allard, *Dopamine and male sexual function.* European urology, 2002. **40**(6): p. 601-608.

80. Fathi Azarbayjani, A., et al., *Transdermal delivery of haloperidol by proniosomal formulations with non-ionic surfactants.* Biological and Pharmaceutical Bulletin, 2009. **32**(8): p. 1453-1458.

81. Ren, C., et al., *Effect of permeation enhancers and organic acids on the skin permeation of indapamide.* International Journal of Pharmaceutics, 2008. **350**(1): p. 43-47.

82. Phillies, G.D., et al., *Mode structure of diffusive transport in hydroxypropylcellulose: water.* The Journal of chemical physics, 2003. **119**(18): p. 9903-9913.

83. Microchem. 2013 [cited 2013 10/25/2013].

84. Mohajerani, E., et al., *Morphological and thickness analysis for PMMA spin coated films.* Journal of Optoelectronics and Advanced Materials, 2007. **9**(12): p. 3901.

85. Luner, P.E. and E. Oh, *Characterization of the surface free energy of cellulose ether films.* Colloids and Surfaces A: Physicochemical and Engineering Aspects, 2001. **181**(1-3): p. 31-48.

86. Van Oss, C.J., *Interfacial forces in aqueous media*. 2006: CRC press.

87. Young, T., *An essay on the cohesion of fluids.* Philosophical Transactions of the Royal Society of London, 1805. **95**: p. 65-87.

88. Zhao, Q., Y. Liu, and E. Abel, *Effect of temperature on the surface free energy of amorphous carbon films.* Journal of Colloid and Interface Science, 2004. **280**(1): p. 174-183.

89. Zhao, Q., et al., *Effect of surface free energy on the adhesion of biofouling and crystalline fouling.* Chemical Engineering Science, 2005. **60**(17): p. 4858-4865.

90. Freitas, A.M. and M.M. Sharma, *Detachment of particles from surfaces: an AFM study.* Journal of Colloid and Interface Science, 2001. **233**(1): p. 73-82.

91. Good, R.J., *Contact angle, wetting, and adhesion: a critical review.* Journal of adhesion science and technology, 1992. **6**(12): p. 1269-1302.

92. Bonn, D., et al., *Wetting and spreading.* Reviews of modern physics, 2009. **81**(2): p. 739.

93. Menczel, J.D. and R.B. Prime, *Thermal analysis of polymers, fundamentals and applications*. 2009: John Wiley & Sons.

94. Clas, S.-D., C.R. Dalton, and B.C. Hancock, *Differential scanning calorimetry: applications in drug development.* Pharmaceutical science & technology today, 1999. **2**(8): p. 311-320.

95. Huynh, P.T., *Solvent-Free Beta-Carotene Nanoparticles for Food Fortification*, in *Food Science*. 2012, Rutgers: New Brunswick. p. 219.

96. Kuru, K. and S. Girgin, *A bilinear interpolation based approach for optimizing hematoxylin and eosin stained microscopical images*, in *Pattern Recognition in Bioinformatics*. 2011, Springer. p. 168-178.

97. Macrae, C.F., et al., *Mercury CSD 2.0-new features for the visualization and investigation of crystal structures.* Journal of Applied Crystallography, 2008. **41**(2): p. 466-470.

98. Snyder, R.L., J. Fiala, and H.J. Bunge, *Defect and microstructure analysis by diffraction*. 1999: Oxford University Press Oxford.

99. Siewert, M., et al., *FIP/AAPS guidelines to dissolution/in vitro release testing of novel/special dosage forms*. AAPS PharmSciTech, 2003. **4**(1): p. 43-52.

100. Sakellariou, P. and R.C. Rowe, *Interactions in cellulose derivative films for oral drug delivery*. Progress in Polymer Science, 1995. **20**(5): p. 889-942.

101. Li, S., D.S. Jones, and G.P. Andrews, *Hot Melt Extrusion: A Process Overview and Use in Manufacturing Solid Dispersions of Poorly Water-Soluble Drugs*. Drug Delivery Strategies for Poorly Water-Soluble Drugs, 2012: p. 325-358.

102. Bajdik, J., et al., *The effect of the solvent on the film-forming parameters of hydroxypropyl-cellulose*. International Journal of Pharmaceutics, 2005. **301**(1): p. 192-198.

103. Wake, W.C., *Theories of adhesion and uses of adhesives: a review*. Polymer, 1978. **19**(3): p. 291-308.

104. Comyn, J., *Theories of adhesion*. Handbook of Adhesives and Sealants, 2006. **2**: p. 1-50.

105. De Boer, M. and P. De Boer, *Thermodynamics of capillary adhesion between rough surfaces*. Journal of Colloid and Interface Science, 2007. **311**(1): p. 171-185.

106. Ata, A., Y.I. Rabinovich, and R.K. Singh, *Role of surface roughness in capillary adhesion*. Journal of adhesion science and technology, 2002. **16**(4): p. 337-346.

107. Erbil, H., *Solid and Liquid Interfaces*. 2006: Blackwell Publishing, Oxford.

108. Dudowicz, J., K.F. Freed, and J.F. Douglas, *New patterns of polymer blend miscibility associated with monomer shape and size asymmetry*. The Journal of Chemical Physics, 2002. **116**(22): p. 9983-9996.

109. Utracki, L.A., ed. *Polymer Blends Handbook*. Vol. 1. 2002, Kluwer Academic Publishers. 651.

110. Qiu, Y., et al., *Developing solid oral dosage forms: pharmaceutical theory & practice*. 2009: Academic Press.

111. Schwahn, D., *Critical to Mean Field Crossover in Polymer Blends*, in *Phase Behaviour of Polymer Blends*. 2005. p. 1-61.

112. Khanna, R. and A. Sharma, *Pattern Formation in Spontaneous Dewetting of Thin Apolar Films*. Journal of Colloid and Interface Science, 1997. **195**(1): p. 42-50.

113. Iyer, K.S. and I. Luzinov, *Surface Morphology of Mechanically Heterogeneous Ultrathin Polymer Films*. Langmuir, 2003. **19**(1): p. 118-124.

114. Jung, M.-H. and H.-S. Choi, *Surface treatment and characterization of ITO thin films using atmospheric pressure plasma for organic light emitting diodes*. Journal of Colloid and Interface Science, 2007. **310**(2): p. 550-558.

115. Dai, Q., R. Gilbert, and J.F. Kadla, *Rheology of Cellulose Liquid Crystalline Polymers (LCPs)*, in *Encyclopedia of Chemical Processing*. 2006. p. 2663-2675.

116. Chang, S.A. and D.G. Gray, *The surface tension of aqueous hydroxypropyl cellulose solutions*. Journal of Colloid and Interface Science, 1978. **67**(2): p. 255-265.

117. Shen, Q., et al., *Re-characterization of the surface properties of non-ionic cellulose ethers by means of column wicking technique*. Colloids and Surfaces A: Physicochemical and Engineering Aspects, 2004. **240**(1-3): p. 107-110.

118. Rials, T., *Thermal and Dynamic Mechanical Properties of Hydroxypropyl Cellulose Films.* Journal of Applied Polymer Science, 1968. **36**: p. 10.

119. Janik, J., R. Tadmor, and J. Klein, *Shear of Molecularly Confined Liquid Crystals. 2. Stress Anisotropy across a Model Nematogen Compressed between Sliding Solid Surfaces.* Langmuir, 2001. **17**(18): p. 5476-5485.

120. Shusser, M. and O.V. Gendelman, *Stability of an evaporating thin polymer film.* International Communications in Heat and Mass Transfer, 2006. **33**(5): p. 564-570.

121. Jameel, A.T. and A. Sharma, *Morphological Phase Separation in Thin Liquid Films: II. Equilibrium Contact Angles of Nanodrops Coexisting with Thin Films.* Journal of Colloid and Interface Science, 1994. **164**(2): p. 416-427.

122. Puri, S., *Surface-directed spinodal decomposition.* Journal of Physics: Condensed Matter, 2005. **17**(3): p. R101.

123. Wise, S.M., J.S. Kim, and W.C. Johnson, *Surface-directed spinodal decomposition in a stressed, two-dimensional, thin film.* Thin Solid Films, 2005. **473**(1): p. 151-163.

124. Zhang, P., *Periodic Phase Separation: A Numerical Study via a Modified Cahn-Hilliard Equation*, in *Mathematics*. 2006, Simon Fraser University.

125. Traille, A. and M. Tentzeris. *Multi-resolution time-domain and level-set techniques for multi-domain/multi-physics/multi-phase simulations*. in *Microwave Symposium Digest (MTT), 2011 IEEE MTT-S International*. 2011. IEEE.

126. da Silva, L.F.M., *Handbook of adhesion technology: with 97 tables*. 2011: Springer.

127. Conti, M. and U.M.B. Marconi, *Interfacial dynamics in rapid solidification processes.* Physica A: Statistical Mechanics and its Applications, 2000. **280**(1): p. 148-154.

128. Weissbuch, I., L. Addadi, and L. Leiserowitz, *Molecular recognition at crystal interfaces.* Science, 1991. **253**(5020): p. 637-645.

129. Boettinger, W.J., et al., *Solidification microstructures: recent developments, future directions.* Acta Materialia, 2000. **48**(1): p. 43-70.

130. Sivakumar, D., et al., *Spreading behavior of an impacting drop on a structured rough surface.* Physics of Fluids (1994-present), 2005. **17**(10): p. 100608.

131. Wang, M.-J., et al., *Dynamic behaviors of droplet impact and spreading: A universal relationship study of dimensionless wetting diameter and droplet height.* Experimental Thermal and Fluid Science, 2009. **33**(7): p. 1112-1118.

132. Sivakumar, D., et al., *Spreading behavior of an impacting drop on a structured rough surface.* Physics of Fluids, 2005. **17**: p. 100608.

133. Aziz, S.D. and S. Chandra, *Impact, recoil and splashing of molten metal droplets.* International journal of heat and mass transfer, 2000. **43**(16): p. 2841-2857.

134. Yablonovitch, E. and T. Gmitter, *Wetting angles and surface tension in the crystallization of thin liquid films.* Journal of The Electrochemical Society, 1984. **131**(11): p. 2625-2630.

135. Caviezel, D., C. Narayanan, and D. Lakehal, *Adherence and bouncing of liquid droplets impacting on dry surfaces.* Microfluidics and Nanofluidics, 2008. **5**(4): p. 469-478.

136. Yarin, A., *Drop impact dynamics: splashing, spreading, receding, bouncing….* Annu. Rev. Fluid Mech., 2006. **38**: p. 159-192.

137. Werner, S.R.L., et al., *Droplet impact and spreading: Droplet formulation effects.* Chemical Engineering Science, 2007. **62**(9): p. 2336-2345.

138. Bourges-Monnier, C. and M.E.R. Shanahan, *Influence of Evaporation on Contact Angle.* Langmuir, 1995. **11**(7): p. 2820-2829.

139. Riegger, L., *Back-end processing in lab-on-a-chip fabrication.* 2010, Universitätsbibliothek Freiburg.

140. Koyama, T. and H. Tanaka, *Generic kinetic pathway of phase separation of deeply quenched polymer solutions: Transient gelation.* EPL (Europhysics Letters), 2007. **80**(6): p. 68002.

141. Tanaka, H., *Universality of viscoelastic phase separation in dynamically asymmetric fluid mixtures.* Physical review letters, 1996. **76**(5): p. 787.

142. Tanaka, H., *Viscoelastic phase separation in complex fluids*, in *Formation and Dynamics of Self-Organized Structures in Surfactants and Polymer Solutions*. 1997, Springer. p. 167-171.

143. Tanaka, H., *Viscoelastic phase separation.* Journal of Physics: Condensed Matter, 2000. **12**(15): p. R207.

144. Lee, H., et al., *Mussel-inspired surface chemistry for multifunctional coatings.* Science, 2007. **318**(5849): p. 426-430.

145. Shen, P., et al., *Wetting of polycrystalline MgO by molten Mg under evaporation.* Materials Chemistry and Physics, 2010. **122**(1): p. 290-294.

146. Picknett, R. and R. Bexon, *The evaporation of sessile or pendant drops in still air.* Journal of Colloid and Interface Science, 1977. **61**(2): p. 336-350.

147. Dhavaleswarapu, H.K., et al., *Experimental investigation of evaporation from low-contact-angle sessile droplets.* Langmuir, 2009. **26**(2): p. 880-888.

148. Wang, Z., et al., *Evaporation of ethanol-water mixture drop on horizontal substrate.* Drying Technology, 2008. **26**(6): p. 806-810.

149. Golovko, D.S., *Evaporation of Sessile Microdrops Studied with Microcantilevers.* 2008.

150. Birdi, K., D. Vu, and A. Winter, *A study of the evaporation rates of small water drops placed on a solid surface.* The Journal of Physical Chemistry, 1989. **93**(9): p. 3702-3703.

151. Block, L., *Dissolution: An Engineering Perspective.*

152. Savolainen, M., et al., *Better understanding of dissolution behaviour of amorphous drugs by in situ solid-state analysis using Raman spectroscopy.* European Journal of Pharmaceutics and Biopharmaceutics, 2009. **71**(1): p. 71-79.

153. Hancock, B.C. and M. Parks, *What is the True Solubility Advantage for Amorphous Pharmaceuticals?* Pharmaceutical Research, 2000. **17**(4): p. 397-404.

154. Blagden, N., et al., *Crystal engineering of active pharmaceutical ingredients to improve solubility and dissolution rates.* Advanced Drug Delivery Reviews, 2007. **59**(7): p. 617-630.

155. Harris, J.W. and H. Stocker, *Handbook of Mathematics and Computational Science.* 1998, New York: Springer-Verlag.

156. Scharifker, B.R., *Diffusion to ensembles of microelectrodes.* Journal of electroanalytical chemistry and interfacial electrochemistry, 1988. **240**(1): p. 61-76.

157. Dredán, J., I. Antal, and I. Rácz, *Evaluation of mathematical models describing drug release from lipophilic matrices.* International Journal of Pharmaceutics, 1996. **145**(1–2): p. 61-64.

158. Ravelli, V.a.R., R., *Prolonged release formulation technology.* Pharm. Manufact. Int., 1995: p. 171-172.

159. Kalani, M. and R. Yunus, *Effect of supercritical fluid density on nanoencapsulated drug particle size using the supercritical antisolvent method.* International journal of nanomedicine, 2011. **7**: p. 2165-2172.

160. Szepes, A., et al., *Freeze-casting technique in the development of solid drug delivery systems.* Chemical Engineering and Processing: Process Intensification, 2007. **46**(3): p. 230-238.

161. Shoaib, M.H., et al., *Evaluation of drug release kinetics from ibuprofen matrix tablets using HPMC.* Pak J Pharm Sci, 2006. **19**(2): p. 119-124.

162. Su, X.Y., R. Al-Kassas, and A. Li Wan Po, *Statistical modelling of ibuprofen release from spherical lipophilic matrices.* European journal of pharmaceutics and biopharmaceutics, 1994. **40**(2): p. 73-76.

163. Ritger, P.L. and N.A. Peppas, *A simple equation for description of solute release I. Fickian and non-fickian release from non-swellable devices in the form of slabs, spheres, cylinders or discs.* Journal of Controlled Release, 1987. **5**(1): p. 23-36.

164. Korsmeyer, R. and N. Peppas, *Macromolecular and modeling aspects of swelling-controlled systems.* Controlled Release Delivery Systems. New York: Marcel Dekker, 1983: p. 77-90.

165. Kiortsis, S., et al., *Drug release from tableted wet granulations comprising cellulosic (HPMC or HPC) and hydrophobic component.* European journal of pharmaceutics and biopharmaceutics, 2005. **59**(1): p. 73-83.

166. Bravo, S.A., M.C. Lamas, and C.J. Salomon, *In-vitro studies of diclofenac sodium controlled-release from biopolymeric hydrophilic matrices.* J Pharm Pharm Sci, 2002. **5**(3): p. 213-219.

167. Dash, S., et al., *Kinetic modeling on drug release from controlled drug delivery systems.* Acta Pol Pharm, 2010. **67**(3): p. 217-223.

168. Prausnitz, M.R. and R. Langer, *Transdermal drug delivery.* Nat Biotech, 2008. **26**(11): p. 1261-1268.

169. Prausnitz, M.R., S. Mitragotri, and R. Langer, *Current status and future potential of transdermal drug delivery.* Nat Rev Drug Discov, 2004. **3**(2): p. 115-124.

170. Dua, K., et al., *Penetration Enhancers for TDDS: A Tale of the Under Skin Travelers.* Advances in Natural and Applied Sciences, 2009. **3**: p. 95-101.

171. Prausnitz, M.R., et al., *Microneedle-based vaccines*, in *Vaccines for Pandemic Influenza.* 2009, Springer. p. 369-393.

172. Subedi, R., et al., *Recent advances in transdermal drug delivery.* Archives of Pharmacal Research, 2010. **33**(3): p. 339-351.

173. Stead, L.F., et al., *Nicotine replacement therapy for smoking cessation.* Cochrane Database Syst Rev, 2008. **1**(1).

174. O'Malley, S.S., et al., *A controlled trial of naltrexone augmentation of nicotine replacement therapy for smoking cessation.* Archives of Internal Medicine, 2006. **166**(6): p. 667.

175. George, T.P., et al., *Nicotine transdermal patch and atypical antipsychotic medications for smoking cessation in schizophrenia.* American Journal of Psychiatry, 2000. **157**(11): p. 1835-1842.

176. Silver, A.A., et al., *Transdermal nicotine and haloperidol in Tourette's disorder: a double-blind placebo-controlled study.* The Journal of clinical psychiatry, 2001. **62**(9): p. 707-714.

177. Stead, L.F., et al., *Nicotine replacement therapy for smoking cessation.* Cochrane Database of Systematic Reviews, 2012(11).

178. Yin, C. and X. Li, *Anomalous diffusion of drug release from a slab matrix: Fractional diffusion models.* International Journal of Pharmaceutics, 2011. **418**(1): p. 78-87.

179. Fernandes, M., L. Simon, and N.W. Loney, *Mathematical modeling of transdermal drug-delivery systems: analysis and applications.* Journal of membrane science, 2005. **256**(1): p. 184-192.

180. Simon, L., M. Fernandes, and N. Loney. *The use of mathematical modeling and simulation tools to study transdermal drug delivery systems*. in *Bioengineering Conference, 2005. Proceedings of the IEEE 31st Annual Northeast*. 2005. IEEE.

181. Paul DR, M.S., *Diffusional release of a solute froma polymer matrix.* Journal of Membrane Science, 1976. **1**: p. 33-48.

182. **Brown, M.**; Available from: www.igert.org.

183. Sirringhaus, H., et al., *High-resolution inkjet printing of all-polymer transistor circuits.* Science, 2000. **290**(5499): p. 2123-2126.

184. Kim, J.-H., et al., *Evaporation of Sessile Droplets of Dilute Aqueous Solutions Containing Sodium n-Alkylates from Polymer Surfaces: Influences of Alkyl Length and Concentration of Solute.* Langmuir, 2008. **24**(20): p. 11442-11450.